Controls on gold mineralization at the Onaman prospect, northwestern Ontario

by

Olivier Grondin

A thesis submitted to the Faculty of Graduate Studies and Research

in partial fulfillment of the requirements for the degree of

Master of Science

Department of Earth and Planetary Sciences

McGill University, Montreal

July 2001

ABSTRACT

The Onaman property in northwestern Ontario hosts several unusual mesothermal gold occurrences, in which gold is associated with chalcopyrite. This study examines two showings with contrasting mineralization styles. The Ryne showing is underlain by intermediate to felsic metavolcaniclastic rocks, and features a brittle-ductile shear zone with disseminated low-grade gold mineralization, whereas the Hourglass showing contains high concentrations of gold disseminated in narrow felsic dykes.

Mineralization proceeded with an initial stage of pyritization, which decreased aH_2S and fO_2 of the fluid, while coeval carbonatization decreased the pH. These changes in physico-chemical parameters lead to the second mineralization stage, in which pyrite was replaced by arsenopyrite and pyrrhotite. Chalcopyrite and gold co-precipitated and both replaced pyrite. The decrease in aH_2S, which reduced $Au(HS)_2^-$ and $Cu(HS)_2^-$ stabilities, was the principal control of gold and chalcopyrite deposition.

The absence of copper in most mesothermal deposits is explained by the extreme solubility of this metal as a bisulfide complex, which prevents its precipitation as chalcopyrite. The rare occurrence of chalcopyrite at Onaman reflects unusually low solubility of copper due to the combined effects of an abnormally low initial pH of the fluid and a low fluid/rock ratio.

SOMMAIRE

Le projet Onaman, situé au nord-ouest de l'Ontario, comprend plusieurs indices d'or mésothermal inhabituels, dans lesquels l'or est associé à la chalcopyrite. La présente étude fait l'objet de deux indices aux styles de minéralisation différents. L'indice Ryne comprend une zone de cisaillement ductile-cassante dans des roches métavolcaniclastiques intermédiaires à felsiques dans laquelle la minéralisation en or est disséminée et à faible teneur. L'or à l'indice Hourglass est disséminé dans d'étroits dykes felsiques et concentré à de fortes teneurs.

La minéralisation est caractérisée par une pyritization initiale qui a diminué l'activité d'H_2S et la fugacité d'oxygène du fluide, alors que l'altération en carbonates diminuait le pH. Ces changements physico-chimiques ont mené au second stade de minéralization dans lequel la pyrite est remplacée par l'arsénopyrite et la pyrrhotite. Aussi, la chalcopyrite et l'or ont co-précipité et ont tous deux remplacé la pyrite. La réduction en aH_2S a induit une diminution de la stabilité des complexes $Au(HS)_2^-$ et $Cu(HS)_2^-$ et fut le contrôle principal de la précipitation d'or et de chalcopyrite.

L'absence du cuivre dans la plupart des gisements d'or mésothermaux est expliquée par sa solubilité extrême lorsque complexé avec le soufre, ce qui empêche la précipitation de la chalcopyrite. L'association or-chalcopyrite observée à Onaman est due à la solubilité du cuivre inhabituellement faible, puisque le pH de départ du fluide était anormalement faible, ainsi qu'au faible rapport fluide/roche.

PREFACE

This thesis was initiated as a collaboration between the author and his supervisor, Professor A.E. Williams-Jones. The thesis comprises four chapters, of which one is a manuscript that has been submitted for publication to Economic Geology. Data was collected by the author through geochemical studies, petrography, microprobe work, and isotopic studies. Prof. A.E. Williams-Jones provided advice on research methodology, and helped evaluate and interpret research results, and critically reviewed the manuscript of which he is co-author.

The thesis was written in the form of a journal manuscript, entitled *Gold mineralization and wallrock alteration at the Onaman property, Ontario*, in accordance with the regulations put forth by the Faculty of Graduate Studies and Research at McGill University. In addition to the manuscript, an introduction including objectives and a literature review, a chapter on regional geology and a conclusion were included to provide a comprehensive description of the research.

ACKNOWLEDGEMENTS

Thanks to Prof. A.E. Williams-Jones for supervision. I must also thank Cameco Gold Inc. for their support, especially the assistance of geologists Mike Koziol, Ike Osmani, Jacques Samson, and technician Dan Dampier. Many discussions with Emeritus Professor Wally MacLean, J.R. Clark and Drs C. Normand and A. Migdisov helped improve the research. I am very grateful to the Natural Science and Engineering Research Council (NSERC) for financial support through a PGS-A scholarship, and a CRD research grant to AEW-J.

Many thanks to the professors who taught me geology at UQAM, and to James Moorhead for his help with understanding the world of geology. I must also thank Mr. Glenn Poirier for his assistance with the electron microprobe analyses, and Mr. Sang-Tae Kim and the people at Geotop for their help with the C & O isotopes.

Special thanks are given to my fellow graduate students, including Charles Maurice, Sandy Archibald, Kate Ault, Annick Chouinard, Jonah Resnick, people involved with the McGill Student Chapter of the Society of Economic Geologists, and to my friend Amélie for her support. I must also point that out I am thankful to all the staff at the EPS department, who are providing exceptional assistance despite being surrounded by dysfunctionality at McGill University.

TABLE OF CONTENTS

LIST OF FIGURES

LIST OF TABLES

LIST OF APPENDICES

CHAPTER 1

General statement

INTRODUCTION

Archean mesothermal gold mineralization, also described as lode-gold, has been studied extensively in the past 50 years. Canadian and Australian deposits have been compared, and several genetic models have been proposed to explain the genesis of epigenetic gold-only deposits in similar geological settings all over the world. This class of deposits is found in greenstone belts composed of both volcanic rocks and clastic sediments, e.g. the Abitibi Belt, Canada (Hodgson, 1993), and Yilgarn Block, Australia (Groves et al. 1989). Characteristic features are a high Au:Ag ratio (between 1:1 and 10:1), an extensive vertical continuity, carbonate-dominated hydrothermal alteration except at high metamorphic grades, a spatial association with felsic intrusions, and a temporal association with regional metamorphism. The deposits form near major faults and on subsidiary structures that are parts of regional deformation corridors characterized by faults and high-strain zones of a brittle to brittle-ductile nature (Groves et al. 1989). These faults act as fluid conduits, are associated with strong carbonate-rich hydrothermal alteration (Hodgson, 1993, Phillips, 1986), and are commonly localized around the contacts between different lithofacies, e.g., the Cadillac break (Hodgson and MacGeehan, 1982). Fluids travel long distances vertically and mineralization is developed along much of the transport path, which implies interaction between the fluid and a variety of host rocks (Mikucki, 1988). The depth of formation of mesothermal gold deposits ranges from 3 to 18 km, corresponding to pressures of 1 to 5 kbar, and to a temperature range from 200 to 700°C (Ridley et al. 1996). However, most deposits form at depths of 3 to 12 km, (i.e., pressures of 1 to 4 kbar) and temperatures of 250 to 400°C (Hodgson, 1993). The geological context for mesothermal gold deposits usually involves the presence of

three rock groups: High-Mg mafic and ultramafic volcanic and intrusive rocks, clastic sedimentary rocks, and felsic intrusions. Most deposits are hosted by mafic or ultramafic metavolcanic rocks, especially when classified as "medium temperature" (Mueller and Groves, 1991), and the metamorphic grade is greenschist facies. The affinity of the host rocks is usually tholeiitic, e.g., at Kirkland Lake (Kishida and Kerrich, 1987), Chibougamau (Dubé et al. 1987), in the Yilgarn Block (Mueller and Groves, 1991, Phillips, 1986), and in most of the Abitibi belt (Hodgson and Hamilton, 1989).

Mineralization

Gold mineralization in mesothermal deposits is usually of two major types: 1) gold-bearing quartz and quartz-carbonate veins, veinlets and stockworks; and 2) disseminated gold in altered wallrock with pyrite-quartz-carbonate-albite replacement zones. Minerals associated with gold mineralization are quartz, carbonates, albite, sericite, pyrite, arsenopyrite, pyrrhotite and other sulfides, tellurides, tourmaline, scheelite, and molybdenite (Hodgson, 1993). As a consequence of the vertical extension of these deposits, gold mineralization rarely disappears at depth, although grades and lateral extent of alteration may decrease (Ridley et al. 1996). Also, pyrrhotite replaces pyrite as the major sulfide phase associated with gold at increasing depth, as seen in the Hollinger-McIntyre mine near Timmins (Hodgson, 1993), and Australian deposits of the Yilgarn Block (Ridley et al. 1996). This is thought to be a result of the decreasing degree of sulfidation (Mueller and Groves, 1991). High gold values have been successfully correlated with alteration assemblages, especially the coincidence of muscovite (sericite) and albite (Kishida and Kerrich, 1987).

Alteration

Hydrothermal alteration is probably the most discussed and studied feature of mesothermal gold deposits and is generally zoned laterally, although the actual mineral assemblages developed vary with the host-rock lithology (Böhlke, 1989), the metamorphic facies, and the temperature of the fluid. The alteration is generally not zoned vertically, suggesting that the distances of vertical fluid advection are orders of magnitude greater than those of lateral infiltration (Ridley et al. 1996). For mesothermal gold mineralization hosted in rocks metamorphosed to greenschist facies, the lateral zonation starts with the occurrence of distal chlorite coexisting with relict primary pyroxene and metamorphic minerals. This zone has been referred to as the outer propylitic zone, and can be followed for distances of tens to hundreds of meters from the lode system (Mueller and Groves, 1991). Calcite is commonly associated with distal chlorite (Dubé et al. 1987). Moving inward, the chlorite is gradually replaced by carbonates and albite to form a zone dominated by ankerite and albite adjacent to the mineralized veins or hosting disseminated mineralization (Mountain and Williams-Jones, 1995). Sericite is also found in the mineralized zone, along with pyrite (Mueller and Groves, 1991). The carbonate alteration is represented by different minerals depending on the host rock, and is commonly zoned from calcite distal to mineralization, to Fe-rich carbonates closer to the lodes (Smith and Kesler, 1985). The carbonate zone is best developed in mafic volcanic rocks (Groves et al. 1989), in which Fe- and Mg-carbonates are the main alteration minerals (Guha et al. 1991); in rocks of felsic and intermediate composition, calcite is the main carbonate mineral (Hodgson, 1993).

Ore fluid chemistry

The nature of the fluids responsible for mesothermal gold mineralization is broadly known as a result of numerous studies of fluid inclusion thermometry and chemistry, and alteration assemblage stability. This review is based on the work of Mikucki (1998). Fluid inclusion studies have shown that the hydrothermal fluid involved in mesothermal gold mineralization is dominantly aqueous, and rich in carbon dioxide (0.05-0.25 X_{CO_2}). Methane seems to be important only in reduced carbon-rich environments, such as graphitic shales. Salinity is relatively low (<10 wt % equivalent NaCl). The small concentration of chlorine also explains the low mobility of base metals in lode-gold environments (Phillips, 1986).

Phase diagrams illustrating the stability conditions of alteration assemblages indicate that mineralization occurs at a near-neutral or slightly alkaline pH (5.2-6.8), which, in the case of greenschist facies host rocks, is buffered by albite and sericite assemblages. The dissociation of HCl° and $H_2CO_3^{\circ}$ with cooling decreases the pH of the fluid and the excess H^+ is fixed in the wallrock by sericite, along with alkalis (Na, K) transported by the fluid. Based on silicate-sulfide and sulfide-oxide (magnetite) assemblages, the oxidation state of the fluid is fairly constant, in the field of reduced sulfur. The sulfur content of the fluid decreases with decreasing temperature.

Physico-chemical controls of mineralization

Under mesothermal conditions, gold is transported in the fluid mainly as a bisulfide complex (Seward, 1973), $Au(HS)_2^-$ being the dominant species in neutral to slightly alkaline conditions (Benning and Seward, 1996). Chloride complexes are unimportant at greenschist facies conditions as they are only favored at low pH, high oxygen fugacity, high chlorinity, and high temperature (Gammons et al. 1997). It was thought that the role of Au(HS)° would increase at higher temperatures (Benning and Seward, 1996), but recent studies have shown that Au(HS)° is important only at temperatures under 300°C, the lower limit of the range of fluid temperatures at which mesothermal deposits are predicted to form (Mikucki, 1998).

Gold mineralization occurs when aqueous gold complexes become unstable as a result of a change in the physico-chemical conditions. One of the most important of these changes is a lowering of aH_2S as a result of sulfidation of the wallrock through pyritization. This serves to destabilize the species $Au(HS)_2^-$ by reversing the complexation reaction:

$Au + 2H_2S + ¼O_2 = Au(HS)_2^- + H^+ + ½H_2O$.

The high Fe/(Fe+Mg) ratios of the host rocks, and the common association of gold with Fe-sulfides support the sulfidation model (Groves et al. 1989). Another change that can be favorable for gold deposition is the lowering of aH^+ as a result of the carbonatization of the wallrock (Ridley et al. 1996), in the reaction:

$Au + 2HS^- + H^+ + ¼O_2 = Au(HS)_2^- + ½H_2O$.

Other mechanisms involve the carbonatization of minerals containing oxidized iron (magnetite) that will oxidize the fluid (Hodgson, 1993), and unmixing of H_2O and CO_2, coupled with fluid-rock interaction that would lower the CO_2 content. This process has been proposed to explain the mineralization at the Sigma mine in Val d'Or (Guha et al. 1991), where a rapid drop of pressure due to fracturing could have caused the unmixing of CO_2 from the aqueous phase (Robert and Kelly, 1987). Other possible gold depositing processes discussed in the past include the adiabatic and conductive cooling of the ore fluid, mixing with another fluid (Mikucki, 1998), and pH increase accompanying sericitization of feldspar in the wallrock (Hodgson, 1993).

PROBLEM AND OBJECTIVES

The Onaman prospect is the object of a mining exploration project, and comprises several gold occurrences, hosted by different lithologies, and reflecting more than one mineralization style. Conventional exploration methodologies, including geophysical surveys, were unsuccessful at finding new targets for the company, Cameco Gold Inc. The research project discussed in this thesis was therefore designed to develop a new exploration approach based on an understanding of the geochemical controls of the gold mineralization.

Although the geochemical signature for mesothermal gold mineralization varies among deposits (Hodgson and McGeehan, 1982), many features of the process are shared, including the transfer from the fluid phase to the rock of CO_2, K, S, H_2O, and Na (Guha et al. 1991). Recognition of these features is important because of their potential to increase

the size of the exploration target. A major interest of this study was therefore to identify the signature of the hydrothermal event that produced the gold. This was accomplished by deciphering the effects of hydrothermal activity on the rocks hosting the deposit, i.e., the alteration, and relating these to the physico-chemical controls of gold mineralization. The study is based mainly on information from two gold occurrences, namely the Ryne and Hourglass showings.

METHODOLOGY

The objectives of the research were pursued with the help of:

1) A program of fieldwork at the Onaman property, Ontario, including drill core logging, trench mapping, and sampling of rocks for petrographic and geochemical analyses.

2) Geochemical analyses by INAA, four-acid digestion ICP, and ICP-MS for elements related to economic mineralization, by ICP-MS for major and trace elements, by a XRF-pressed pellet method for a selection of trace elements, by cold-vapor for Hg, and by Leco induction furnace for C and S. The geochemical data acquired were used to determine the mass changes accompanying alteration.

3) Compilation of the data acquired by Cameco Gold Inc., including bulk-rock analyses, that were used in the mass transfer calculations.

4) Petrographic examination to identify primary and secondary minerals and determine the textural relationships among them.

5) Microprobe analyses to determine the chemical composition of ore and gangue minerals, correlate chemical variations with changes in textural relationships, and calculate mineral activities.

6) Sulfur isotopic analyses of pyrite grains to determine the source of sulfur. The pyrite grains were manually separated from the crushed samples, or mechanically concentrated.

7) Carbon and oxygen isotopic analyses of ankerite to determine the source of carbon and the source of the fluid.

8) Thermodynamic analysis of stability relationships among alteration and mineralization minerals.

PREVIOUS WORK

Mining and exploration

The Onaman project is located in an area that has been intensively prospected since the 1910's. Several past and present mineral exploration properties are located nearby, and prospectors have regularly staked claims in the area since the first gold discovery in 1915. The Tash-Orn Mines, situated 8km northwest of the Onaman property, produced 320 kg of test gold ore grading 32 g/t in 1917. Six kilometers northwest of Onaman, the Adair prospect produced 34 tons of gold ore yielding 14 g/t from a 10m vertical shaft in 1924. A small mine was established during the 1930's north of Tashota Station, eleven kilometers NNW of the Onaman project but did not produce any ore (Amukun, 1977). A shaft was sunk to 100m at the Wascanna mine prospect seven kilometers northwest of Onaman that produced 450 kg of test gold ore grading 36 g/t in 1937. The Tashota-Goldfields mine, located 13 km south of Onaman, produced a total of 395 kg of gold, 465 kg of silver and 260 tons of copper between 1935 and 1938 (Thurston, 1980). However, all gold exploitation in the Tashota area has been minor and overshadowed by the

important production from the Beardmore-Geraldton mining camp, 60km south of the Onaman property.

The most extensive modern exploration of Onaman and surrounding areas was in the 1970's and included trenching, diamond drilling and underground development (Amukun, 1977), and prior to the current exploration by Cameco Gold Inc., only Sherrit Gordon Limited, Noranda Exploration Co. Ltd. and Holmer Gold Mines have explored in the area, and their work was limited to geophysical surveys, some trenching and reconnaissance diamond drilling on areas overlapping the Onaman property (Osmani, 1999). Cameco Gold Inc. carried out trenching, channel sampling, and diamond drilling on the property in 1998 and 1999 (Osmani, 1999).

Research

Academic work in the area includes an early study of the gold potential of the Onaman area (Girvin, 1924), a study of the structural controls of mineralization in the Tashota-Goldfields mine (Flaherty, 1936) and an alteration study of a massive sulfide occurrence 14 kilometers SSW of the Onaman property (Osterberg et al. 1987). Regionally, McBride (1987) related gold mineralization of the Beardmore-Tashota area to tectonic evolution, Anglin et al. (1988) constrained the timing of gold and base metal mineralization of this area using U-Pb geochronology, and Anglin and Franklin (1989) used Pb isotopic data to investigate the source of this mineralization. Finally, a MSc thesis mapping project including an alteration study is currently underway at the Marshall Lake Cu-Zn-Ag prospect, 15km northwest of Onaman, and (Straub, 2000).

MAPPING

Gledhill (1925) produced the first geological map of the Onaman area, which was subsequently remapped by the Ontario Geological Survey in the 1970's, at a scale of 1:31,680. Gold mineralization received only cursory attention in this latter mapping program, the information coming mainly from assessments file by mining companies. Most of the detailed mapping was reserved for the Beardmore-Geraldton segment, which has produced more than 4.1 million ounces of gold and 250,000 ounces of silver from 19 mines. This gold mineralization is largely epigenetic (Anglin et. al. 1988), and related to iron formations. The deposits occur mainly in veins, shear zones and breccias (Mason and McConnell, 1983).

The area was mapped most recently in the 1990's by the Ontario Geological Survey. This work was at a regional scale, and only fieldwork summaries have been published to this date (G. Stott, personal communication). Finally, Cameco Gold personnel prepared detailed geological maps in 1997-8 of an area of 19 km^2 (18 unpatented mining claims representing 119 claim units).

CHAPTER 2

Regional and property geology

REGIONAL GEOLOGY

Lithology

The Onaman property is situated in the Gzowski-Oboshkegan area, interpreted to be one of the volcanic centers of the Onaman-Tashota greenstone belt, which is located in the Eastern Wabigoon Region (EWR) of the Wabigoon Subprovince of the Superior Province, northwestern Ontario (Fig. 1). This part of the Wabigoon Subprovince still is poorly understood, in part because the typical Wabigoon stratigraphy, which is dominated by mafic metavolcanic rocks at the base of a supracrustal rock sequence, is apparently not present (Blackburn et al., 1991). No mafic flows were found in the Gzowski-Oboshkegan area. However, it has been observed that metavolcanic units in the EWR are clustered around volcanic centers (Blackburn and Johns, 1988), such as the Gzowski-Oboshkegan center.

The Onaman-Tashota area is separated from the better-studied Beardmore-Geraldton belt by a sequence of andesitic to rhyolitic south-younging volcanic rocks (Blackburn et al. 1991), and comprises the northern, east-west striking segment of a z-shaped greenstone belt. The southwest-northeast trending part of the "z" links the Onaman-Tashota belt with the Beardmore-Geraldton greenstone belt, 60 km to the south. This central part of the greenstone belt consists predominantly of mafic metavolcanic rocks, and includes a narrow body of conformable felsic metavolcanics. Felsic intrusives and migmatitic rocks occur on both sides of the belt, which has been intruded by younger mafic rocks

(Thurston, 1980). The northern part of the belt comprises the Tashota (western end) and Gledhill Lake (eastern end) areas, which were mapped separately by the OGS, and can be distinguished by the relative abundance of mafic and felsic rocks. The Gledhill Lake area comprises equal proportions of mafic and felsic metavolcanics, subordinate clastic and chemical sediments (sandstones and iron formation) and minor proportions of mafic intrusives (Amukun, 1980). By contrast, the Tashota area is composed mainly of mafic metavolcanic and intrusive rocks, except the Onaman property, where intermediate to felsic metavolcanic rocks predominate. Clastic sedimentary rocks are also present (Amukun, 1977).

Metamorphism and regional structure

The metamorphic grade of the Wabigoon Subprovince is mainly mid to lower amphibolite facies and lower than that of the adjacent subprovinces. Temperature and pressure are estimated to have been generally about 500-600°C, and <3.4 Gpa, respectively (Easton, 2000). Higher metamorphic grades occur at the margins of the subprovince, and maximum temperature and pressure are estimated to have been 750°C and 0.3 to 0.4 GPa respectively. Peak metamorphism is interpreted to have postdated major folding events (Blackburn et al., 1991). Metamorphic grades in the Onaman-Tashota greenstone belt were generally lower than elsewhere in the Wabigoon Subprovince, varying from lower greenschist to lower amphibolite facies (Amukun, 1977). On the Onaman property, regional metamorphic grades were from lower to mid-greenschist facies, which is evident from the presence of chlorite, sericite, albite, iron oxides and carbonates. Rocks with mineral assemblages representative of hornblende

hornfels facies occur close to a granitoid stock, in the southwest part of the property (Osmani, 1999).

The rocks of the Onaman area have been severely deformed, and exhibit penetrative deformation from at least two tectonic events (Amukun, 1977), although up to seven episodes of deformation have been identified in other parts of the Wabigoon Subprovince (Blackburn et al. 1991). Regional folding is poorly understood because of the lack of outcrops in the Onaman area. Interpreted axial planes have a northeast trend, and isoclinal folds have been interpreted on the basis of dips and lack of closure. Two major fault trend directions are observed: NNW (N10°) and WNW (N45°) (Amukun, 1977).

Geochronology

Published ages of volcanism vary widely. A rhyolite from the Onaman River area was dated at 2769 Ma from U-Pb isotopic ratios in zircons (Anglin et al. 1988). Some volcanic rocks of the EWR have Pb model ages older than 2.8 Ga (Blackburn et al. 1991), and galena from a massive sulfide occurrence south of the Onaman project was dated ca. 2900 Ma (Anglin and Franklin, 1989). It should be noted, however that model Pb ages are notoriously unreliable.

PROPERTY GEOLOGY

Geological staff of Cameco Gold mapped the Onaman property at a scale of 1:5000 in 1997 and 1998 (Melrose, 1998), and reported the results of their work in a series of

unpublished company reports (Fig. 2). The following geological description is based on a 1999 report by Osmani.

The property is underlain by steeply dipping massive to pillowed mafic metavolcanics and vesicular flows, which are overlain by a thick sequence of intermediate to felsic metavolcaniclastic rocks. Thin units of siltstone and argillite occur within both the mafic and intermediate to felsic volcaniclastics, while conglomerate overlies the latter. Several gabbro bodies and quartz-feldspar porphyry and felsite dykes intrude this sequence, and were intruded in turn by late Archean granitoid dykes and stocks, and Proterozoic diabase dykes of the Matachewan (2.45 Ga) and Marathon (2.17 Ga) swarms.

Mafic metavolcanics

The basal mafic metavolcanics are both phyric and aphyric, and range from fine- to medium-grained. They cover approximately one fifth of the property and are concentrated in the north. Their thickness is unknown. Weak carbonate and chloritic alteration is widely observed. Geochemically, these rocks are tholeiitic to calc-alkaline in affinity.

Intermediate metavolcaniclastics

The overlying intermediate to felsic metavolcaniclastic sequence consists dominantly of pyroclastic and epiclastic rocks, comprising mainly lapilli tuff, blocky tuff, tuff breccia, and finer-grained crystal and ash tuff. Lithic fragments are commonly quartz- and

plagioclase-phyric in an aphyric to quartz-phyric, chloritized and sericitized matrix. The matrix can be difficult to discern from the fragments when the latter are tightly packed because the matrix and fragments are compositionally similar. Fragments with coarse quartz and feldspar crystals are probably derived from quartz-feldspar porphyry intrusions, which were emplaced in the intermediate to felsic metavolcaniclastic rock sequence. Primary textures are preserved only in fragments. Based on whole-rock geochemical analyses (Osmani, 1999), the intermediate to felsic volcaniclastics have a calc-alkaline affinity and are largely dacitic in composition. Andesitic and rhyodacitic varieties occur locally.

Metasedimentary rocks

Clastic metasediments are a minor rock type on the property but are widely distributed. They occur mainly as lenses (a few cm to 20m thick) interbedded in the intermediate to felsic metavolcaniclastic units, and less commonly in the mafic metavolcanics, and consist mainly of argillite (locally graphitic) and agillaceous siltstone. A thin unit of polymictic conglomerate with interbedded siltstone, wacke, and quartz arenite overlies the intermediate to felsic metavolcaniclastics uncomformably. The clasts in these conglomerates are angular to rounded, range in diameter from a centimeter up to 1 m, and are composed of mafic and intermediate to felsic metavolcanics, siltstone and argillite, quartz-feldspar porphyry, and gabbro. Granitic clasts are rarely found, except in one bed, in which they are a minor component.

Intrusions

Gabbro stocks, dykes and sills cover a quarter of the property and vary from fine- to coarse-grained, although most are medium-grained. Locally, they may be porphyritic with plagioclase crystals commonly reaching up to 7 cm in length. Xenoliths of country rocks are found in the larger intrusions. Magnetite is commonly present, particularly in the northern part of the property where the gabbros produce strong magnetic anomalies. Geochemically, the gabbros are similar to the mafic metavolcanics. An ultramafic dyke was identified from bulk-rock geochemical analyses of samples from outcrop and drill core.

Felsic stocks, dykes and sills occur throughout the property and are largely porphyritic, containing quartz and feldspar phenocrysts, and locally amphibole. Three generations of felsic intrusions can be distinguished. Older stocks and dykes consist of medium- to coarse-grained calc-alkaline to mildly alkaline granitoid rocks (diorite, monzonite and monzodiorite and rare lamprophyres), and their REE trends are similar to the sanikutoids emplaced during the late Archean in the Superior Province. Their emplacement was probably coeval with that of the polymictic conglomerate, since these intrusions cut the conglomerate, which contains granitic clasts. Two generations of hypabyssal felsic dykes were distinguished from the older late Archean granitoids on the basis of their textures. Their exact timing relative to the granitoids is unclear. Early quartz-feldspar porphyries and felsite dykes are tonalitic and are invariably deformed and altered, suggesting pre-deformation emplacement. By contrast, younger porphyries and aphyric dykes are typically granodiritic in composition, and generally massive to weakly foliated. Quartz-

feldspar porphyries of both ages are typically calc-alkaline, suggesting that some of these intrusions are subvolcanic sills related to the metavolcaniclastics, whereas felsite dykes are weakly alkaline and may be related to the late Archean granitoid stocks.

Diabase dykes are the youngest rocks on the property. They are massive, magnetic, and range in width from <1m up to 60m. Two types occur: 1) N to NE striking, fine-grained to aphanitic, 2) NW striking and plagioclase-phyric. No crosscutting relationship was observed in outcrop.

Structure

Rocks on the property have been subjected to two major episodes of regional deformation. The dominant foliation was produced by D_2, and is generally conformable with bedding and layering in the metavolcanic rocks, striking west to west-southwest and dipping steeply northward. D_1 fabrics are locally preserved in D_2 fold closures. Based on primary sedimentary features such as flame structures and graded bedding in metasiltstone units, younging directions are toward the south; in addition, minor asymmetric Z-folds and bedding-cleavage relationships indicate that the metavolcanic-metasedimentary sequence on the property forms the north limb of a south-verging overturned syncline (Thomas, 1998). Evidence of refolded minor structures, varying from mesoscopic open folds through to tight isoclinal folds, is preserved in several parts of the property, particularly to the south of the Ryne showing. Thus, the rock sequence forms the central part of an E-NE-trending D_1 antiform that has been refolded about a NE-trending D_2 axis to produce a synform.

Faults on the property have northwesterly or northeasterly trends. They have been observed in drill core as narrow zones of brecciation (0.1 to 3m) and interpreted geophysically. The fault movements are unknown (Amukun, 1977), and these structures are characterized by local offset lithologic contacts and limited flattening. Shear zones are also observed on the property and may be distinguished from the faults by their greater width (5 to 25m), a strong penetrative foliation and intense flattening of clasts. Locally, there are narrow bands of reduced grain size and mm-scale laminae interpreted to represent mylonitic shears. An absence of kinematic indicators suggests non-rotational strain or pure shear flattening. The intense flattening and absence of large veins suggest a brittle-ductile behavior of the shear zone. Brittle structures are represented by micro-veinlets within the shear zone, which are locally cut by a series of narrow (< 20cm) NW-trending shear fractures (Reidel shears, or extensional crenulation cleavages) that host deformed veinlets and associated alteration.

Shear zones typically represent a major structural control on mesothermal gold mineralization, and the Onaman property is no exception. The largest of the shear zones and the most prominent structure at Onaman is the Ryne Deformation Zone (RDZ). The RDZ is 15 to 25 m wide, and trends W-NW for 250 m (in outcrop) across the south-central part of the property, before it is disrupted or truncated by NE-trending cross-faults. However, based on geophysical and drill hole data, the RDZ is interpreted to extend 1.5 km west from the Ryne showing (Fig. 2), toward the Knucklethumb Lake area (Osmani, 1999). The RDZ is characterized by well-developed schistosity, flattening of volcanic/volcaniclastic/sedimentary clasts, and intense hydrothermal alteration. Other

important shear zones on the property include two NW-trending structures that extend between the Green Jimmy and MVP gold showings (Fig. 2), and between the Big Bear and Hourglass gold showings. These shear zones were mainly interpreted by magnetic and induced polarization anomalies, but in outcrop, they also display intense flattening and hydrothermal alteration.

Alteration and mineralization

All outcrops sampled display evidence of intense hydrothermal alteration, which makes the distinction between regional metamorphism and alteration difficult. No fresh equivalents of the altered lithofacies were found. Least-altered samples of intermediate to felsic metavolcaniclastic rocks are carbonatized (calcite), and in some cases sericitized and chloritized. In mineralized zones, calcite is replaced by ankerite, giving weathered surfaces a rusty color. Evidence of silicification and albitization is observed locally in outcrop and drill core, both in mineralized and unmineralized zones.

Gold showings on the property display three main styles of mineralization: 1) disseminated in intensively altered shear zones (Ryne, Big Bear, Cabin); 2) disseminated in shallow intrusions, e.g., felsite dykes and porphyries (Hourglass); and 3) hosted in pyrite-chalcopyrite-pyrrhotite-bearing quartz-carbonate veins (Big Bear, MVP, Green Jimmy) and quartz-tourmaline veins (Claimline). The shear and intrusion-related styles of mineralization are the most important in terms of economic potential. These showings commonly do not share the same lithology, and consequently, alteration assemblages and mineralization styles differ among them.

CHAPTER 3

Journal manuscript

Gold mineralization and wallrock alteration at the Onaman property, Ontario

Olivier Grondin and Anthony E. Williams-Jones

Olivier Grondin
Earth and Planetary Sciences, McGill University
3450 University Street, Montreal, Qc H3A 2A7
grondin@eps.mcgill.ca

Anthony E. Williams-Jones
Earth and Planetary Sciences, McGill University
3450 University Street, Montreal, Qc H3A 2A7
willyj@eps.mcgill.ca

Submitted to: Economic Geology

ABSTRACT

The Onaman property in northwestern Ontario hosts several mesothermal gold showings that are unusual because of the association of the gold with minor copper mineralization and the contrasts in lithologies and structural setting. This study focuses on two showings selected to represent the principal miineralization styles. The Ryne showing is underlain by intermediate to felsic metavolcaniclastic rocks, and features a brittle-ductile shear zone hosting disseminated gold mineralization and high-grade quartz-tourmaline microveinlets, whereas high-grade disseminated gold in the Hourglass showing is hosted by narrow felsic dykes.

Similar alteration and mineralization parageneses are present at both showings. Early quartz-albite alteration of the groundmass was overprinted by intense and pervasive carbonatization. Sericitization and chloritization occurred later. Ankerite is the dominant carbonate mineral in mineralized zones, and only calcite is present in unmineralized rocks. Altered/mineralized rocks are enriched in Na and Ca, depleted in K, and Fe and Mg behaved coherently and underwent minor gains and losses. Mineralization was coeval with carbonatization and quartz ± albite ± carbonate ± tourmaline veining, and involved deposition of pyrite and its subsequent replacement by arsenopyrite, pyrrhotite, chalcopyrite, and native gold/electrum. Chalcopyrite and gold crystallized together.

Native gold and electrum compositions cluster in three groups based on their Ag concentration, and more than one compositional group is commonly represented in a single sample.

Oxygen and carbon isotopic ratios of ankerite suggest a metamorphic origin for the fluid, and a possible mantle source for carbon. Sulfur isotopic ratios in pyrite correlate positively with gold grades.

A model is proposed in which deformation of the volcanic pile lead to the formation of a shear zone, and created dilational zones allowing dyke intrusion. Fluids of possible metamorphic origin rose along the pathways created by the shear zones and the dykes. An initial stage of mineralization represented by pyritization of the host rock reduced sulfur activity and oxygen fugacity. Contemporaneous carbonatization decreased pH. This evolution of the fluid produced the second mineralization stage, namely the replacement of pyrite by pyrrhotite and the penecontemporaneous crystallization of native gold and chalcopyrite. The changes in fO_2, pH and aH_2S favored gold deposition by decreasing its solubility, while pH and sulfur activity decreases promoted chalcopyrite deposition. In the case of both gold and chalcopyrite, decreasing H_2S was the principal control of mineralization.

The unusual occurrence of genetically contemporaneous gold and chalcopyrite in the Onaman mesothermal showings is explained by the fact that initial pH and fluid-rock ratio were significantly lower than for most deposits of this class, thereby enabling both

gold and chalcopyrite to saturate in the ore fluids and deposit when reductions in aH_2S destabilized $Au(HS)_2^-$ and $Cu(HS)_2^-$.

INTRODUCTION

Although Archean greenstone-hosted mesothermal gold mineralization has been the subject of intense study in a large number of deposits over the past 50 years, most of these studies have focused on gold- or gold-silver-only variants hosted by large quartz vein systems (Robert and Kelly, 1987; Smith et al., 1984). Relatively few studies have been carried out on disseminated mesothermal gold mineralization (see Poulsen, K.H., 1996, for a review; Issigonis, 1980), most of which is younger than Archean e.g., the gold deposits in the Appalachian orogeny (Ryan and Smith, 1998; Evans, 1996) or developed in rocks of high metamorphic grade, e.g., some of the shear zone and disseminated lode deposits described by Groves (1993). The number of studies describing copper-bearing mesothermal gold deposits is similarly small (e.g., Jiang, 2000; Gaboury and Daigneault, 1999). Indeed, in most mesothermal gold deposits, copper concentrations are expected to be below those of the host volcanic pile (Kerrich and Fryer, 1981; Groves and Foster, 1993) and predictably so because base metals, which are transported predominantly as a chloride complexes, are not mobile in the low salinity, intermediate pH fluids that transport the gold (Wood, 1987; Lydon, 1980).

In this paper, we describe a rare example of disseminated Archean mesothermal gold mineralization and coexisting low-grade copper in the Onaman-Tashota greenstone belt of the Archean Superior Province in Canada, and propose a model that explains the genesis of the Onaman showings, and similar mesothermal gold deposits elsewhere.

GEOLOGICAL SETTING

Regional geology

The Onaman property is situated near the Gzowski-Oboshkegan volcanic center of the Onaman-Tashota greenstone belt, in the Eastern Wabigoon Region of the Wabigoon Subprovince of the Superior Province, northwestern Ontario (Fig 1) (Blackburn et al., 1991). Stratigraphically, the Onaman-Tashota belt is dominated by a sequence of basal tholeiitic pillowed basalts and overlying calc-alkaline intermediate to felsic metavolcaniclastic rocks. Thin units of iron formation and clastic metasediments are intercalated in both sequences, and both locally overlie the intermediate to felsic metavolcaniclastic rocks (Amukun, 1977). Intrusive rocks include gabbro, diorite and lamprophyre, and later large batholitic complexes of granitic intrusives (Fig. 1). The Onaman property is located in an area underlain mainly by intermediate to felsic metavolcaniclastic rocks, and minor clastic sedimentary rocks (Fig. 2).

Rocks in the Onaman-Tashota greenstone belt were strongly deformed and display a foliation defined by the alignment of micas and amphiboles, and the elongation of pyroclastic fragments. Regional folding and faulting is still poorly understood due to the lack of outcrop (Amukun, 1977). Peak metamorphism postdated shearing and regional folding events (Blackburn et al. 1991), and ranged from lower greenschist to lower amphibolite facies.

Property geology

The following description is based largely on the mapping of Osmani (1999). The stratigraphic sequence on the Onaman property begins with an unknown thickness of massive to pillowed and weakly carbonatized and chloritized mafic metavolcanics of tholeiitic to calc-alkaline affinity. These rocks are overlain by intermediate to felsic metavolcaniclastic rocks, both pyroclastic and epiclastic, comprising lapilli tuff, blocky tuff, tuff breccia, finer-grained crystal and ash tuff, and fragmental rocks of unknown origin. The fragments are commonly quartz- and plagioclase-phyric, and are hosted by a matrix of fine-grained quartz, chlorite, sericite and carbonate. Generally, the composition of the matrix and fragments is similar, which makes distinction between them difficult, where the fragments are tightly packed. On the basis of their chemical composition, these rocks are interpreted to be mainly dacitic and of calc-alkaline affinity. Locally, compositions may range from andesitic to rhyodacitic.

Metasedimentary rocks occur largely as lenses of argillite, graphitic argillite, and siltstone interbedded in the intermediate to felsic metavolcaniclastics, and, to a lesser extent, intercalated in the mafic flows. A thin unit of polymictic conglomerate, siltstone, wacke and quartz arenite overlies the intermediate to felsic metavolcaniclastics. The clasts in the conglomerate are angular to rounded, and can measure up to 1m in length. Graded bedding and flame structures in metasedimentary units indicate a younging direction to the south.

Metagabbro plugs, dykes and sills of tholeiitic affinity intrude the mafic metavolcanics and the intermediate to felsic metavolcaniclastics, and larger intrusions contain xenoliths of these units. They are generally medium-grained, although fine-grained gabbros and plagioclase-phyric varieties with crystals measuring up to 7 cm in length occur locally. A single ultramafic dyke was also identified.

Three generations of felsic intrusions have been mapped on the property, although two of them and perhaps all may be related. The earliest intrusions form stocks, dykes and sills of diorite, monzonite and monzodiorite and rarely lamprophyre, are medium to coarse grained, and range in chemical affinity from calc-alkaline to mildly alkaline. They are thought to be of late Archean age as their REE profiles are similar to those of sanikutoids of that age in the Superior Province. These intrusions cut the polymictic conglomerate. This, and the occurrence of granitic clasts, suggests that their emplacement was coeval with coarse clastic sedimentation. Younger felsic intrusions occur exclusively as dykes, and comprise a set of pre-deformation (and alteration) quartz-feldspar porphyries and felsites of tonalitic composition, and a set of massive, relatively undeformed and unaltered porphyries and aphyric dykes of granodiritic composition. Both generations of porphyries are of calc-alkaline affinity, but felsite dykes are weakly alkaline.

The youngest intrusions on the property are Proterozoic diabase dykes, which are generally massive and magnetic, and range in thickness from <1 m up to 60 m. Two varieties are discernable, one being fine-grained to aphanitic and N- to NE- trending, and the other being plagioclase-phyric and NW-trending. No crosscutting relationships were observed between these two classes of diabase dyke.

Structural geology

Two regional deformation events affected the rocks at Onaman. The first of these, D_1, produced a major E-NE-trending antiform. However, other evidence of this deformation is not preserved except in the closures of D_2 folds where D_1 fabrics, e.g., a crenulated foliation, were recognized. The dominant foliation was produced by D_2 and is evident as a well-developed schistosity striking west to west-southwest, and dipping steeply to the north. The foliation is generally parallel to bedding and layering in the metavolcaniclastics, and is discordant only in the cores of rare mesoscopic NW-plunging isoclinal folds and the E-NE trending antiform referred to above. This structure was refolded during D_2 to produce a large south-verging overturned NE-trending syncline, as indicated by minor Z-folds and bedding-cleavage relationships (Thomas, 1998).

Faults, observed in the field, and inferred from narrow (0.1 to 3m) brecciation zones in drill core logs, regional lineaments and geophysical data, are common on the property, and follow two major trends, NW and NE. They locally offset lithological contacts and display limited clast flattening.

Brittle-ductile shear zones are also common, and are distinguished from the faults by their strong penetrative foliation and clast flattening, and locally, narrow bands of mylonitic shearing. The absence of kinematic indicators suggests non-rotational strain or pure shear flattening. The shear zones are typically 15 to 20 m wide, and reflect a dominantly ductile deformation regime, in which brittle responses are restricted to narrow (< 20 cm)

NW-trending fractures (Reidel shears, or extensional crenulation cleavages) hosting deformed microveinlets.

The most important shear zone from the perspective of mineralization is the Ryne Deformation Zone (RDZ), which trends 278°/70°N and is discussed in the section on mineralized showings. Two other important shear zones, because of their spatial relation to mineralization, occur between the Green Jimmy and MVP gold showings, and between the Big Bear and Hourglass showings, and trend NW (Fig. 2). These shear zones were identified in outcrop (flattened fragments, strong foliation, hydrothermal alteration) and from magnetic and induced polarization surveys.

Metamorphism

Regional metamorphic grade reached lower to mid-greenschist facies as indicated by the occurrence of mineral assemblages in the metavolcaniclastic rocks containing chlorite, sericite, albite and calcite, and biotite in mafic intrusives. Talc was observed in an ultramafic dyke. Adjacent to granitoid stocks in the Knucklethumb Lake area, the metavolcaniclastic rocks also underwent thermal metamorphism to hornblende hornfels facies and contain fine-grained red-brown garnets.

MINERALIZED SHOWINGS

Although ten gold occurrences have been discovered on the Onaman property, our research focused almost exclusively on the Ryne and Hourglass showings, which are the

two largest and best mineralized of these occurrences. They also represent the two main styles of mineralization, namely disseminated gold in a shear zone, and gold hosted by felsite dykes, respectively. Finally, they are the two most intensely explored occurrences, and those for which most information is therefore available.

Ryne showing

The Ryne showing consists of a trench measuring 170 by 35 m, located in the southwest part of the property (Fig. 2), and is mainly underlain by W-NW striking intermediate to felsic volcaniclastic rocks and polymictic conglomerate (Fig. 3). Intrusive rocks are also common, and take the form of large dykes of gabbro, common quartz-feldspar porphyry, aphyric felsite dykes, and late lamprophyre. Rare Proterozoic diabase dykes are also observed. However, the dominant feature of the Ryne showing is a 15- to 25 m-wide shear zone that trends W-NW for 250 m (in outcrop) before being truncated by NE-trending faults. Based on magnetic and drill hole data, the Ryne deformation zone or RDZ extends 1.5 km west of the Ryne showing (Osmani, 1999). The RDZ is manifested by clast flattening in the metavolcaniclastic and sedimentary rocks, by a strongly developed schistosity, and intense hydrothermal alteration. It hosts all the gold mineralization, and is locally concordant with the metavolcaniclastics-conglomerate contact.

Gold mineralization is mainly disseminated and broadly associated with pyritization and carbonatization (ankerite), which give the rocks a rusty color. Gold also occurs in quartz-tourmaline ± ankerite microveinlets, and rare quartz-tourmaline veins (<1 cm thick).

Grades are erratic, but numerous samples yielded assays >5 g/t over 3.5 meters, and a grab sample from a zone of visible gold yielded over 2000 g/t Au.

Hourglass showing

The Hourglass showing consists of a stripped area measuring 45 by 25 m underlain by intermediate to felsic metavolcaniclastics similar to those at the Ryne showing, and intruded by two generations of felsic dykes (Fig. 4); an early, locally porphyritic variety, and later aphyric felsite. Both types are folded and therefore predated D_2 deformation. Early felsic dykes, including porphyries, generally trend N-S, have a variable apparent thickness reaching up to 2 m, are deformed, display light hydrothermal alteration, and are composed mainly of a mixture of plagioclase, quartz and amphibole. The later felsite dykes are more common, are generally oriented sub-parallel to the main foliation (WNW), are heavily altered, boudinaged, and their apparent thickness is generally <0.5 m. They are composed mainly of quartz and albite, with minor ankerite and sericite.

Gold in the Hourglass showing is hosted almost exclusively by the later aphyric felsite dykes, and is generally higher grade than at the Ryne showing; the best assay result yielded 169.9 g/t over 0.5 m. The host rocks are unmineralized, except adjacent to felsite dykes (within 2m of their contacts) where grades reach up to 2 g/t.

The Ryne and Hourglass showings are only 700 m apart, but their stratigraphic relationship is unclear because of faulting in the area. However, the Hourglass showing is on strike with the Big Bear showing and the two may be joined by a fault/shear

(photolineament). Although there is no sign of intense shearing at Hourglass and the metavolcaniclastics are only moderately foliated, the Big Bear showing locally displays a strongly developed foliation. The Ryne showing is located south of this tie line, but NE-SW and N-S faults are found west and east of the showing, respectively, and could have displaced the Ryne "block" southward.

Alteration petrography

Metavolcaniclastic rocks immediately outside the two mineralized showings (Ryne and Hourglass) are composed of a fine-grained matrix of quartz and albite, and scattered quartz and plagioclase phenocrysts, which are present in both the matrix and fragments. They are altered pervasively by calcite, which replaced plagioclase and filled interstices in quartz eyes. Calcite was overprinted by sericite, and sericite microveinlets cut across zones of calcite. Sericite also replaced plagioclase crystals partially, or completely where they escaped prior alteration by calcite; pseudomorphs composed of sericite and calcite are common. Chlorite is an important constituent of the metavolcaniclastic rocks, and, together with sericite, makes up to 15 to 50 % of the modal mineralogy. The proportions of sericite and chlorite vary from 5 to 50 and 10 to 30 modal %, respectively, according to the host lithology, creating chlorite-green zones and sericite-white zones in intermediate metavolcaniclastics and felsic metavolcaniclastics, respectively. Zones of pervasive chlorite cut sericite zones where both minerals are present, although the distribution of chlorite is also lithologically controlled. Minor proportions of ilmenite and rutile are common. Rutile typically replaced ilmenite, forming skeletal crystals of the latter. Late-stage calcite veinlets were observed.

Mineralized metavolcaniclastic rocks have been replaced almost totally by secondary minerals. The only relicts of primary mineralogy are common quartz eyes in porphyritic fragments, and less commonly, the outlines of carbonatized and sericitized plagioclase phenocrysts. Early alteration is represented by fine-grained quartz (30 to 70 % of the modal mineralogy) and subordinate albite in the matrix, and albitization of plagioclase phenocrysts. This alteration was overprinted by pervasive carbonate alteration, which is the main alteration stage at the Ryne showing, generally representing between 15 and 35 % of the modal mineralogy. The most common carbonate mineral is ankerite, which replaced both the groundmass and plagioclase phenocrysts (Fig. 5b); the latter are preserved as pseudomorphs composed of carbonate and sericite (Fig. 5d). Ankerite fills embayments in quartz (Fig. 5e), and therefore also post-dated this mineral. Similar textural relationships are observed with albite. Ankerite, however, pre-dated sericite, as shown by the occurrence of sericite crystals cutting across pervasive ankerite zones and large ankerite crystals (Fig. 5f). Dolomite is restricted to a zone of high-grade mineralization, and occurs in veinlets that also contain ankerite and calcite in minor proportions (Fig. 5c). The dolomite fills spaces around ankerite rhombs, and was therefore introduced later than ankerite. Tourmaline occurs locally in the groundmass and in some veinlets, and pre-dates sericite (Fig. 5a), but its limited occurrence precluded interpretation of textural relationships with early alteration minerals. Sericite is locally present as a pervasive alteration product (it generally comprises <10 modal % but locally up to ~25 modal % of the rock), in which crystals are either parallel to the main foliation or to veinlets. Chlorite and biotite developed late, replacing sericite. Where both minerals are present, textural evidence shows that chlorite was replaced by biotite.

Up to three generations of veinlet are present (including late-stage calcite-only veinlets). The first generation veinlets contain ankerite accompanied by variable proportions of quartz and albite. These veinlets are variably oriented and commonly cut each other. The second generation comprises veinlets consisting only of sericite. These veinlets cut across ankerite patches, and insinuate between crystals in ankerite-quartz-albite veinlets. Late-stage calcite-only veinlets cut across all other mineral fabrics, and are not considered to have played an important role in the gold mineralizing event.

Intermediate to felsic metavolcaniclastic rocks are hydrothermally altered throughout the Hourglass showing, and display evidence of an alteration sequence similar to that of the Ryne showing. Early albitization and silicification were overprinted by extensive carbonatization, followed by pervasive sericitization of the groundmass and late chloritization. Felsite dykes of the Hourglass showing also display a similar alteration paragenesis (Fig. 6), despite their higher silica content. Relicts of plagioclase phenocrysts are preserved as pseudomorphs composed of quartz and albite, and early alteration of the groundmass is represented by a mixture of the same minerals (up to 75% modal quartz). Quartz-albite veinlets cut the groundmass, and were followed by a set of quartz-albite-pyrite ± Au veinlets. Pervasive ankerite alteration was contemporaneous with or later than the formation of these latter veinlets. Strongly deformed dykes are commonly the most altered and may contain up to 30 modal % ankerite. By contrast, less deformed massive felsite dykes show little carbonate alteration, even where highly mineralized. Chlorite was found in trace amounts in only one sample of felsite dyke, and biotite is totally absent.

Mineralization and ore mineralogy

Pyrite is generally the main sulfide phase in mineralized rocks at both the Ryne and Hourglass showings, comprising between 2 and 10% and less than 5% of the modal mineralogy, respectively. Two generations of pyrite were identified based on textural relationships. Early pyrite was the first sulfide mineral deposited, and is generally anhedral, but locally may exhibit a euhedral habit. The second generation occurs as irregular overgrowths of globular shape on the early pyrite grains. Both types of pyrite are common, though generally one generation predominates in any given sample. Early pyrite frequently shows evidence of having been fractured, suggesting pre-deformation precipitation of older pyrite.

In addition to pyrite, pyrrhotite, arsenopyrite and chalcopyrite are commonly present at both showings, although in minor proportions (locally, pyrrhotite is the principal sulfide at the Ryne showing), while molybdenite occurs sparsely, and only at the Ryne showing. Arsenopyrite replaced pyrite along fractures, filled embayments (Fig. 7f), and formed inclusions in pyrite interpreted to be located along annealed grain boundaries between crystals. At the Ryne showing, arsenopyrite also occurs as disseminated euhedral crystals, as globular overgrowths on arsenopyrite or pyrite euhedra, and in the cores of tourmaline crystals.

Pyrrhotite is either disseminated in the groundmass or formed by replacing pyrite (Fig 7a), as is evident from its occurrence as a rim on pyrite crystals or as inclusions in

aggregates of annealed pyrite grains (the inclusions are located along grain boundaries). Pyrrhotite also postdated arsenopyrite, filling embayments and fractures in crystals of this mmineral (Fig. 7b).

Chalcopyrite is a minor mineral that occurs primarily as disseminations in the groundmass. Commonly, however, it fills fractures in pyrite or occurs along boundaries between pyrite grains (Fig. 7d), and as strings of inclusions interpreted to represent replacement of pyrite by chalcopyrite along boundaries of annealed grains. In many cases, curvilinear fracture-like features passing through pyrrhotite or chalcopyrite "inclusions" in pyrite confirm the interpretation of replacement along grain boundaries.

The only gold-bearing minerals identified are native gold and electrum. Gold grains commonly exhibit a close spatial relationship with pyrite, occurring at the margins of pyrite grains (Fig. 7e), and as inclusions-like replacements along annealed boundaries within composite pyrite crystals. Native gold grains at Ryne occur in quartz-tourmaline-ankerite veinlets (Fig. 7c), but are also disseminated in the host rocks. At the Hourglass showing, the gold is disseminated mainly in the silicified felsite dykes.

In many cases, the native gold is more closely associated with chalcopyrite than with pyrite, commonly occuring as inclusions in chalcopyrite that has replaced pyrite (Fig. 7d). Where chalcopyrite is included in pyrite, the chalcopyrite may contain an inclusion of native gold, suggesting possible co-precipitation of the two minerals. As discussed above, these inclusions are interpreted to represent replacement along annealed boundaries. Native gold and electrum were also observed in contact with sericite,

ankerite, pyrrhotite and arsenopyrite. These textural relationships suggest that gold precipitated after the first generation of pyrite, and penecontemporaneously with chalcopyrite, pyrrhotite, arsenopyrite (Fig. 8), and ankerite. Mineralization occured after silicification and albitization, but contemporaneously with carbonatization (Fig. 6).

MASS CHANGES DURING ALTERATION

Mass changes during alteration and mineralization were estimated using an immobile element technique (MacLean and Kranidiotis, 1987; Barrett and MacLean, 1994). Aluminum, titanium, zirconium and yttrium were interpreted to be immobile from their co-linearity on isocon diagrams (Grant, 1986) (Fig 9). However, Zr fractionates early in calc-alkaline rocks, preventing its use in monitoring mass changes during their alteration, and Y was only analyzed in a small proportion of samples. Aluminum and titanium were selected to monitor the extent of alteration, and provide information on igneous fractionation. The alteration study was limited to metavolcaniclastic rocks that could be identified as lapilli tuffs and felsite dykes. Other volcaniclastic rocks were not included in the study due to their geochemical heterogeneity. For the same reasons, mass change calculations were not conducted on the conglomerate present at the Ryne showing. Bulk-rock geochemical analyses were performed by Actlabs Inc., and additional bulk-rock geochemical data were compiled from company reports (the analyses were performed by Chemex Labs Inc.).

The lack of fresh rock in the Onaman area makes the calibration of igneous fractionation trends difficult, as alteration concentrates or dilutes immobile elements, thus displacing

data on a binary immobile element diagram away from or towards the origin, respectively. In order to overcome this problem, Archean calc-alkaline suites from the literature (Gélinas et al., 1977; Goodwin, 1977; Hallberg et al., 1976; Ujike and Goodwin, 1987; Stott, personal communication, 2000) were compared to Onaman rocks on Al_2O_3-TiO_2 diagrams, and used to establish the magmatic evolution (Fig. 10). Representative geochemical analyses of metavolcaniclastic rocks from the Ryne and Hourglass showings, and felsite dykes of the Hourglass are given in Table 1.

The results of mass change calculations (Table 2) show that lapilli tuffs from Ryne lost from 5 to 20 % of their original Si (% of original wt.% value), but that felsite dykes at Hourglass gained from 5 to 50 % Si. Both lithologies generally gained Na, at least locally (Ryne), a feature manifested by albitization and albite veining. Felsite dykes at Hourglass gained an average of 46 % of their original sodium, whereas lapilli tuffs from the Ryne showing locally lost up to 82 % Na, but elsewhere gained up to 50 % Na. The sodium gains for both lithologies correlate positively with gold grades (Fig. 11), and suggest that albitization of lapilli tuffs and felsite dykes promoted gold deposition. Iron and Mg underwent variable mass losses and gains, but behaved coherently i.e., where Fe was lost, Mg was also lost, and vice-versa (Fig. 12a). Both volcaniclastic rocks and felsite dykes underwent severe potassium mass losses averaging –25 (omitting outliers) and –1040 %, respectively, and 10 to 65 % calcium was added to both rock types, as a result of carbonatization (Fig. 12b).

Correlation coefficients were determined for ~30 trace elements. Significant weak positive correlations for gold at Ryne were established with Cu (0.51, n=38), W (0.30,

n=32), Hg (0.63, n=9), Te (0.37, n=11), S (0.35, n=21) and Sb (0.41, n=13). Base metals other than copper do not correlate with gold, and silver concentrations are generally below the detection limit (< 1 ppm). As shown on Fig. 13, Cu concentrations above 50 ppm, W concentrations above 10 ppm, and Sb concentrations above 1ppm correspond to gold grades above 0.1 g/t. Tellurium values above the detection limit (> 0.1 ppm) generally occur in samples with gold grades greater than 1 g/t. Sulfur concentration increases steadily with gold grade. Between 0 and 2.0 wt.% total sulfur, the gold concentration increases from 0.005 to 10 g/t. In contrast to the Ryne showing, only Hg correlates positively with gold grade in the Hourglass felsites. The concentrations of S, Sb, Cu, W and Te are consistently low, even in the best mineralized samples, and are comparable to background values at the Ryne showing.

MINERAL CHEMISTRY

Hydrothermal minerals were analyzed using a JEOL 8900 electron microprobe with a focused beam and an acceleration voltage of 20 kV for sulfides and gold, a 5 μm diameter beam and an acceleration voltage of 15 kV for micas and feldspars, and a 10 μm diameter beam and an acceleration voltage of 15 kV for carbonate minerals.

Alteration minerals

The alteration minerals analyzed were carbonates, plagioclase, sericite, chlorite and biotite. Ankerite is the most voluminous carbonate in both the Ryne and Hourglass showings, and ranges in composition from $Ca_{1.00}Mg_{0.46}Fe_{0.54}(CO_3)_2$ to

$Ca_{1.00}Mg_{0.67}Fe_{0.33}(CO_3)_2$. In a single polished thin section (PTS), the concentration of MgO can vary by as much as 5 wt.% and FeO by as much as 8 wt.%. At the Hourglass showing, ankerite is also the dominant carbonate mineral, and MgO and FeO concentrations also vary by up to 5 and 6 wt.%, respectively, in a single PTS. There is a weak positive correlation between gold grade and Mg concentration in the carbonate (Fig. 14), and, moreover, the highest gold grades are associated with the occurrence of dolomite.

Despite several different textural and mineralogical associations, all plagioclase feldspar is nearly pure albite (Ab_{97}). Regionally, albite is likely a product of metamorphism (i.e., the original plagioclase yielded albite and calcite), as well as constituting a significant local alteration mineral associated with mineralization. Other minerals analyzed include sericite, which is phengitic muscovite with up to 4.9 wt.% FeO, 2.2 wt.% MgO, and 0.8 wt.% Na_2O, biotite, which is intermediate in composition between annite and eastonite, and iron-rich chlorite.

Gold and sulfide minerals

Pyrite, arsenopyrite and pyrrhotite were analyzed for Fe, As, Co, Cu, Ni, Zn and S. Arsenopyrite was also analyzed for Mn. Chalcopyrite was analyzed for Cu, Fe, As, Ni and S, and sphalerite was analyzed for Zn, Fe, Ni, Mn and S. Native gold and electrum were analysed for Au, Ag, Hg and Cu.

Pyrite compositions at Ryne and Hourglass are similar, with As, Co, and Ni being the only significant impurities. Arsenic concentrations range from <0.03 (detection limit) to 2.77 wt.% (avg = 0.25 wt.%), Co from 0.01 (detection limit) to 1.83 wt.% (avg = 0.05 wt.%), and Ni from 0.01 (detection limit) to 0.53 wt.% (avg = 0.04 wt.%). The highest concentrations of arsenic occur in the cores of crystals. However, this is not true for cobalt or nickel, which, although zonally distributed, may be concentrated towards the cores or rims of grains. Furthermore, not only do Co and Ni not correlate with As, they do not correlate with each other. The As content of early pyrite is generally higher than that of the overgrowths and ranges from 0.05 to 1.63 wt.%, while that of the overgrowths, ranges from 0.04 to 0.85 wt.%.

The average composition of arsenopyrite is $Fe_{0.94}As_{0.89}S$, the only impurities being Co and Ni, which were detected in trace concentrations at both showings. Chalcopyrite generally contains only traces of As and Ni (<0.08 wt.%) and no detectable cobalt. Sphalerite from the Ryne showing has an average iron content of 7.58 wt.% ($Zn_{0.9}Fe_{0.13}S$); concentrations of the other metals analyzed (Ni and Mn) were below the detection limit. No sphalerite was found at Hourglass.

Native gold and electrum grains form three population groupings or clusters based on their Ag content (5 to 12 wt.%, 16 to 21 wt.%, and 23 and 28 wt.%) for both the Ryne and Hourglass showings (Fig. 15). Moreover, 6 out of 17 gold-bearing samples contain grains with compositions that fall into more than one cluster. However, these three compositional classes of native gold/electrum are indistinguishable from their mode of

occurrence. Nevertheless, it may be worth noting that macroscopically visible native gold at the Ryne showing contains <7 wt.% Ag. Copper and mercury concentrations were below the detection limit (0.08 and 0.3 wt.%, respectively).

STABLE ISOTOPES

Oxygen and carbon

Ankerite in mineralized metavolcanics from the Ryne showing and from mineralized felsite dykes from the Hourglass showing was sampled with a low-speed rotary drill for carbon and oxygen isotopic analyses, performed at GEOTOP. Isotopic ratios for oxygen and carbon, expressed as $\delta^{18}O$ (SMOW) and $\delta^{13}C$ (PDB), have a precision of ±0.2 ‰ and range between 23.5 and 25.1 ‰, and –1.6 and –2.6 ‰, respectively (Table 3). The $\delta^{18}O$ composition of the fluid was calculated from the equation of Golyshev et al. (1981) for dolomite-H_2O at temperatures of 300 and 400°C. Values of 1000 ln α for dolomite-H_2O are similar to those for calcite-H_2O, and can therefore also be assumed to be similar to those of ankerite-H_2O. Calculated $\delta^{18}O$ values for the fluid at Onaman ranges between 18.2 and 19.6 ‰, and between 20.9 and 22.4 ‰ at 300 and 400°C, respectively. On a δD-$\delta^{18}O$ diagram (Fig. 16a), the isotopic composition of fluids from Onaman cluster in the box for metamorphic fluids, at much higher $\delta^{18}O$ values than those of typical Archean lode gold deposits and Cretaceous deposits of the Alleghany district from California (Ridley and Diamond, 2000; Böhlke and Kistler, 1986).

The $\delta^{13}C$ ratio of the fluid was calculated using the dolomite-CO_2 fractionation equation of Ohmoto and Rye (1979) for 300 and 400°C, and ranges between –1.3 and –0.3 ‰, and –0.5 and +0.5 ‰ for 300° and 400°C, respectively. Carbon isotope ratios cannot evaluate the source of carbon with certainty, but the heavier $\delta^{13}C$ ratios for ankerite at Onaman could be compatible with a mantle origin (~ -5 ‰) fractionated to heavier ratios during metamorphism (Kerrich, 1987). These ratios are similar to those of many deposits in the Superior Province (Fig. 16b), including Hollinger-McIntyre and Dome in the Timmins area (Kerrich, 1990).

Sulfur

Pyrite grains from crushed samples of the Ryne and Hourglass showings were picked manually under a binocular microscope. The $\delta^{34}S$ values for pyrite at the Ryne showing range between +2.0 and +3.3 ‰, and between +4.6 and +6.4 ‰ in felsite dykes of the Hourglass showing (± 1 ‰, CDT) (Table 4). Gold grades correlate positively with heavier sulfur isotopic ratios at the Ryne showing (correlation coefficient of 0.57, n=7), and at the Hourglass showing, where the analysed samples all have gold high gold grades, $\delta^{34}S$ values are consistently high (Fig. 17). A similar correlation has been reported for the Red Lake area where non-auriferous samples yielded lower sulfur isotopic ratios than auriferous samples (El Bilali and Hattori, 1998).

DISCUSSION

Pressure-temperature conditions

Based on mineral assemblages, the mineralization at Onaman falls between two classes of lode gold deposits recognized by Hagemann and Cassidy (2000), in the Yilgarn Craton, Australia. The absence of amphiboles, K-feldspar and Ca-plagioclase restricts temperature-pressure conditions to be below those of the mesozonal class (375-550°C, 2-3 kbar). On the other hand, pyrrhotite and chalcopyrite are typical of mesozonal deposits. Titanium minerals at Onaman include both rutile and ilmenite, which occur in epizonal and mesozonal deposits, respectively. Most structures hosting Archean lode gold mineralization are of a brittle-ductile nature, in rocks of middle- to upper-greenschist metamorphic facies, e.g., Timmins, Golden Mile (Groves and Foster, 1993), and typical pressure and temperature estimates for these deposits vary between 200 and 400°C and 0.5 and 2 kbar, respectively (Mueller and Groves, 1991; Groves et al., 1989; Kishida and Kerrich, 1987; Robert and Kelly, 1987; Smith et al., 1984). As most alteration minerals at Onaman belong to the shallower of the two classes of gold deposits, and two important ore-stage sulfides (pyrrhotite and chalcopyrite) are typical of the mesozonal class, we tentatively infer that the P-T conditions were 2 kbar and 400°C.

Fluid evolution

The principal physicochemical controls on gold deposition and hydrothermal alteration in lode gold deposits are generally thought to be temperature and/or pH and/or oxygen fugacity and/or the activity of reduced sulfur. In this section, we evaluate the evolution of

these parameters at Onaman from mineral stability relationships, sulfur isotopic variations and metal (Au, Cu) solubility data. In so doing we assume that, as hydrothermal mineral assemblages are the same at both Ryne and Hourglass, physicochemical conditions were similar at the two showings.

Phase diagrams were constructed using SUPCRT92 (Johnson et al., 1992) and the revised 1998 SUPCRT database (Shock, 1998), which incorporates recent experimental data for gold bisulfide complexes from Benning and Seward (1996) and gold chloride complexes from Gammons and Williams-Jones (1995). In figure 18, we show the stability fields of minerals in the Fe-O-S system and selected ore and alteration minerals, and the solubility contours of gold and copper as a function of log fO_2 and pH. The concentrations of components such as Na, K, Ca, and Mg were estimated from published analyses. The sodium and chloride ion concentrations were assumed to be 1 m (~6 wt.% NaCl equivalent), which is in the range of the salinity of mesothermal gold ore as estimated from microthermometric measurements of fluid inclusions (Groves and Foster, 1993). The potassium concentration was assumed to be 0.02 m, which corresponds to a Na/K ratio of 50, and is similar to that determined at the Sigma mine (Robert and Kelly, 1987), and in the mesothermal veins of the Bechaz gold mine in the Italian Alps (Diamond et al., 1991). The concentration of Ca was fixed at 0.003 m based on calcite saturation at 400°C and $X_{CO2} \sim 0.1$ (Mikucki and Ridley, 1993). Magnesium concentration was estimated to be 0.0003, one order of magnitude lower than Ca (Diamond et al., 1991; Robert and Kelly, 1987). Carbon concentration was assumed to be 0.1 m, or 10 mole %, which is similar to values from solid probe mass spectrometric analyses of fluid inclusions (Guha

et al., 1991), and corresponds to the value assumed for many lode gold deposits (Perring et al., 1987).

The replacement of pyrite by pyrrhotite constrains the log fO_2 of the ore fluid to a value <-27.5, which is consistent with the occurrence of chalcopyrite; the latter mineral is stable at log fO_2 between –24.3 and –31.3 at the same value of ΣaS. The presence of ankerite ($a$dolomite = 0.6), puts the lower pH boundary at 5.1, whereas the occurrence of pure dolomite limits it locally to a pH above 5.2. A slightly lower pH limit is provided by the occurrence of albite, which replaces paragonite at a pH of 4.7. On the other hand, the absence of K-feldspar and syn- to late-mineralization development of phengitic muscovite suggests that pH did not exceed 6.3 (Fig. 18).

Figure 19 shows the field of stability of ore minerals at minerals at Onaman in terms of log aH_2S and log fO_2 at a pH of 5.5. At log fO_2 values constrained by the replacement of pyrite by pyrrhotite and chalcopyrite (-27.5 to –31.3), log aH_2S will have a value between –1.3 and 0.6.

In addition to broadly constraining fO_2, pH and aH_2S, the phase relationships discussed above also provide some indication of the evolution in these parameters. The replacement of pyrite by pyrrhotite indicates that the fluid evolved to lower fO_2 and aH_2S, while the replacement of plagioclase by sericite suggests that pH decreased (albeit syn- to late-mineralization), since it reflects an environment of lower pH than albitization. This

evolution of the fluid to lower pH is most evident, however, in the intense carbonatization (CO_2 metasomatism) which produced hydrogen ions via the reaction:

$$Fe^{2+}, Mg^{2+} + Ca^{2+} + 2\,CO_2 + 2\,H_2O = Ca(Fe,Mg)(CO_3)_2 + 4\,H^+$$

Further indication of the direction of change in these parameters is provided by the sulfur isotopic data, which correlate positively with gold concentration, i.e., evolved to heavier values. On figure 20, contours of $\delta^{34}S_{pyrite}$ are shown as a function of log fO_2 and pH, from which it can be seen that an evolution towards heavier ratios corresponds to an increase of pH, or a decrease in oxygen fugacity at low or high initial log fO_2, respectively (Ohmoto, 1972). Given the evidence presented above that fO_2 likely decreased with time from conditions of pyrite stability to those of pyrrhotite stability, and that pH also decreased (albite to sericite; carbonatization), the evolution of $\delta^{34}S$ seems best explained by a reduction in fO_2. From the range in $\delta^{34}S$ and the inferred log fO_2 of <-27 during mineralization, the initial value of log fO_2 is interpreted to have been between -25.0 and -25.8.

In summary, the physico-chemical changes of the fluid during mineralization were a drop in aH_2S of nearly 2 log units (from 0.9 to -1.3) and a drop in fO_2 of more than 2.5 log units (from ~-25 to between -27.5 and -31.3), and an unevaluated but significant decrease in pH in the interval 6.3 to 5.1. Whether or not there was an accompanying decrease in temperature is not known.

Physico-chemical controls of mineralization

Experimental studies have shown that gold is present in ore fluids mainly as bisulfide and/or chloride complexes, with the latter predominanting at high temperature and low pH. At the estimated physico-chemical conditions prevailing at Onaman, gold is dissolved dominantly as a bisulfide complex, as shown by the gold solubility contours on figure 18.

Gold precipitation at Onaman may have been triggered by changes in one or more of three physico-chemical parameters. The estimated drop in fO_2 of >2.5 log units would have reduced gold solubility by approximately 0.5 log units, and, if combined with a decrease in pH of 0.5 log units, would have reduced its solubility by 1 log unit (Fig. 18). However, the estimated drop in aH_2S of nearly 2 log units would have reduced gold solubility by no less than five orders of magnitude (Fig. 19). On the other hand, a decrease in temperature would not have promoted gold deposition, as gold shows retrograde solubility at temperatures in the range of those estimated for the Onaman deposit (Fleet and Knipe, 2000). Based on the above, we conclude that the gold deposited largely in response to the reduction in aH_2S, but that the reductions in fO_2 and pH may also have contributed to gold deposition.

As is the case for gold. experimental studies have shown that copper dissolves predominantly as bisulfide and chloride complexes in hydrothermal fluids (Mountain and Seward, 1999; Xiao et al., 1998). In figure 18, we show solubility contours for chalcopyrite, with the copper dissolved as $Cu(HS)_2^-$ and $Cu(Cl)_2^-$, and as is evident from

this figure, $Cu(HS)_2^-$ predominates at the physico-chemical conditions estimated for the Onaman showings. It was assumed that either pyrite or pyrrhotite provided the iron needed to produce chalcopyrite. An important feature of this diagram is that the solubility of copper as chalcopyrite reaches a minimum (<10 ppm) on the pyrite-pyrrhotite join at a pH of 4, and then increases to a value of >10 000 ppm (1 wt.%) at the H_2S-HS^- predominance boundary. At the conditions of fO_2 and pH initially prevailing at Onaman, the solubility would have been about 1000 ppm, and, if the ore fluid was at or near saturation with chalcopyrite, decreases in pH, fO_2 or H_2S would have induced deposition of this mineral. From the distribution of solubility contours, it can be seen that the interpreted decrease in pH would have reduced chalcopyrite solubility by 1 log unit per pH unit (Fig. 18). However, although the accompanying decrease in fO_2 would have further reduced chalcopyrite solubility while pyrite was stable, this effect would have reversed as conditions evolved to those where pyrrhotite is stable, i.e., chalcopyrite solubility would actually have increased (Fig. 18). By contrast, the estimated decrease of aH_2S by 2 log units would have reduced chalcopyrite solubility by nearly 2 log units. We therefore conclude that, as for gold, the decrease in aH_2S was the principal control of chalcopyrite deposition.

Geological mechanisms

Mineralization at Onaman proceeded in two main stages, namely a first stage of pyritization, and a second stage in which pyrrhotite replaced pyrite and native gold co-precipitated with chalcopyrite. Pyritization, which accompanied carbonatization, involved replacement of iron-bearing minerals in the host rock by sulfur introduced from

the fluid, as shown by the additions of sulfur to the rocks and the comparatively minor changes in iron. The effect of this pyritization on the fluid was the sharp drop in aH_2S reported above, and a decrease in fO_2 due to the oxidation of the primary minerals. These changes produced the conditions necessary for the second stage of mineralization, namely the replacement of pyrite by pyrrhotite, and the deposition of gold and chalcopyrite. The reductions in aH_2S and fO_2 stabilized pyrrhotite in favor of pyrite and the reduction in aH_2S destabilized $Au(HS)_2^-$ and $Cu(HS)_2^-$, causing deposition of native gold and chalcopyrite. The strong positive correlation between Au and S (Fig. 13), which applies equally to lapilli tuffs, fragmental volcanic rocks, and mafic and felsic intrusives, and the general absence of pyrite in unmineralized rocks, confirms the hypothesis that pyritization was the principal control of gold mineralization at Onaman. Volumetrically, the most important effect of fluid-rock interaction was the conversion of calcium and ferro-magnesian silicate minerals to ankerite. However, the resultant decrease in the pH of the fluid probably played a relatively minor role in promoting gold mineralization.

An interesting feature of the gold mineralization, as noted earlier, is that Au/Ag ratios in native gold/electrum define three broad compositional groupings, more than one of which is represented in the same thin section. According to Gammons and Williams-Jones (1995), such variations can be caused by fluctuations in temperature, aS_2, fO_2, Cl^- concentration, pH, and total Au/Ag of the system. A variation in fO_2 of 3 log units, or in aH_2S of 0.4 log units, or a combination of the two (initial Au/Ag_{system} ratio ranging from 3 to 10), which is similar to and less than the estimated changes in these parameters, respectively, would produce the observed variations in native gold/electrum composition. In both the predominance fields of pyrite and pyrrhotite, pH has no effect on native

gold/electrum composition (Gammons and Williams-Jones, 1995). Athough we cannot know the cause of these fluctuations, one explanation is that seismic pumping (Sibson, 1975) produced extreme variation of fluid flux and that this lead to periods of fluid- and rock-buffering of the fluid composition during which fO_2 and aH_2S were alternatively high and low, respectively.

Genetic model

The proposed geological model for the emplacement of the gold mineralization at Onaman involves the formation of a regional shear zone during Archean accretion in a pile of volcaniclastic rocks. The deformation weakened the pile, producing dilation zones that allowed intrusion of felsic dykes, and the development of shear zones such as that at the Ryne showing. Fluids carrying gold and other metals, notably copper, in solution rose along these pathways. Based on their oxygen isotopic composition and relatively high content of CO_2, the fluids are interpreted to have been of metamorphic origin. These fluids produced albitization and intense carbonatization and pyritization, which had the effect of lowering fO_2, pH and particularly aH_2S in the fluid. As a result, pyrite was replaced by pyrrhotite, and gold and chalcopyrite saturated in the solution. Gold was disseminated, and concentrated in small discontinuous veinlets at the Ryne showing, where brittle-ductile conditions precluded the development and maintenance of large open structures. At the Hourglass showing, the fluids were focussed along the same zones of dilatation into which the dykes were intruded, and likely deposited gold in small microfractures produced by contraction of the dykes during cooling.

Significance of chalcopyrite

One of the important characteristics of mesothermal gold deposits is that they are almost invariably depleted in base metals like copper relative to their host rocks (Kerrich and Fryer, 1981; Groves and Foster, 1993). The conventional explanation for this is that the physico-chemical conditions under which gold is mobilized (near neutral pH, intermediate fO_2) are not favorable for base metal transport because the latter dissolve predominantly as chloride complexes, which require low pH and high fO_2 (Lydon, 1980; Wood, 1987). We propose, however, that a far more plausible explanation, which is supported by the results of this study, is that copper is simply too soluble (as a bisulfide complex) to even saturate in the fluid, and is consequently flushed through the system. Not only does this explain the common lack of copper in mesothermal gold deposits, but it also explains the widely reported depletion of this metal from the host rocks. In those rare cases where copper concentrates, such as at Onaman, it does so because initial pH was low, and the ores formed under conditions in which the hydrothermal system was rock-buffered because of low fluid-rock ratios.

CONCLUSION

1. The Onaman property displays two styles of potentially economic gold mineralization, one in which the gold is disseminated in a shear zone hosted by intermediate to felsic metavolcaniclastics, and the other in which the gold is concentrated in felsite dykes intruding metavolcaniclastic rocks.
2. Processes active during wallrock alteration and mineralization at the Onaman property were the same at the two gold showings, suggesting a single gold event in which

wallrock alteration began with early silicification and albitization, followed by carbonatization, pyritization and late sericitization and chloritization.

3. Mineralization was penecontemporaneous with carbonatization, and occurred in two stages, namely the early replacement of iron minerals in the wallrock by pyrite, and the later replacement of pyrite by arsenopyrite, pyrrhotite, and spatially associated gold and chalcopyrite.
4. Oxygen isotopic ratios of ankerite suggest a metamorphic origin, and carbon isotopic ratios are similar to those of large deposits of the Superior Province for which a mantle origin has been proposed. Sulfur isotopic ratios correlate positively with gold grades, and reflect an evolution to lower fO_2-pH conditions.
5. Pyritization of the host rock was the major control on gold and chalcopyrite deposition, reducing sulfur activity, and destabilizing the bisulfide complexes for both Au and Cu. The sulfidation of the wallrock also reduced fO_2, which favored gold deposition, but only decreased chalcopyrite solubility when pyrite was the dominant Fe-sulfide. Carbonatization of the host rock also helped promote the deposition of both gold and chalcopyrite by lowering the pH and reducing their solubilities. The decrease in aH_2S was the dominant factor in the deposition of gold and chalcopyrite.
6. Copper, which is transported as a bisulfide complex in mesothermal gold-bearing ore fluids, is generally too soluble to deposit as chalcopyrite and is therefore flushed through the system. Mesothermal gold deposits in which copper is associated with gold, such as Onaman, are rare cases where low pH ensured low copper solubility and chalcopyrite was therefore able to deposit through mechanisms similar to those responsible for gold mineralization.

ACKNOWLEDGEMENTS

O. Grondin gratefully acknowledges the support of a Natural Sciences and Engineering Research Council (NSERC) post-graduate scholarship. Financial support for the research was provided by a research grant from Cameco Gold Inc. and a matching research grant from the NSERC-CRD program to AEW-J. We also thank Cameco Gold Inc. for access to the field area, drill core and internal reports, and the assistance of company geologists Mike Koziol, Ike Osmani and Paul Coad. We thank W.H. MacLean, A. Migdisov, J.R. Clark and C. Normand for helpful discussions and G. Poirier and S.T. Kim for assistance during SEM and oxygen and carbon isotope analyses, respectively.

CHAPTER 4

Conclusion

Research in the Onaman-Tashota greenstone belt has been limited to a few government reports and unpublished theses. This study compiles the available information and reports the results of detailed field observations, petrographical analyses, geochemical and isotopic correlations, mass balance calculations, and thermodynamic modeling of an unusual mesothermal gold deposit characterized by genetically contemporaneous gold and copper mineralization. Hydrothermal alteration and mineralization have similar parageneses in two gold showings of contrasting lithology, suggesting a single mineralizing event. Gold is disseminated in a shear zone hosted by intermediate to felsic metavolcaniclastics at the Ryne showing, and is concentrated in felsite dykes at the Hourglass showing. Textural relationships among alteration minerals suggest that early quartz-albite alteration formed a fine-grained groundmass, and was followed by a major episode of pervasive carbonate metasomatism, overprinted by sericitization and late chloritization. In mineralized zones, ankerite is the dominant carbonate, whereas calcite is the main carbonate elsewhere.

Mineralization was contemporaneous with the ankerite alteration and quartz ± carbonate ± albite ± tourmaline veining, and began with an initial stage of pyritization. Pyrite was replaced by arsenopyrite and then pyrrhotite, and simultaneously by chalcopyrite and gold.

Altered and mineralized rocks are enriched in Na, represented by albitization, and Ca due to carbonatization, but depleted in K. Sodium metasomatism occurred in zones favorable for gold deposition and Na gains correlate positively with gold grades. Iron and magnesium behave coherently and were both gained and lost.

Ankerite oxygen isotopic ratios suggest a metamorphic origin for the fluid, and carbon isotopic ratios are similar to those of large gold deposits of the Superior Province for which a mantle origin has been proposed. Pyrite sulfur isotopic ratios and gold grades correlate positively, the former reflecting an evolution of the fluid to lower conditions of fO_2 and pH.

Thermodynamic modeling of mineral stability relationships and metal solubility show that pyritization lowered H_2S activity by consumption of sulfur and lowered oxygen fugacity by oxidizing iron-bearing minerals in the host rocks. Gold and copper were both transported predominantly as bisulfide complexes, and were destabilized by reduced aH_2S. Host rock pyritization also decreased fO_2, which favored gold deposition, but only promoted chalcopyrite deposition when pyrite was the dominant Fe-sulfide. CO_2 metasomatism promoted destabilization of both gold and copper complexes by reducing pH. Sufidation was the principal cause of gold and minor copper mineralization, reducing metal solubilities by several orders of magnitude, a conclusion that is supported by the positive correlation between gold and total sulfur in metavolcaniclastic rocks of the Ryne showing.

Fluctuations in oxygen fugacity and H_2S activity of the fluid were responsible for the variable composition of native gold and electrum observed. Such fluctuations may have been due to seismic pumping of the fluid, which would have produced extreme variations in the fluid flux, and therefore alternations between fluid and rock buffering of the fluid compositon, during which fO_2 and aH_2S would have been high and low, respectively.

The unusual gold-chalcopyrite association observed at Onaman is explained by the low pH of the ore fluid. Contrary to what has been assumed previously, copper is transported as a bisulfide complex at conditions typical for mesothermal gold deposits. At such conditions, copper is too soluble to be concentrated and is therefore flushed from the system. Mesothermal gold deposits where copper is associated with gold, such as Onaman, are rare cases where initial pH was low enough to permit copper saturation in the fluid and deposition of chalcopyrite. In such cases, chalcopyrite deposition is triggered by the same mechanisms that are effective for gold mineralization, and promoted by low fluid/rock ratio.

Observations and interpretations of mineralization at Onaman place this gold occurrence between the greenschist- and amphibolite-facies hosted classes of lode gold deposits. In conlcusion, the Onaman gold prospect is a mesothermal gold deposit in which copper was introduced along with gold because pH conditions were low enough to destabilize both gold and copper bisulfide complexes. In other respects, it shares a common genesis with other lode gold deposits in similar geological settings.

REFERENCES

Amukun, S.E., 1980, Geology of the Gledhill Lake Area, Ontario Geological Survey, Report 198, Ministry of Natural Resources, 78 p.

Amukun, S. E., 1977, Geology of the Tashota Area, Ontario Geological Survey, Report 167, Ministry of Natural Resources, 90 p.

Anglin, C.D., and Franklin, J.M., 1989, Preliminary lead isotope studies of base metal and gold mineralization in the eastern Wabigoon Subprovince, northwestern Ontario; *In* Current Research, Part C, Geological Survey of Canada, Paper 89-1C, p. 285-292.

Anglin, C.D., Franklin, J.M., Loveridge, W.D., Hunt, P.A., and Osterberg, S.A., 1988, Use of zircon U-Pb ages of felsic intrusive and extrusive rocks in eastern Wabigoon Subprovince, Ontario, to place constraints on base metal and gold mineralization; *In* Radiogenic Age and Isotopic Studies, Report 2, Geological Survey of Canada, Paper 88-2, p.109-115.

Barrett, T.J., and MacLean, W.H., 1994, Mass changes in hydrothermal alteration zones associated with VMS deposits of the Noranda area, Exploration and Mining Geology, v. 3, p. 131-160.

Benning, L.G., and Seward, T.M., 1996, Hydrosulphide complexing of Au(I) in hydrothermal solutions from 150-400 degrees C and 500-1500 bar, Geochimica et Cosmochimica Acta, v. 60, no. 11, p. 1849-1871.

Blackburn, C.E., and Johns, G.W., 1988, A stratigraphic reconnaissance of the eastern Wabigoon Subprovince; *In* Summary of Field Work and Other Activities 1988, Ontario Geological Survey, Miscellaneous Paper 141, p.163-168.

Blackburn, C.E., Johns, G.W., Ayer, J., and Davis, D.W., 1991, Wabigoon Subprovince *In* Thurston, P.C., Williams, H.R., Sutcliffe, R.H., Stott, G.M., eds., Geology of Ontario, Ontario Geological Survey, Special Volume 4, part 1, p. 303-381.

Böhlke, J.K., 1989, Comparison of metasomatic reactions between a common CO_2-rich vein fluid and diverse wall rocks: intensive variables, mass transfers, and Au mineralization at Alleghany, California, Economic Geology, v. 84, p. 291-327.

Böhlke, J.K., and Kistler, R.W., 1986, Rb-Ar, and stable isotope evidence for the ages and sources of fluid components in gold-bearing quartz veins in the northern Sierra Nevada foothills metamorphic belts, Economic Geology, v. 81, p. 296-322.

Diamond, L.W., Jackman, J.A., and Charoy, B., 1991, Cation ratios of fluid inclusions in a gold-quartz vein at Brusson, Val d'Ayas, northwestern Italian Alps: Comparison

of bulk crush-leach results with SIMS analyses of individual inclusions, Chemical Geology, v. 90, p. 71-78.

Dubé B., Guha, J., and Rocheleau, M., 1987, Alteration patterns related to gold mineralization and their relation to CO_2/H_2O ratios, Mineralogy and Petrology, v. 37, p. 267-291.

Easton, R.M., 2000, Metamorphism of the Canadian shield, Ontario, Canada. I. The Superior Province, Canadian Mineralogist, v. 38, p. 287-317.

El Bilali, H., and Hattori, K., 1998, High C-13 and S-34 in carbonate and sulfide minerals associated with gold at the Red Lake greenstone belt; evidence from deformation zones and Campbell Mine *In* Abstracts with programs, Geological Society of America, 1998 meeting, v. 30, p. 369-370.

Evans, D.T.W., 1996, Epigenetic gold occurrences, eastern and central Dunnage Zone, Newfoundland, Government of Newfoundland and Labrador, Geological Survey, Mineral Resource Report (St. John's), 1996, 135p.

Flaherty, G.F., 1936, Mechanics of structure at Tashota Goldfields Mine, Tashota, Ontario, Transactions of the Canadian Institute of Mining and Metallurgy and of the Mining Society of Nova Scotia, no. 39, p. 723-738.

Fleet, M.E., and Knipe, S.W., 2000, Solubility of native gold in H-O-S fluids at 100-400 °C and high H2S content, Journal of Solution Chemistry, v. 29, p. 1143-1157.

Gaboury, D., and Daigneault, R., 1999, Evolution from sea floor-related to sulfide-rich quartz vein-type gold mineralization during deep submarine volcanic construction: The Géant Dormant gold mine, Archean Abitibi belt, Canada, Economic Geology, v. 94, p. 3-22.

Gammons, C.H., Yu, Y., and Williams-Jones, A.E., 1997, The disproportionation of gold (I) chloride complexes at 25 to 200°C, Geochimica et Cosmochimica Acta, v. 61, p. 1971-1997.

Gammons, C.H., and Williams-Jones, A.E., 1995, Hydrothermal geochemistry of electrum: Thermodynamic constraints, Economic Geology, v. 90, p. 420-432.

Gélinas, L., Brooks, C., Perrault, G., Carignan, J., Trudel, P., and Grasso, F., 1977, Chemo-stratigraphic divisions within the Abitibi volcanic belt, Rouyn-Noranda district, Quebec *In* Volcanic regimes in Canada, W.R.A. Baragar, L.C. Coleman and J.M. Hall eds., Geological Association of Canada, Special Paper 16, p. 265-295.

Girvin, H.H., 1924, Geology of the Onaman gold area [Ontario], Canadian Mining Journal, v. 45, p. 899-900.

Gledhill, T.L., 1925, Tashota-Onaman gold area, District of Thunder Bay; Ontario Department of Mines, v.34, part 6, p. 65-85. Accompanied by map 34G.

Golyshev, S.I., Padalko, N.L., and Pechenkin, S.A., 1981, Fractionation of stable oxygen and carbon isotopes in carbonate systems, Geochemistry International, v. 18, p. 85-99.

Goodwin, A.M., 1977, Archean volcanism in Superior Province, Canadian Shield *In* Volcanic regimes in Canada, W.R.A. Baragar, L.C. Coleman and J.M. Hall eds., Geological Association of Canada, Special Paper 16, p. 205-241.

Grant, J.A., 1986, The isocon diagram - A simple solution to Gresen's equation for metasomatic alteration, Economic Geology, v. 81, p. 1976-1982.

Groves, D.I., 1993, The crustal continuum model for late-Archaean lode-gold deposits of the Yilgarn Block, Western Australia, Mineralium Deposita, v. 28, p. 366-374.

Groves, D.I., and Foster, R.P., 1993, Archaean lode gold deposits *In* Gold metallogeny and exploration, R.P. Foster ed., p. 63-103.

Groves, D.I., Barley, M.E., and Ho, S.E., 1989, Nature, genesis, and tectonic setting of mesothermal gold mineralization in the Yilgarn Block, Western Australia, *In*, Keays, R.R., Ramsay, W.R.H., and Groves, D.I., eds., The geology of gold deposits: the perspective in 1988, Economic Geology, Monograph 6, p. 71-85.

Guha, J., Huan-Zhang, L., Dubé, B., Robert, F., and Gagnon, M., 1991, Fluid characteristics of vein and altered wall rock in Archean mesothermal gold deposits, Economic Geology, v. 86, p. 667-684.

Hagemann, S.G., and Cassidy, K.F., 2000, Archean orogenic lode gold deposits *In* Gold in 2000, S.G. Hagemann and P.E. Brown eds., p. 9-68.

Hallberg, J.A., Johnston, C., and Bye, S.M., 1976, The Archaean Marda igneous complex, Western Australia, Precambrian Research, vol. 3, p. 111-136.

Hodgson, C.J., 1993, Mesothermal lode-gold deposits, *In* Kirkham, R.V., Sinclair, W.D., Thorpe, R.I., and Duke, J.M., eds., Mineral deposit modeling, Geological Association of Canada, Special Paper 40, p. 635-678.

Hodgson, C.J., and Hamilton, J.V., 1989, Gold mineralization in the Abitibi greenstone belt: end-stage result of Archean collisional tectonics?, *In*, Keays, R.R., Ramsay, W.R.H., and Groves, D.I., eds., The geology of gold deposits: the perspective in 1988, Economic Geology, Monograph 6, p. 86-100.

Hodgson, C.J., and McGeehan, P.J., 1982, A review of the geological characteristics of "gold-only" deposits in the Superior Province of the Canadian Shield, *In* Hodder,

R.W., and Petruks, W., eds., Geology of Canadian gold deposits, Canadian Institute of Mining and Metallurgy, Special Volume 24, p. 211-229.

Issigonis, M.J., 1980, Occurrence of disseminated gold deposits in porphyries in Archaean Abitibi belt, northwest Quebec, Canada, Transactions of the Institution of Mining and Metallurgy (Section B: Applied Earth Science), v. 89, p. 157-158.

Johnson, J.W., Oelkers, E.H., and Helgeson, H.C., 1992, SUPCRT92: A software package for calculating the standard molal thermodynamic properties of minerals, gases, aqueous species, and reactions from 1 to 5000 bars and 0° to 1000°C, Computers and Geosciences, v. 18, p. 899-947.

Jyang, N., 2000, Hydrothermal fluid evolution associated with gold mineralization at the Wenyu mine, Xiaoqinling district, China, Resource Geology (Tokyo 1998), v. 50, p. 103-112.

Kerrich, R., 1990, Carbon-isotope systematics of Archean Au-Ag vein deposits in the Superior Province, Canadian Journal of Earth Sciences, v. 27, p. 40-56.

Kerrich, R., 1987, The stable isotope geochemistry of Au-Ag vein deposits in metamorphic rocks *In* Stable isotope geochemistry of low temperature processes, T.K. Kyser ed., Mineralogical Association of Canada Short Course Handbook v. 13, p. 287-336.

Kerrich, R., and Fryer, B.J., 1981, The separation of rare elements from abundant base metals in Archean lode gold deposits: Implications of low water/rock source regions, Economic Geology, v. 76, p. 160-166.

Kishida, A., and Kerrich, R., 1987, Hydrothermal alteration zoning and gold concentration at the Kerr-Addison Archean lode gold deposit, Kirkland Lake, Ontario, Economic Geology, v. 82, p.649-690.

Lydon, J.W., 1980, The behaviour of metals in hydrothermal systems with emphasis on gold; Workshop on epithermal deposits, Geoscience Forum, Whitehorse, Yukon (preprint).

MacLean, W.H., and Kranidiotis, P., 1987, Immobile elements as monitors of mass transfer in hydrothermal alteration: Phelps Dodge massive sulfide deposit, Matagami, Quebec, Economic Geology, v. 82, p. 951-962.

Mason, J.K., and McConnell, C.D., 1983, Gold mineralization in the Beardmore-Geraldton area; *In* Colvine, A.C., editor, The geology of gold in Ontario, Ontario Geological Survey, Miscellaneous Paper 110, p.84-97.

McBride, D.E., 1987, Gold mineralization and its position in the geological evolution of the Beardmore-Tashota area, Canadian Institute of Mining Bulletin, v. 80, no. 900, p. 51-58.

Melrose, D.M., 1998, Cameco Corporation – 1997 Exploration program, Onaman River and West Onaman projects, Oboshkegan township, Ontario, Unpublished report.

Mikucki, E.J., 1998, Hydrothermal transport and depositional processes in Archean lode-gold systems: a review, Ore Geology Reviews, v. 13, p. 307-321.

Mikucki, E.J., and Ridley, J.R., 1993, The hydrothermal fluid of Archaean lode-gold deposits at different metamorphic grades: compositional constraints from ore and wallrock alteration assemblages, Mineralium Deposita, v. 28, p. 469-481.

Mountain, B.W., and Seward, T.M., 1999, The hydrosulphide/sulphide complexes of copper(I): Experimental determination of stoichiometry and stability at 22°C and reassessment of high temperature data, Geochimica et Cosmochimica Acta, v. 63, p. 11-29.

Mountain, B.W., and Williams-Jones, A.E., 1995, Mass transfer and the path of metasomatic reactions in mesothermal gold deposits: An example from Flambeau Lake, Ontario, Economic Geology, v. 91, p. 302-321.

Mueller, A.G., and Groves, D.I., 1991, The classification of Western Australian greenstone-hosted gold deposits according to wallrock-alteration mineral assemblages, Ore Geology Reviews, v. 6, p. 291-331.

Ohmoto, H., 1972, Systematics of sulfur and carbon isotope in hydrothermal ore deposits, Economic Geology, v. 67, p. 551-579.

Ohmoto, H., and Rye, R.O., 1979, Isotope of sulfur and carbon *In* Geochemistry of Hydrothermal deposits, H.L. Barnes ed., p. 509-567.

Osmani, I.A., 1999, Cameco Corporation – 1998-99 Exploration program, Onaman project, Oboshkegan township, Northwestern Ontario, Unpublished report, 65 p.

Osterberg, S.A., Morton, R.L., and Franklin, J.M., 1987, Hydrothermal alteration and physical volcanology of archean rocks in the vicinity of the Headway-Coulee massive sulfide occurrence, Onaman area, Northwestern Ontario, Economic Geology, v. 82, p. 1505-1520.

Perring, C.S., Groves, D.I., and Ho, S.E., 1987, Constraints on the source of auriferous fluids for Archaean gold deposits *In* Recent advances in understanding Precambrian gold deposits, S.E. Ho and D.I. Groves eds., p. 287-306.

Phillips, G.N., 1986, Geology and alteration in the Golden Mile, Kalgoorlie, Economic Geology, v. 81, p. 779-808.

Poulsen, K.H., 1996, Disseminated and replacement gold *In* Geology of Canadian Mineral Deposit Types, O.R. Eckstrand, W.D. Sinclair, and R.I. Thorpe eds., p. 383-392.

Ridley, J.R., and Diamond, L.W., 2000, Fluid chemistry of orogenic lode gold deposits and implications for genetic models *In* Gold in 2000, S.G. Hagemann and P.E. Brown eds., p. 141-162.

Ridley, J., Mikucki, E.J., and Groves, D.I., 1996, Archean lode-gold deposits: fluid flow and chemical evolution in vertically extensive hydrothermal systems, Ore Geology Reviews, v. 10, p. 279-293.

Robert, F., and Kelly, W.C., 1987, Ore-forming fluids in Archean gold-bearing quartz veins at the Sigma mine, Abitibi greenstone belt, Québec, Canada, Economic Geology, v. 82, p. 1464-1482.

Ryan, R.J., and Smith, P.K., 1998, A review of the mesothermal gold deposits of the Meguma Group, Nova Scotia, Canada, Ore Geology Reviews, v. 13, p. 153-183.

Shock, E. L., 1998, slop98.dat - Sequential-access thermodynamic datafile to be used as input to program cprons92, a code that converts sequential files into their direct-access equivalent (dslop98.dat), which is used by program SUPCRT92, http://zonvark.wustl.edu/geopig/slop98.dat.

Seward, T.M., 1973, Thio complexes of gold and the transport of gold in hydrothermal ore solutions, Geochimica et Cosmochimica Acta, v. 37, p.379-399.

Sibson, R.H., Moore J.M., and Rankin, A.H., 1975, Seismic pumping; a hydrothermal fluid transport mechanism, Journal of the Geological Society of London, v. 131, Part 6, p. 653-659.

Smith, T.J., and Kesler, S.E., 1985, Relation of fluid inclusion geochemistry to wallrock alteration and lithogeochemical zonation at the Hollinger-McIntyre gold deposit, Timmins, Ontario, Canada, Canadian Institute of Mining Bulletin, v. 78, no. 876, p. 35-46.

Smith, T.J., Cloke, P.L., and Kesler, S.E., 1984, Geochemistry of fluid inclusions from the McIntyre-Hollinger gold deposit, Timmins, Ontario, Canada, Economic Geology, v. 79, p. 1265-1285.

Straub, K.H., 2000, Geochemistry of hydrothermal alteration and its relation to base-metal mineralization in the Marshall Lake area, northern margin of the Onaman-Tashota greenstone belt, Project Unit 99-011, *In* Summary of field work and other activities 2000 (OFR 6032), Ontario Geological Survey, p. 26.1-26.14.

Thomas, D., 1998, Onaman project, Ontario; Alteration, mineralization and structural controls at the Ryne and Hourglass showings, Appendix 1 of: Cameco Corporation –

1998-99 Exploration program, Onaman project, Oboshkegan township, Northwestern Ontario, Unpublished report, 17 p.

Thurston, P. C., 1980, Geology of the Northern Onaman Lake Area, Ontario Geological Survey, Report 208, Ministry of Natural Resources, 81 p.

Ujike, O., and Goodwin, A.M., 1987, Geochemistry and origin of Archean felsic metavolcanic rocks, central Noranda area, Quebec, Canada, Canadian Journal of Earth Sciences, v. 24, p. 2551-2567.

Wood, S.A., 1987, Applications of a multiphase ore mineral solubility experiment to the separation of base metals and gold mineralization in Archean greenstone terrains, Economic Geology, v. 82, p. 1044-1048.

Xiao, Z., Gammons, C.H., and Williams-Jones, A.E., 1998, Experimental study of copper(I) chloride complexing in hydrothermal solutions at 40 to 300°C and saturated water vapor pressure, Geochimica et Cosmochimica Acta, v. 62, p. 2949-2964.

FIGURES

Figure 1: Regional geology of the Onaman-Tashota greenstone belt (Adapted from Stott, personal communication, 2001).

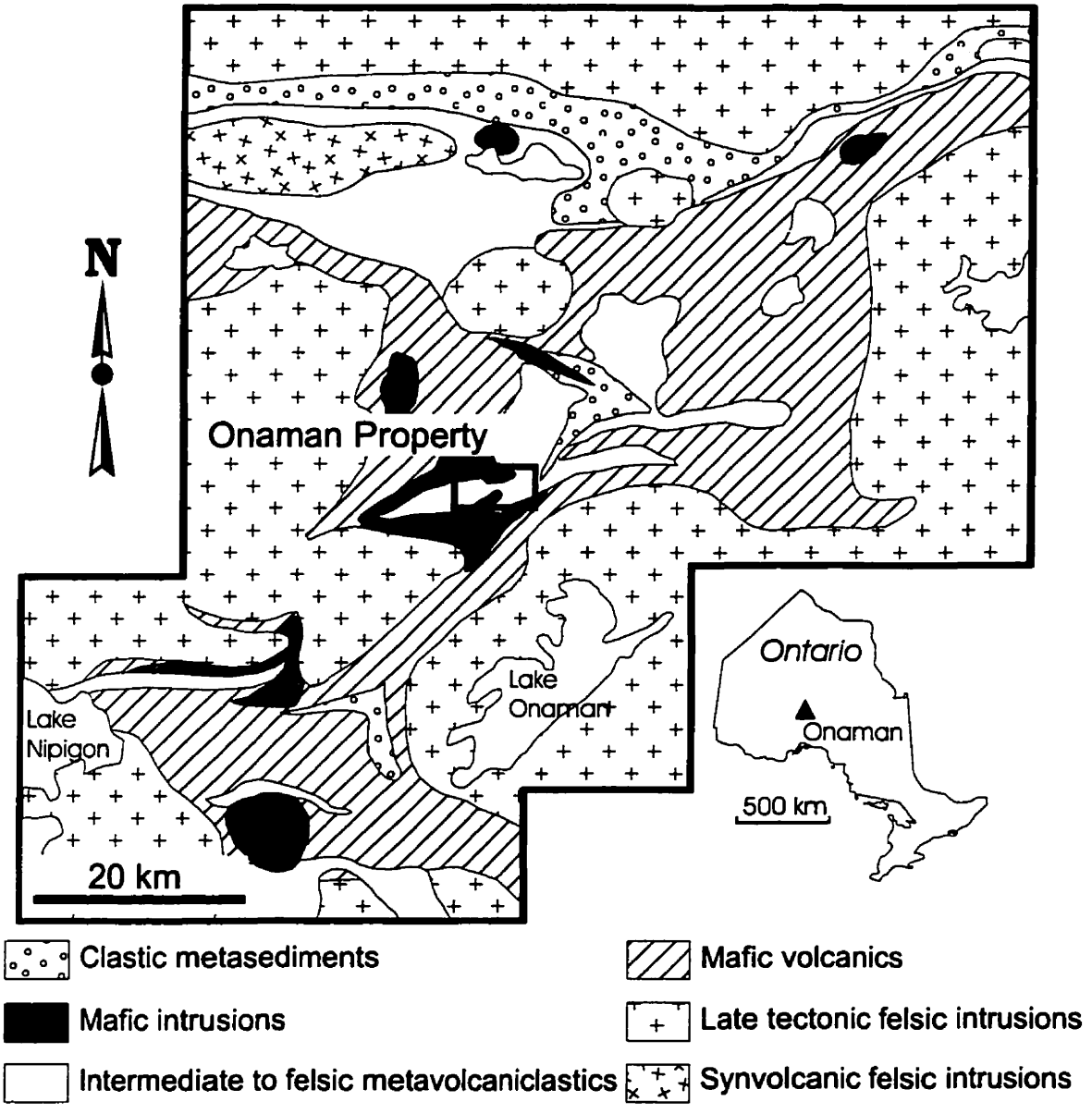
N
Onaman Property
Lake
Nipigon
Lake
Onaman
20 km
Ontario
Onaman
500 km
Clastic metasediments
Mafic intrusions
Intermediate to felsic metavolcaniclastics
Mafic volcanics
Late tectonic felsic intrusions
Synvolcanic felsic intrusions

Figure 2: Geological map of the Onaman property (Adapted from Osmani, 1999).

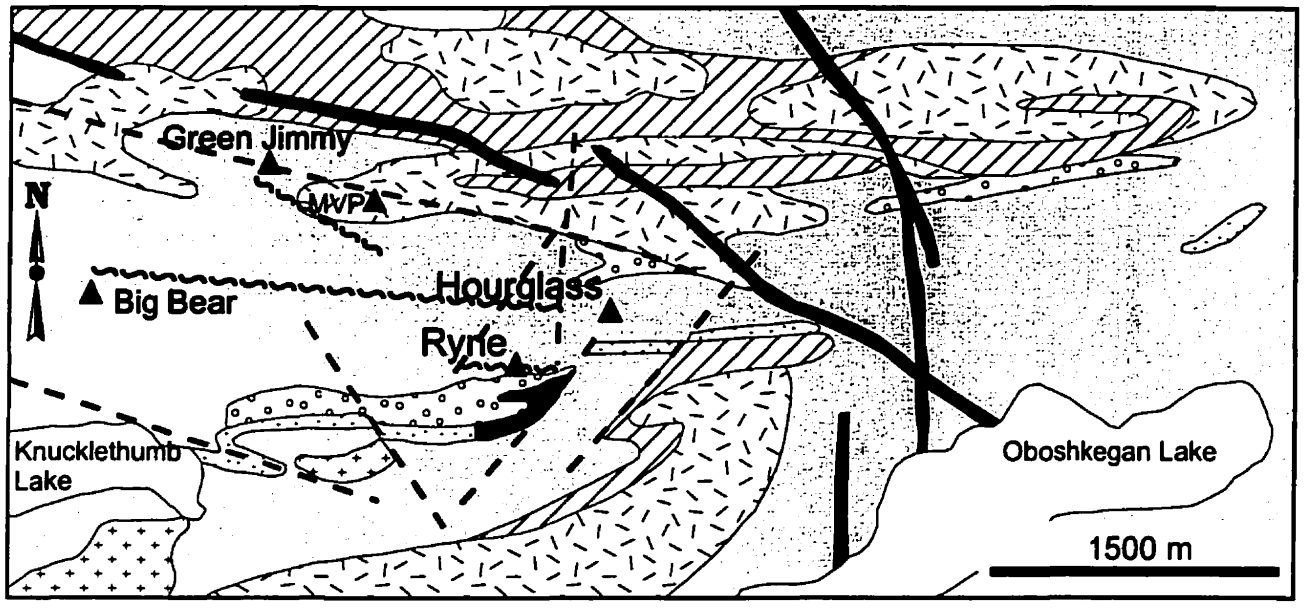
Green Jimmy
MVP
N
Big Bear
Hourglass
Ryrie
Knucklethumb Lake
Oboshkegan Lake
1500 m
Siltstone
Conglomerate
Intermediate to felsic metavolcaniclastics
Mafic metavolcanics
Diabase dyke
Granitoid intrusives
Gabbro
Quartz-feldspar porphyry
Gold showing
Fault
Shear zone

Figure 3: Geological map of the Ryne showing (Adapted from Osmani, 1999).

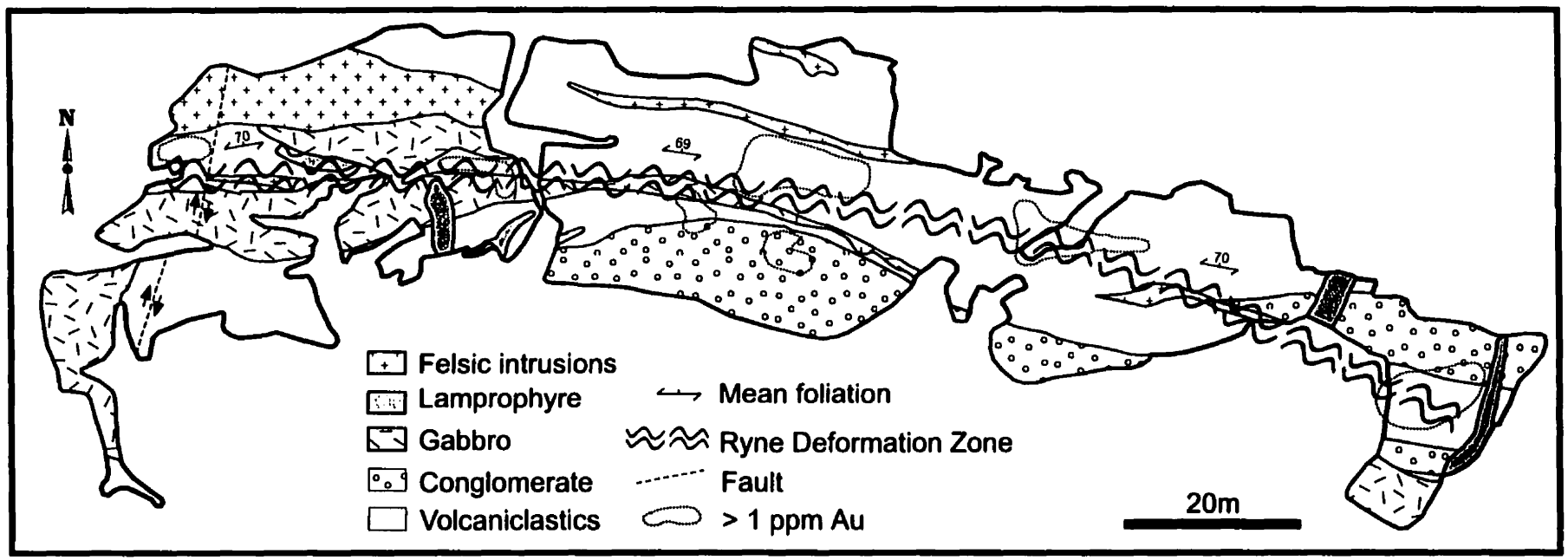
N
70
69
70
Felsic intrusions
Lamprophyre
Gabbro
Conglomerate
Volcaniclastics
Mean foliation
Ryne Deformation Zone
Fault
> 1 ppm Au
20m

Figure 4: Geological map of the Hourglass showing (Adapted from Osmani, 1999).

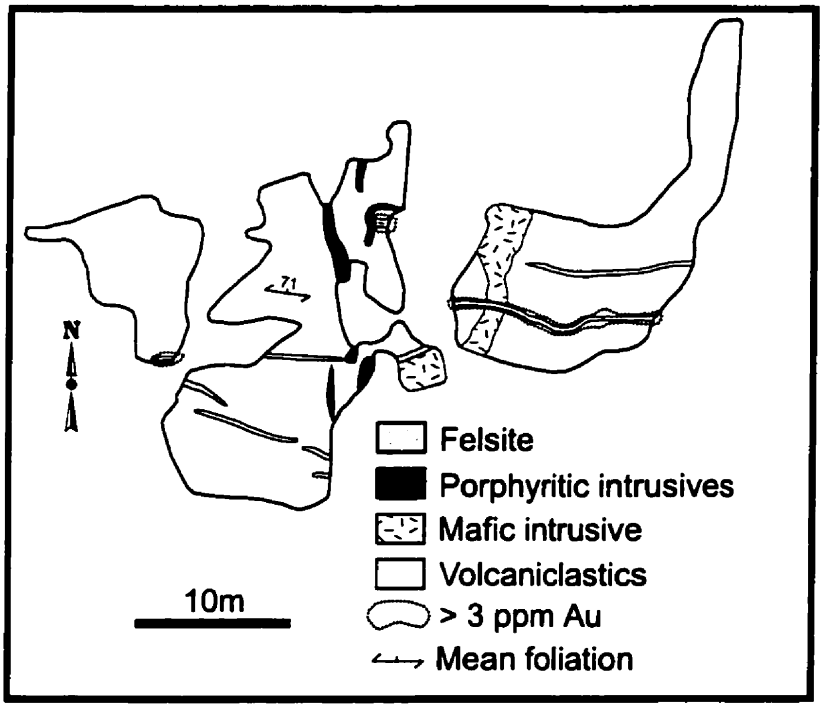
N
71
10m
Felsite
Porphyritic intrusives
Mafic intrusive
Volcaniclastics
> 3 ppm Au
Mean foliation

Figure 5: Photomicrographs in transmitted light, crossed polars. A: Tourmaline (dark elongated crystal) replaced by sericite (light crystals) (Ryne). B: Alteration of twinned albite by ankerite. Late sericite is concentrated along the edge of the albite phenocryst (Hourglass). C: Carbonate vein composed of ankerite rhombs and late dolomite filling (dark) (Ryne). D: Sericite-ankerite pseudomorphs in a fine-grained groundmass of quartz and albite (Ryne). E: Ankerite filling embayment in quartz crystals (Ryne). F: Twinned ankerite crystal replaced by pervasive sericite (Ryne). Ab: albite, Ak: ankerite, Qtz: quartz, Tur: tourmaline, Ser: sericite, Dol: dolomite.

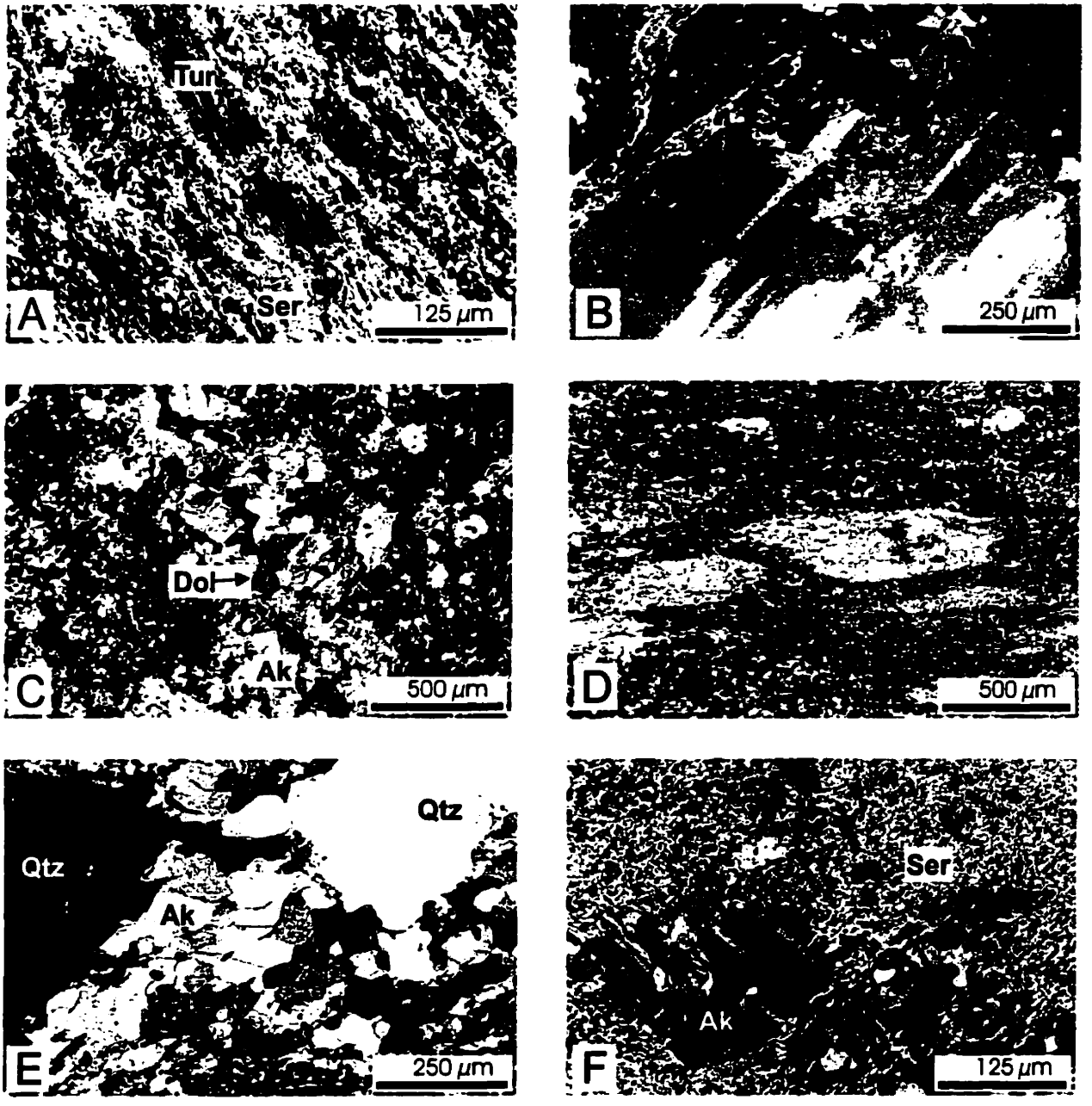
Tur
Ser
A
125 μm
B
250 μm
Dol
Ak
C
500 μm
D
500 μm
Qtz
Qtz
Ak
E
250 μm
Ser
Ak
F
125 μm

Figure 6: Alteration mineral paragenesis of the Ryne and Hourglass showings.

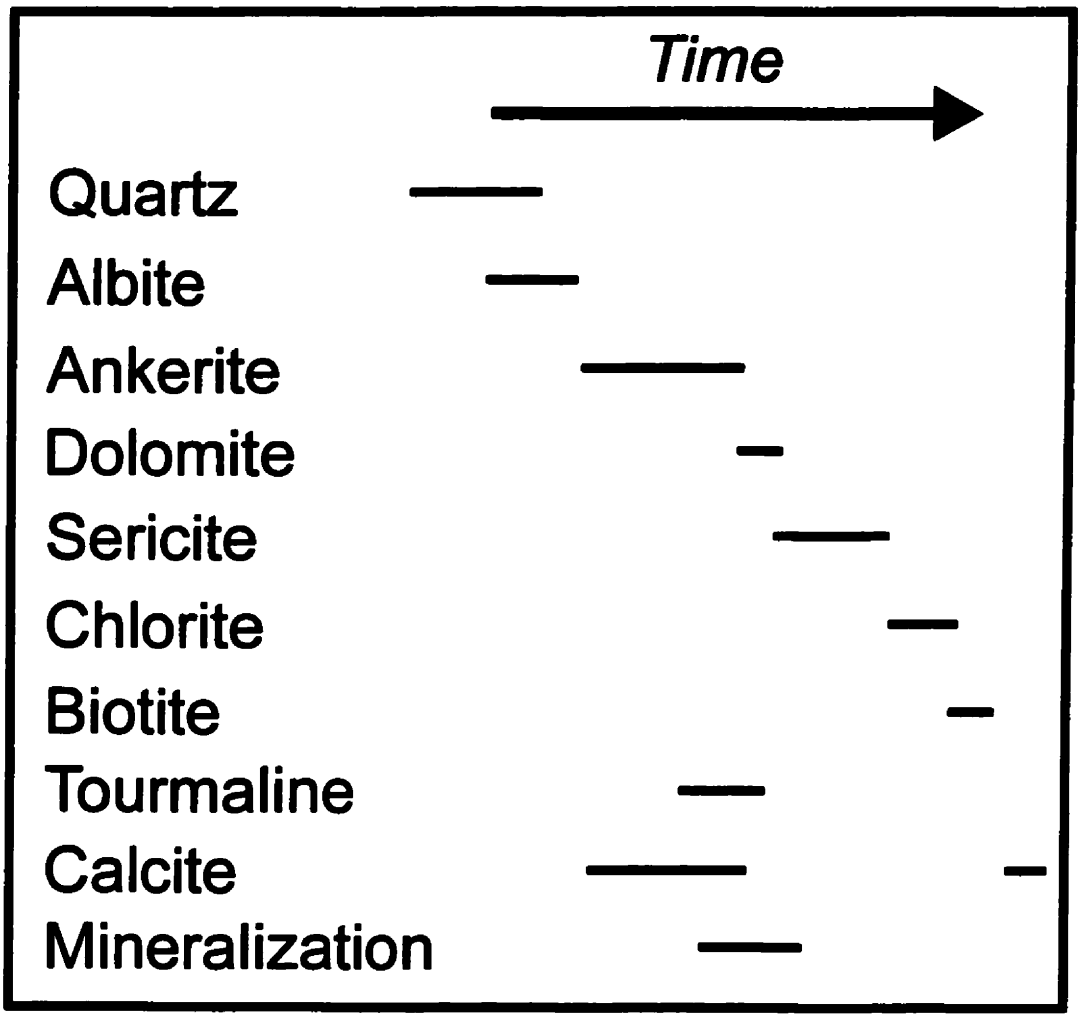
Time
Quartz
Albite
Ankerite
Dolomite
Sericite
Chlorite
Biotite
Tourmaline
Calcite
Mineralization

Figure 7: Photomicrographs in reflected light of textural relationships among ore minerals. All photomicrographs are from the Ryne showing. A: Replacement of pyrite by pyrrhotite. Note embayments in pyrite filled by pyrrhotite. B: Nucleation of pyrrhotite on arsenopyrite boundary. Small chalcopyrite grains replaced pyrrhotite. C: Free gold surrounding fractured and weathered pyrite grains. D: Composite chalcopyrite and native gold inclusions in pyrite representing replacements of the latter along annealed fractures or grain boundaries. E: Native gold overgrown on pyrite. F: Arsenopyrite (dashed outline) replacing pyrite. Note free grains of arsenopyrite in groundmass left of the pyrite crystal. Py: pyrite, Ccp: chalcopyrite, Apy: arsenopyrite, Au: gold, Po: pyrrhotite.

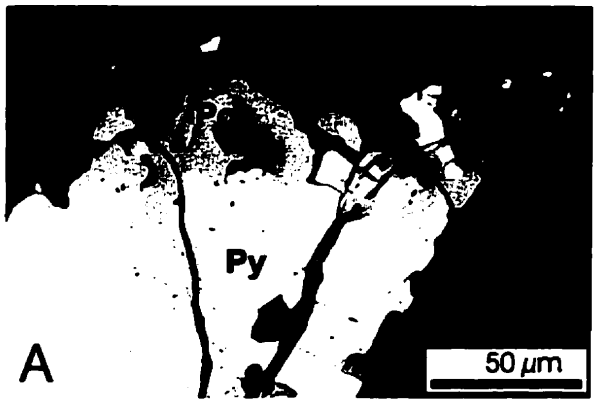
Py
A
50 µm

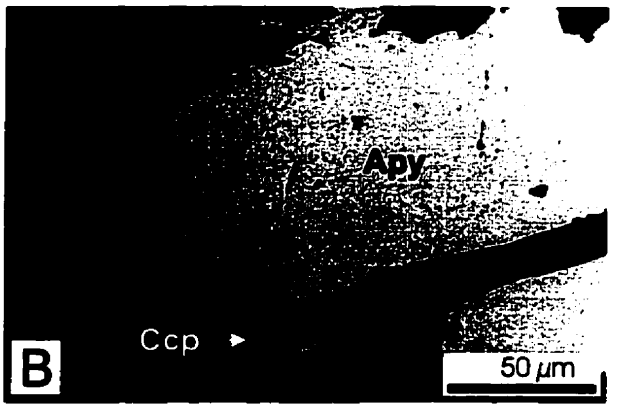
Apy
Ccp
B
50 µm

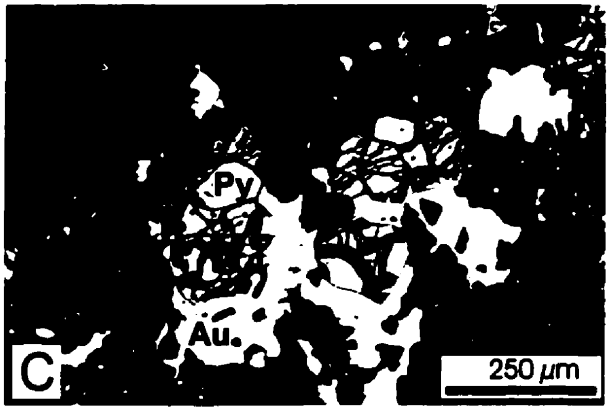
Py
Au
C
250 µm


Ccp
Py
Au
D
50 µm

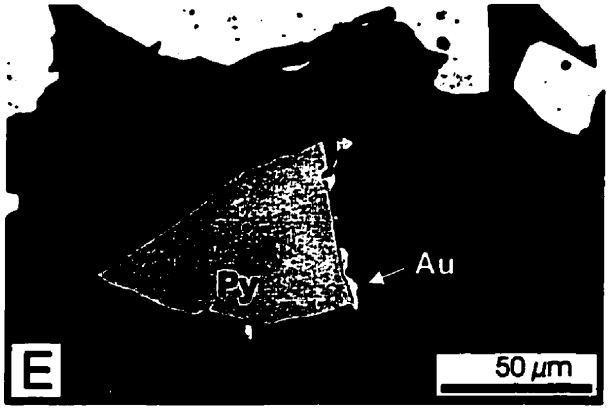
Au
Py
E
50 µm

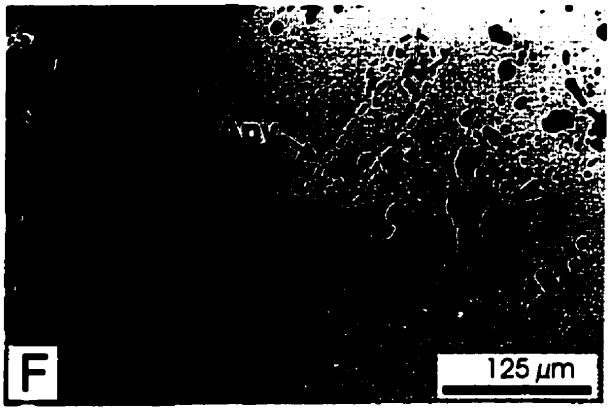
F
125 µm

Figure 8: Ore mineral paragenesis of the Ryne and Hourglass showings.

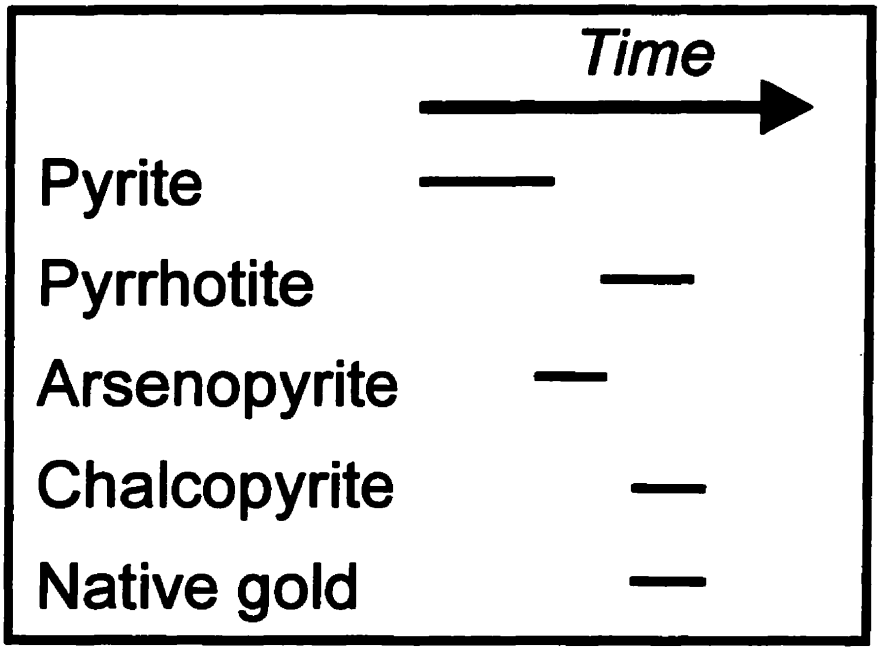
Time
Pyrite
Pyrrhotite
Arsenopyrite
Chalcopyrite
Native gold

Figure 9: Isocon diagram comparing element concentrations of least altered vs altered rock. The numbers in front of the element or oxide are scaling factors. Concentrations of Zr and Y are expressed in ppm.

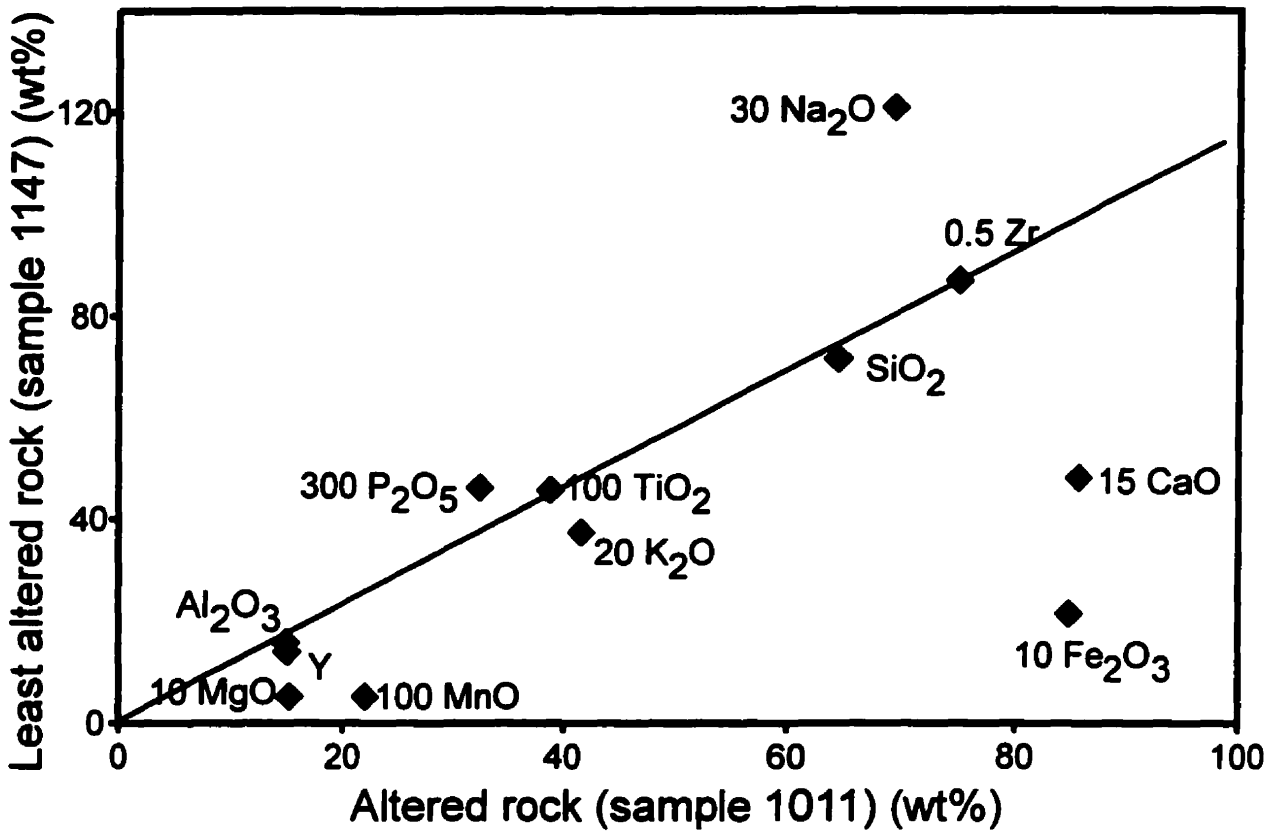
Least altered rock (sample 1147) (wt%)
120
80
40
0
0
20
40
60
80
100
Altered rock (sample 1011) (wt%)
30 Na2O
0.5 Zr
SiO2
300 P2O5
100 TiO2
15 CaO
20 K2O
Al2O3
Y
10 Fe2O3
10 MgO
100 MnO

Figure 10: Comparison of the compositions of variably altered lapilli tuffs from the Ryne showing and felsite dykes from the Hourglass showing with those of suites of fresh calc-alkaline rocks reported by Gélinas et al. (1977), Goodwin (1977), Hallberg et al. (1976), and Ujike and Goodwin (1987). The magmatic trend shows the fractionation of aluminum and titanium during magmatic differentiation. The alteration line represents the dilution or concentration of immobile elements in an altered rock with a precursor composition located at the intersection of the alteration line and the magmatic trend.

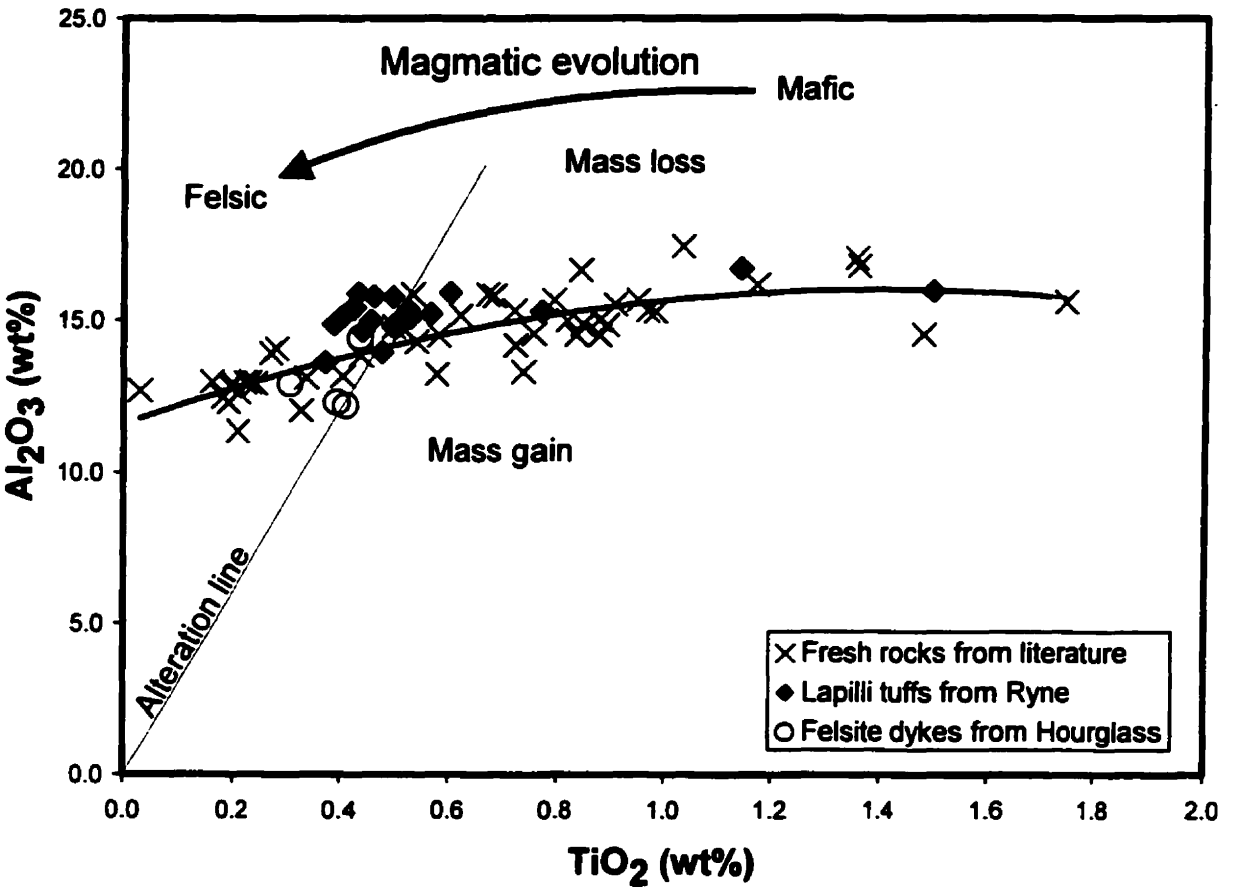
Magmatic evolution
Mafic
Felsic
Mass loss
Mass gain
Alteration line
Fresh rocks from literature
Lapilli tuffs from Ryne
Felsite dykes from Hourglass
25.0
20.0
15.0
10.0
5.0
0.0
0.0
0.2
0.4
0.6
0.8
1.0
1.2
1.4
1.6
1.8
2.0
Al2O3 (wt%)
TiO2 (wt%)

Figure 11: Mass changes of sodium in lapilli tuffs from the Ryne showing and felsite dykes from the Hourglass showing as a function of gold grade. Results reported in % of original wt% value.

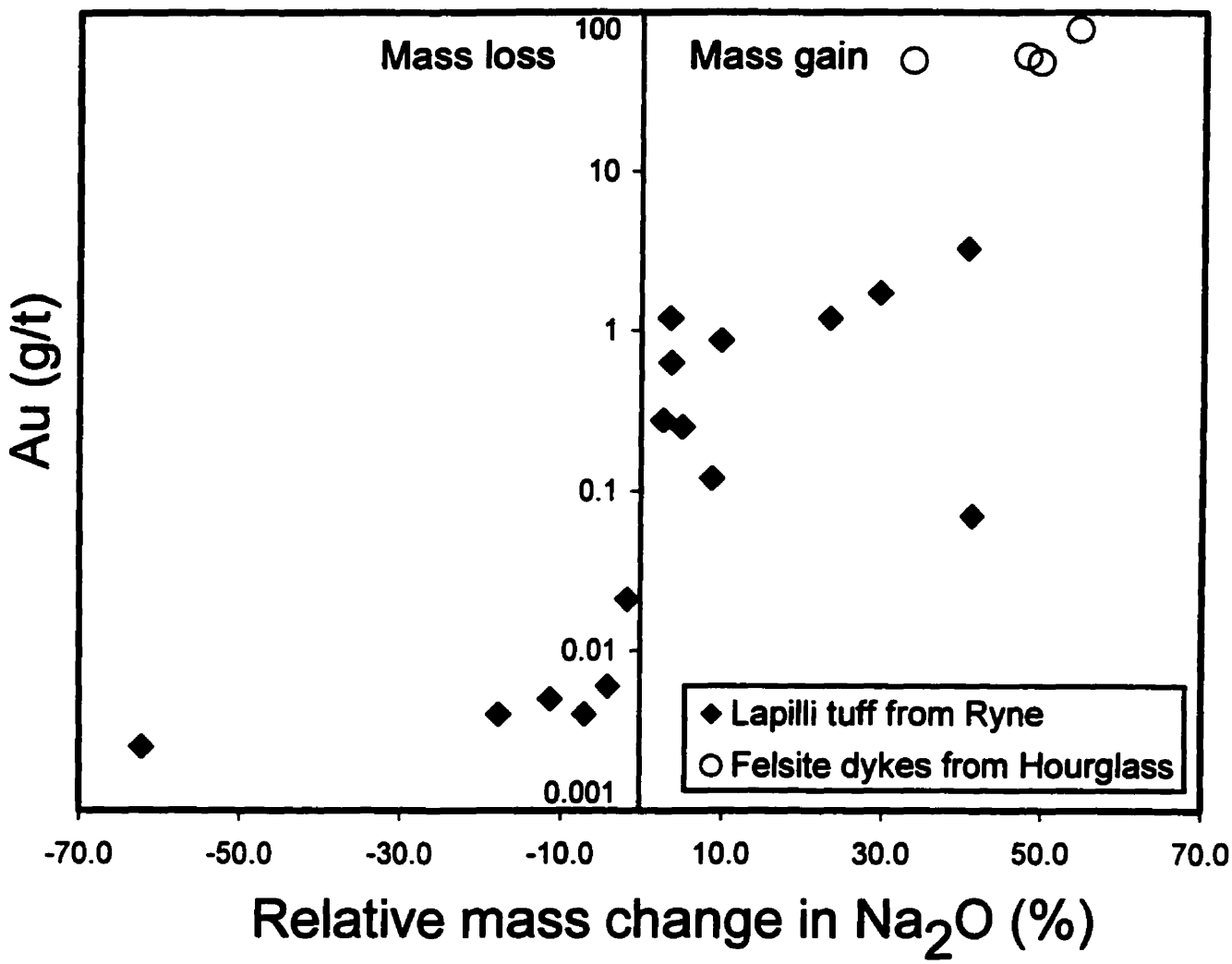
Mass loss
Mass gain
100
10
1
0.1
0.01
0.001
Au (g/t)
Lapilli tuff from Ryne
Felsite dykes from Hourglass
-70.0
-50.0
-30.0
-10.0
10.0
30.0
50.0
70.0
Relative mass change in Na_2O (%)

Figure 12: Mass changes for selected major element oxides in lapilli tuffs from the Ryne showing and felsite dykes of the Hourglass showing. Note the coherent behavior of Fe and Mg (A), the general addition of Ca and the extreme depletion in K (B).

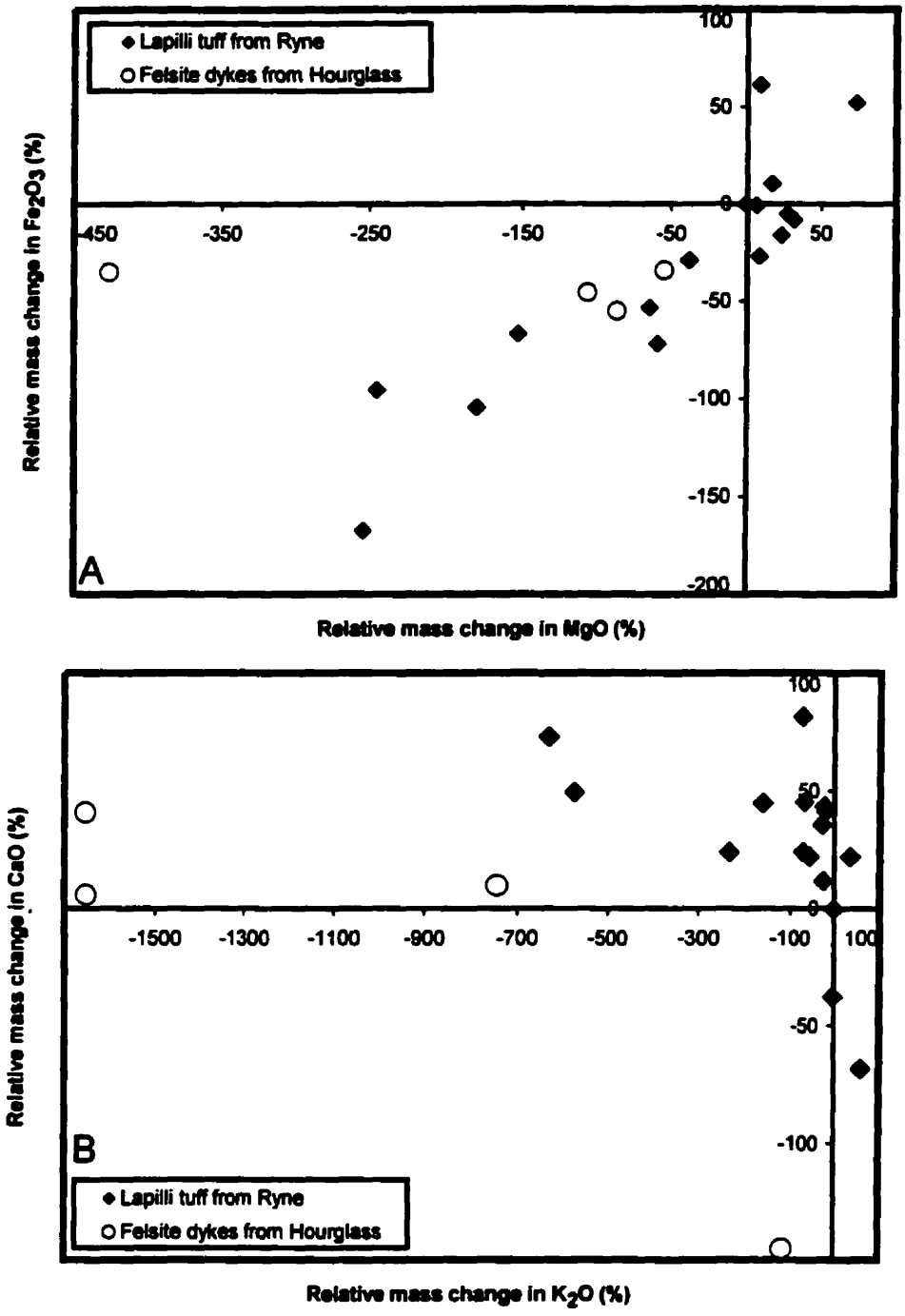
Lapilli tuff from Ryne
Felsite dykes from Hourglass
Relative mass change in Fe_2O_3 (%)
Relative mass change in MgO (%)
A
100
50
0
-50
-100
-150
-200
-450
-350
-250
-150
-50
50
Relative mass change in CaO (%)
Relative mass change in K_2O (%)
B
-1500
-1300
-1100
-900
-700
-500
-300
-100
100

Figure 13: Binary plots of bulk rock gold concentration versus the concentrations of other trace elements.

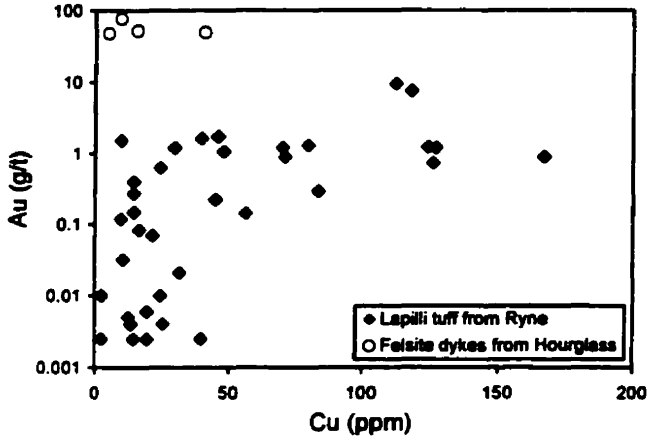
Au (g/t)
100
10
1
0.1
0.01
0.001
0
50
100
150
200
Cu (ppm)
Lapilli tuff from Ryne
Felsite dykes from Hourglass

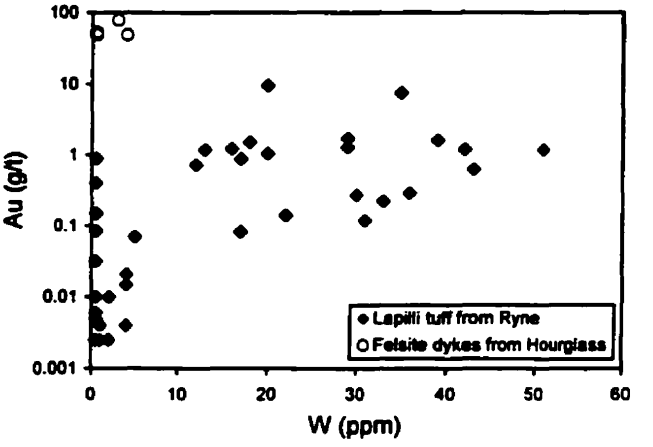
Au (g/t)
100
10
1
0.1
0.01
0.001
0
10
20
30
40
50
60
W (ppm)
Lapilli tuff from Ryne
Felsite dykes from Hourglass

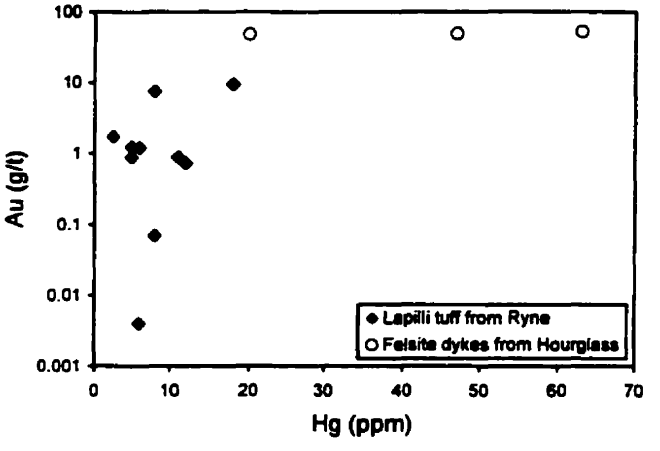
Au (g/t)
100
10
1
0.1
0.01
0.001
0
10
20
30
40
50
60
70
Hg (ppm)
Lapilli tuff from Ryne
Felsite dykes from Hourglass

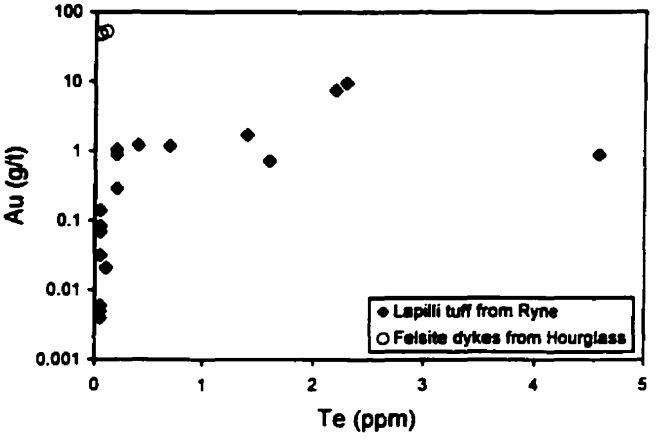
Au (g/t)
100
10
1
0.1
0.01
0.001
0
1
2
3
4
5
Te (ppm)
Lapilli tuff from Ryne
Felsite dykes from Hourglass

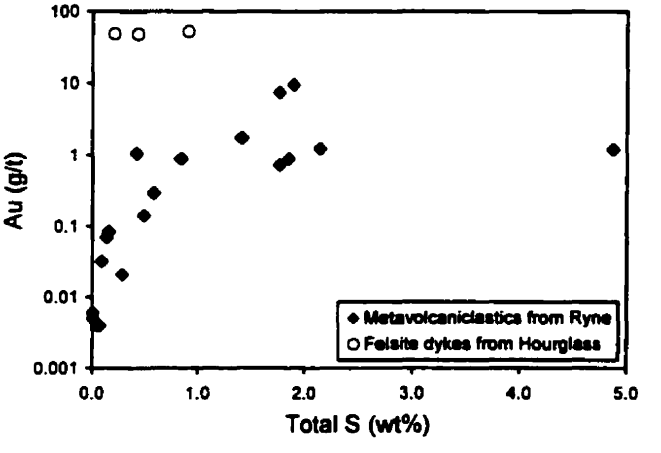
Au (g/t)
100
10
1
0.1
0.01
0.001
0.0
1.0
2.0
3.0
4.0
5.0
Total S (wt%)
Metavolcaniclastics from Ryne
Felsite dykes from Hourglass

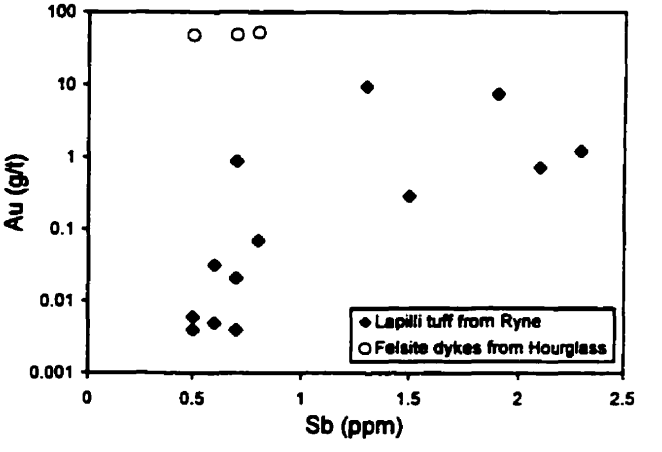
Au (g/t)
100
10
1
0.1
0.01
0.001
0
0.5
1
1.5
2
2.5
Sb (ppm)
Lapilli tuff from Ryne
Felsite dykes from Hourglass

Figure 14: Gold assays as a function of carbonate mineral composition.

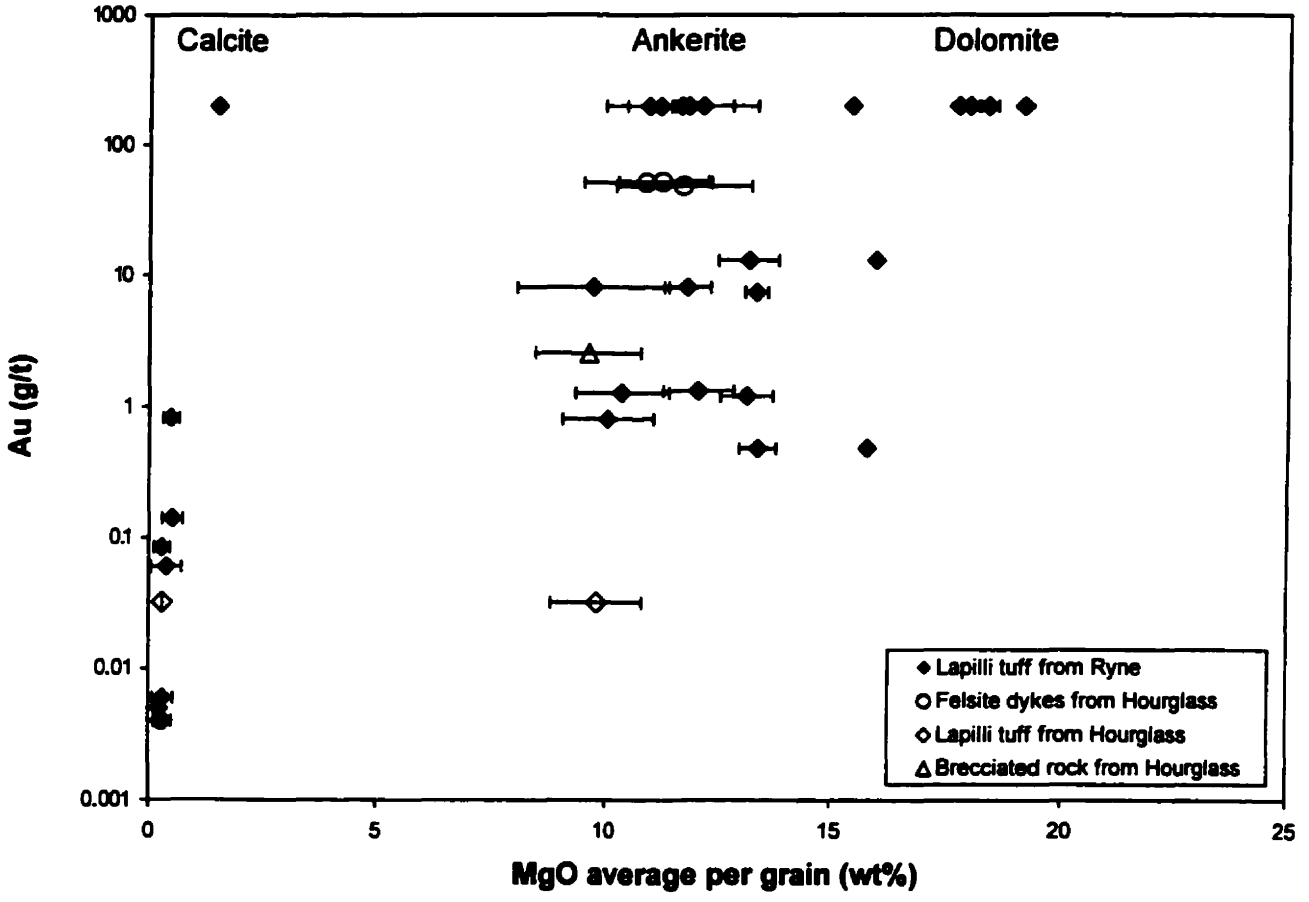
Calcite
Ankerite
Dolomite
1000
100
10
1
0.1
0.01
0.001
Au (g/t)
0
5
10
15
20
25
MgO average per grain (wt%)
Lapilli tuff from Ryne
Felsite dykes from Hourglass
Lapilli tuff from Hourglass
Brecciated rock from Hourglass

Figure 15: The silver content of native gold and electrum from metavolcaniclastics of the Ryne showing and felsite dykes of the Hourglass showing. Note that there are three clusters of Ag concentration: A, B and C, and that individual samples contain native gold and electrum grains with compositions falling in more than one cluster. Samples containing native gold/electrum with composition in more than one cluster are distinguished from other samples (black) by different patterns. Each bar reflects the average composition of up to 10 grains.

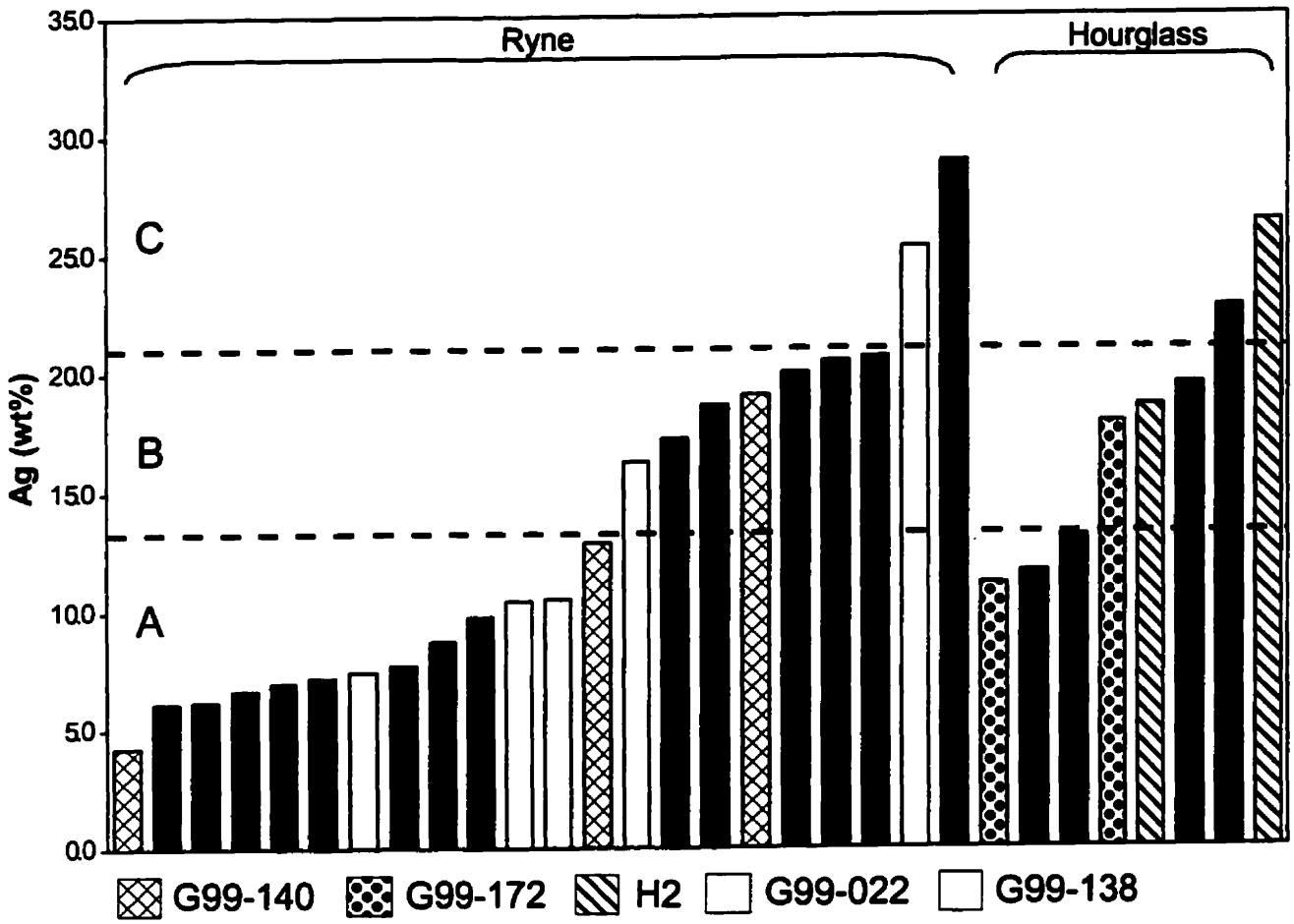
Ryne
Hourglass
35.0
30.0
25.0
20.0
15.0
10.0
5.0
0.0
Ag (wt%)
C
B
A
G99-140
G99-172
H2
G99-022
G99-138

Figure 16: A: Interpreted oxygen isotopic compositions of the Onaman ore fluid compared to those of magmatic water, metamorphic water, meteoric water, and ore fluids of other lode gold deposits. Adapted from Ridley and Diamond, 2000. B: Oxygen and carbon isotopic composition of ankerite from Onaman compared to carbonate minerals of other gold deposits. Adapted from Kerrich, 1990.

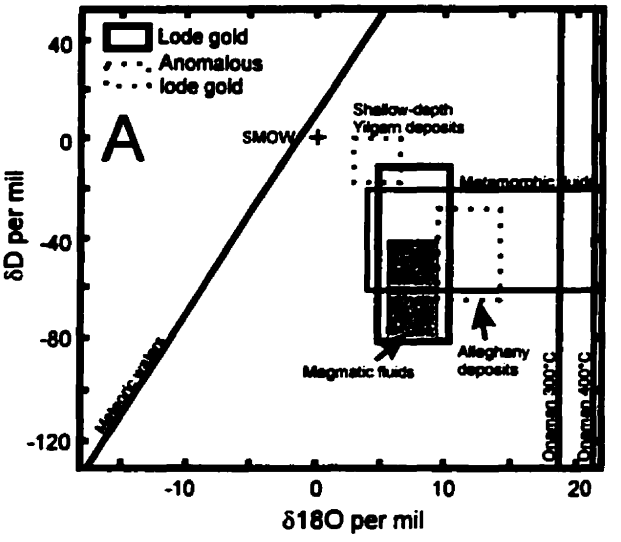
Lode gold
Anomalous
lode gold
A
SMOW
Shallow-depth
Yilgarn deposits
Metamorphic fluid
Meteoric water
Magmatic fluids
Alleghany
deposits
Onaman 300°C
Onaman 400°C
40
0
-40
-80
-120
-10
0
10
20
δD per mil
δ18O per mil

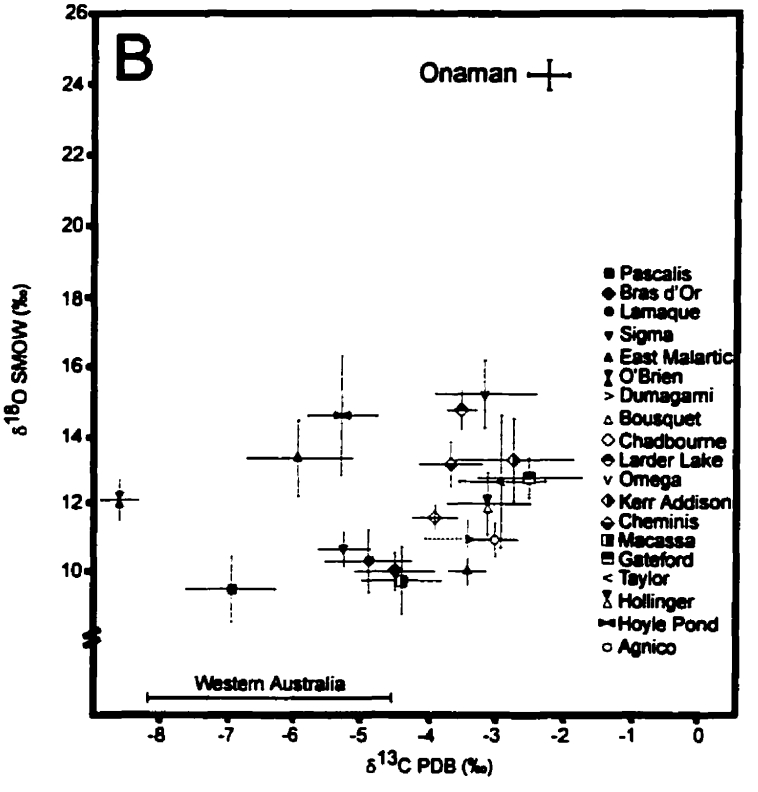
B
Onaman
Pascalis
Bras d'Or
Lamaque
Sigma
East Malartic
O'Brien
Dumagami
Bousquet
Chadbourne
Larder Lake
Omega
Kerr Addison
Cheminis
Macassa
Gateford
Taylor
Hollinger
Hoyle Pond
Agnico
Western Australia
26
24
22
20
18
16
14
12
10
-8
-7
-6
-5
-4
-3
-2
-1
0
δ18O SMOW (‰)
δ13C PDB (‰)

Figure 17: Sulfur isotopic composition of pyrite from lapilli tuff from the Ryne showing and felsite dykes of the Hourglass showing as a function of gold grade.

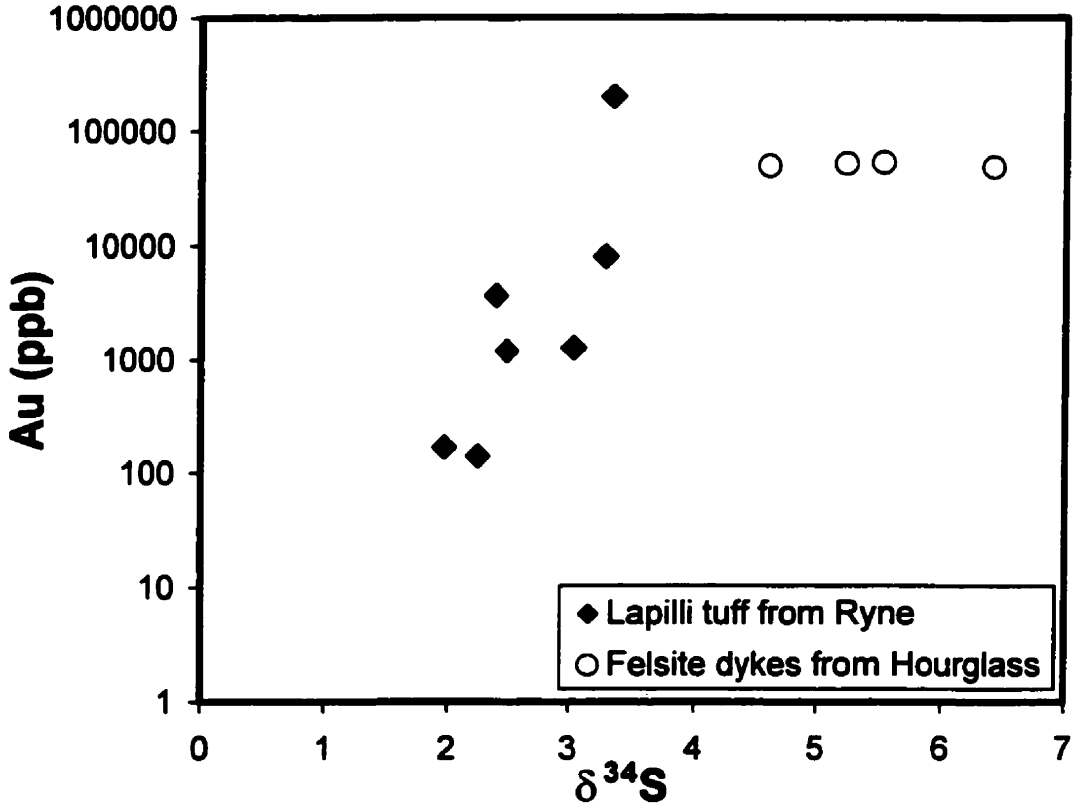
1000000
100000
10000
1000
100
10
1
Au (ppb)
0
1
2
3
4
5
6
7
δ34S
Lapilli tuff from Ryne
Felsite dykes from Hourglass

Figure 18: Phase diagram showing the stability fields of ore and selected alteration minerals at pressure-temperature conditions estimated for the Onaman property. Contours of gold solubility in ppb for Cl-complexes (low pH) and bisulfide complexes (neutral pH), and contours of chalcopyrite solubility in ppm are also shown (dotted line: Cu(HS)2-; dashed line: CuCl2-). The star indicates the approximate initial composition of the mineralizing fluid. SS: 0.1 m; [Cl-]: 1.0 m; [C]: 0.1 m; [Ca]: 0.001 m; [Mg]: 0.0001 m; [Na]: 0.1 m; [K]: 0.002 m. Py: pyrite, Po: pyrrhotite, Hem: hematite, Mag: magnetite, Ccp: chalcopyrite, Bn: bornite, Pg: paragonite, Ab: albite, Ms: muscovite, Kfs: K-feldspar.

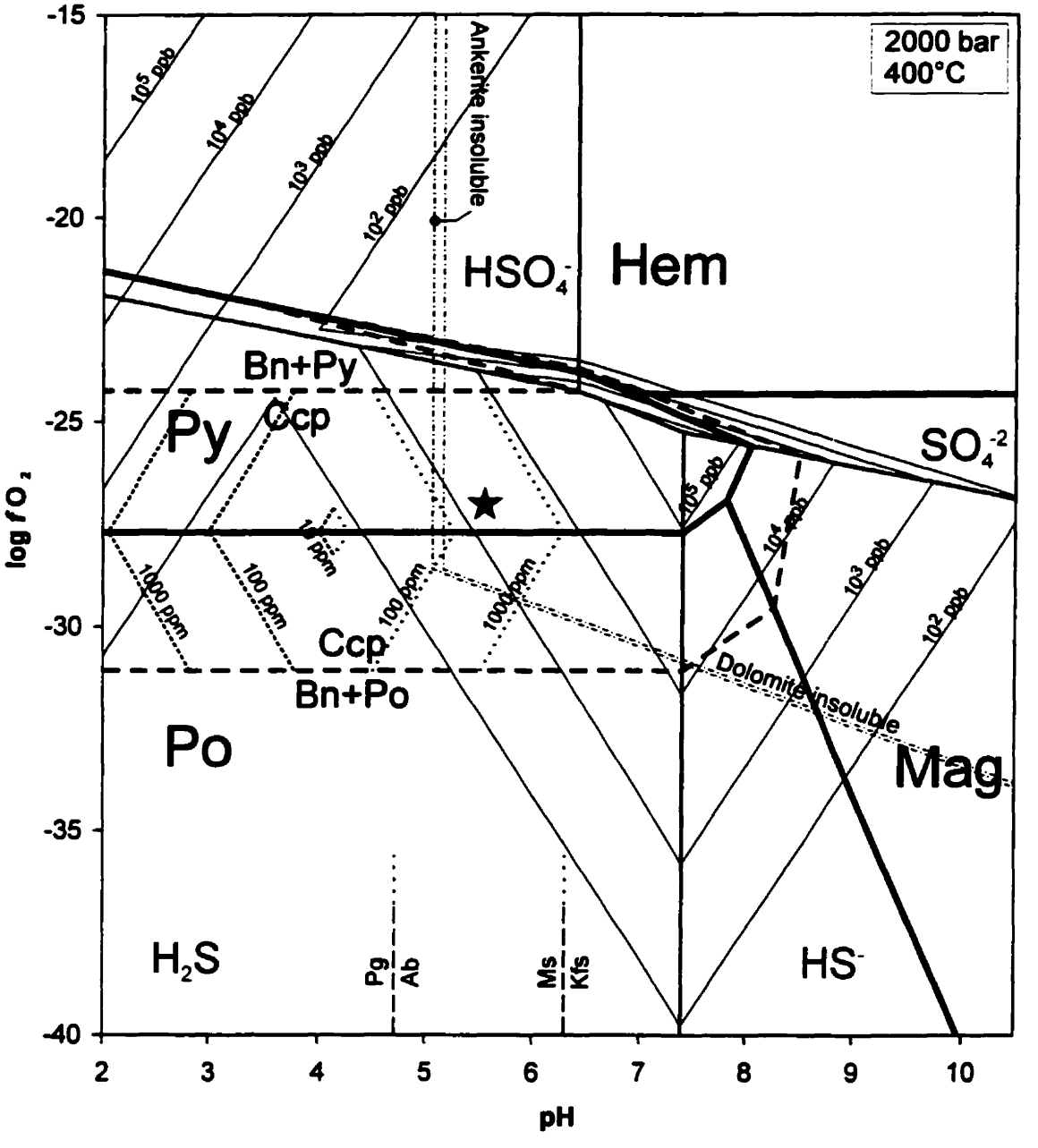
2000 bar
400°C
Ankerite insoluble
HSO4-
Hem
Bn+Py
Py
Ccp
SO4-2
Ccp
Bn+Po
Po
Dolomite insoluble
Mag
H2S
HS-
Pg
Ab
Ms
Kfs
log fO2
pH
-15
-20
-25
-30
-35
-40
2
3
4
5
6
7
8
9
10

Figure 19: Phase diagram showing the predominance boundaries of minerals in the Fe-O-S system, the gold solubility in ppb and the chalcopyrite solubility in ppm, both as bisulfide complexes, under the estimated physico-chemical conditions at Onaman. Star indicates initial position of mineralizing fluid. [Cl-]: 1.0 m. See figure 18 for mineral abbreviations.

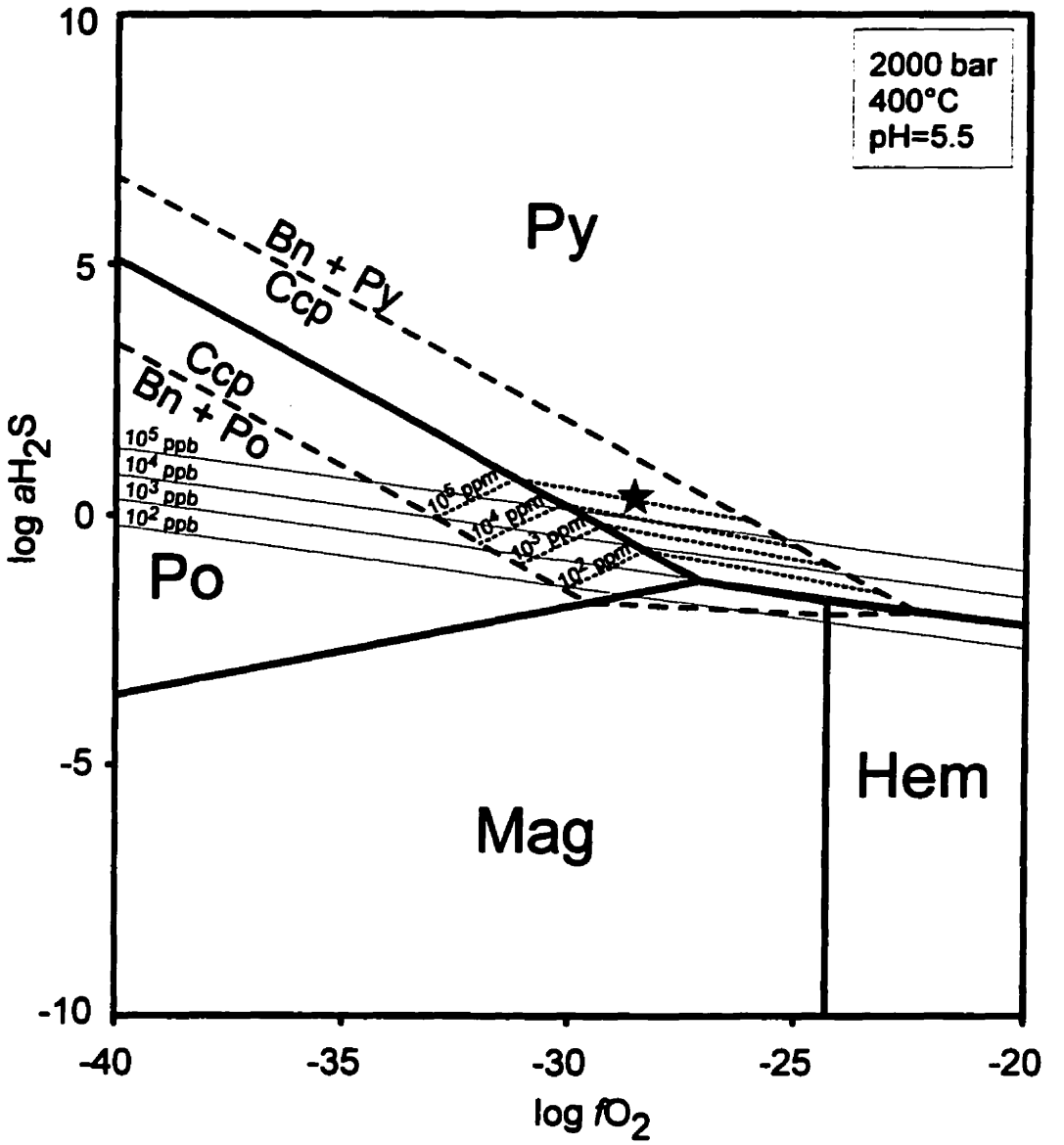
2000 bar
400°C
pH=5.5
Py
Bn + Py
Ccp
Ccp
Bn + Po
10^5 ppb
10^4 ppb
10^3 ppb
10^2 ppb
10^5 ppm
10^4 ppm
10^3 ppm
10^2 ppm
Po
Mag
Hem
10
5
0
-5
-10
-40
-35
-30
-25
-20
log aH_2S
log fO_2

Figure 20: Phase diagram showing the stability fields of ore minerals and contours of δ34S for H_2S, calculated using the method described by Ohmoto (1972). Conditions and mineral abbreviations are identical to those of figure 18. The path starting at the star and following the arrow will produce heavier pyrite and the replacement of pyrite by pyrrhotite. Solubility contours of gold and chalcopyrite have been omitted for clarity, but are identical to those of figure 18.

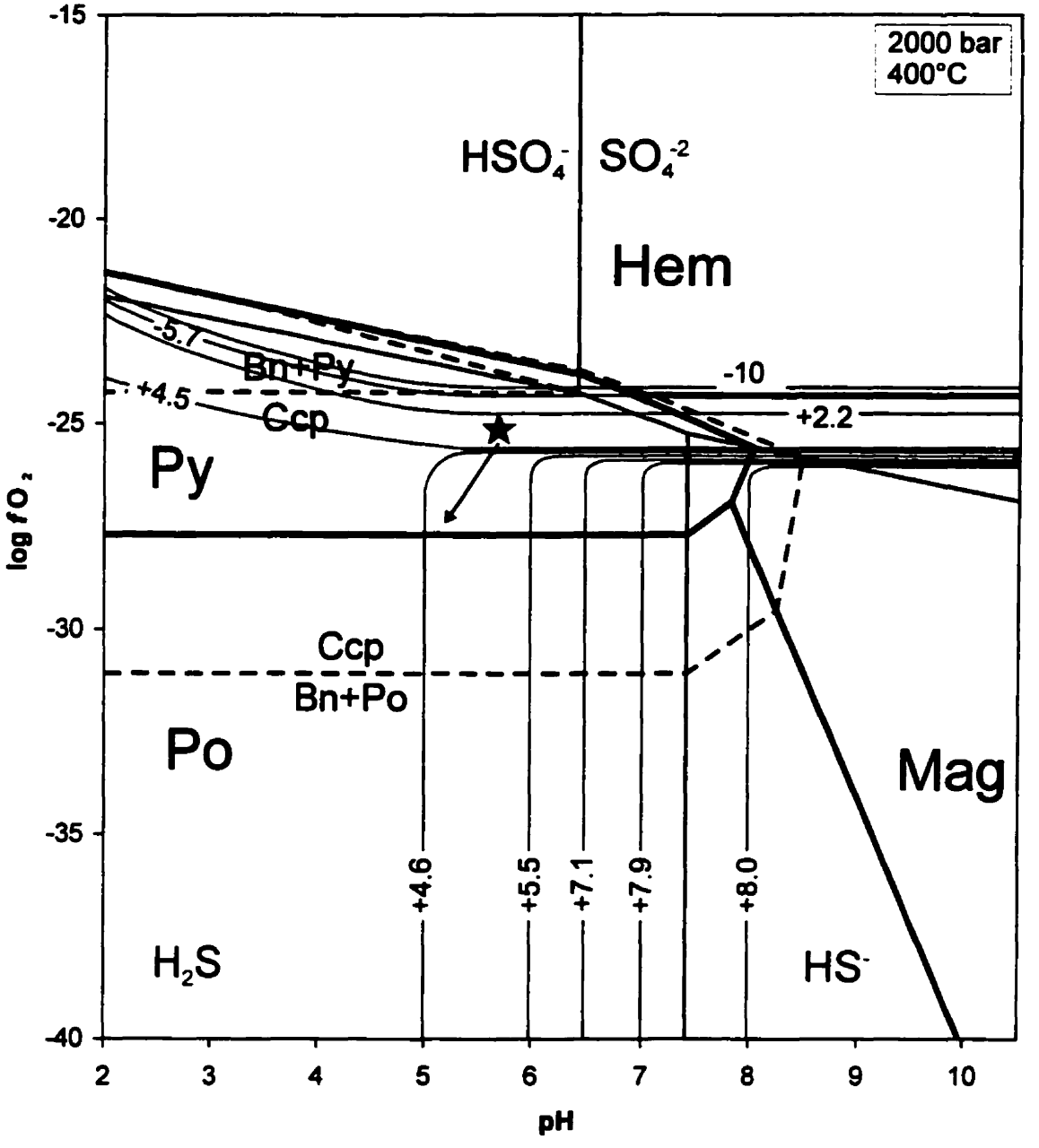
2000 bar
400°C
HSO4-
SO4-2
Hem
-5.7
Bn+Py
+4.5
Ccp
-10
+2.2
Py
Ccp
Bn+Po
Po
Mag
+4.6
+5.5
+7.1
+7.9
+8.0
H2S
HS-
log fO2
pH
-15
-20
-25
-30
-35
-40
2
3
4
5
6
7
8
9
10

TABLES

Table 1. Major (wt%), metals and trace element content of typical rocks at Onaman

	Metavolcaniclastic Ryne 1147	Metavolcaniclastic Ryne (mineralized) 1033	Metavolcaniclastic Hourglass 8859	Felsite dyke Hourglass 1150
SiO2	71.74	61.92	71.26	73.86
TiO2	0.46	0.43	0.50	0.31
Al2O3	15.79	10.90	14.96	12.90
Fe2O3	2.15	9.92	3.41	2.43
MnO	0.05	0.26	0.04	0.04
MgO	0.52	3.73	0.95	0.60
CaO	3.22	8.73	2.00	2.14
Na2O	4.03	1.37	5.08	7.45
K2O	1.87	2.69	1.66	0.19
P2O5	0.15	0.06	0.13	0.09
TOTAL	100	100	100	100
LOI	3.05	12.29	3.19	3.03
Total S	0.01	2.15	0.09	0.44
Total C	0.54	3.27	0.63	0.75
Au ppb	5	1230	32	48200
Ag ppb	<400	600	<400	1900
Cu ppm	13	124	11	5
Zn ppm	46	71	70	33
Sb ppm	0.6	2.3	0.6	<1
W ppm	<1	16	<1	4
Zr ppm	174	57	149	84
Y ppm	14	14	12	8
Nb ppm	5	2	4	2

Table 2. Representative mass balance calculation results for selected elements

	Metavolcaniclastic Ryne 1147 5 ppb Au		Metavolcaniclastic Ryne (mineralized) 1029 7500 ppb Au		Metavolcaniclastic Hourglass 8859 32 ppb Au		Felsite dyke Hourglass 1150 48200 ppb Au	
	Absolute (wt%)	Relative %	Absolute (wt%)	Relative %	Absolute (wt%)	Relative %	Absolute (wt%)	Relative %
SiO2	-8.56	-11.94	-3.42	-5.88	-2.26	-3.18	3.54	4.79
Fe2O3	-2.25	-104.51	2.80	34.23	-1.58	-46.22	-0.83	-34.37
MgO	-0.94	-178.92	1.34	37.20	-0.90	-94.61	-0.32	-54.17
CaO	0.78	24.17	5.37	63.65	-0.74	-36.84	0.88	40.98
Na2O	-0.46	-11.34	3.29	50.06	0.87	17.17	3.69	49.46
K2O	-1.33	-71.08	-1.40	-184.51	-1.14	-68.65	-3.07	-1652.97

Table 3. Carbon and oxygen isotopic ratios of ankerite

		δ13C (vs PDB)	δ18O (vs SMOW)	Fluid δ18O 300°C	Fluid δ18O 400°C
022	Ryne	-2.4	23.6	18.2	20.9
090	Ryne	-2.2	24.3	18.9	21.7
154	Hourglass	-2.2	24.2	18.8	21.5
175	Ryne	-2.5	24.2	18.8	21.6
176	Hourglass	-2.6	24.1	18.7	21.4
R3	Ryne	-2.3	23.9	18.5	21.2
142	Ryne	-1.6	25.0	19.6	22.4
024	Ryne	-2.2	24.0	18.6	21.4

Analyses performed by Centre GEOTOP, Université du Québec à Montréal.

Table 4. Sulfur isotopic ratios of pyrite

Sample	Location	Lithology	Au (ppb)	δ34S
G99-011	Ryne	Metavolc.	140	2.2
G99-022	Ryne	Metavolc.	8090	3.3
G99-023	Ryne	Metavolc.	1270	3.0
G99-031	Ryne	Mass. sulfide	170	2.0
G99-066	Ryne	Metavolc.	1200	2.5
G99-088	Ryne	Mass. sulfide	3690	2.4
G99-175	Ryne	Metavolc.	200000	3.3
G99-152	Hourglass	Felsite	49200	4.6
G99-154	Hourglass	Felsite	51450	5.2
G99-172	Hourglass	Felsite	52500	5.5
G99-176	Hourglass	Felsite	48200	6.4

Analyses performed by EIL, University of Waterloo.

APPENDIX A

Bulk-rock geochemistry

	ONA97-1-17	ONA97-1-34	OG99C-1146	OG99C-1147	OG99C-8859	ONA97-1-1001
	Ryne Lapilli tuff	Ryne Lapilli tuff	Ryne Lapilli tuff	Ryne Lapilli tuff	Ryne Lapilli tuff	Ryne Lapilli tuff
Au g/t	0.006	0.021	0.004	0.005	0.032	0.07
SiO2 wt%	70.99	71.23	60.38	71.74	71.26	68.70
TiO2	0.42	0.40	0.44	0.46	0.50	0.37
Al2O3	15.44	15.13	14.65	15.79	14.96	13.62
Fe2O3	2.41	2.40	12.90	2.15	3.41	2.52
MnO	0.06	0.04	0.35	0.05	0.04	0.07
MgO	0.85	0.49	1.72	0.52	0.95	0.76
CaO	4.14	3.84	4.78	3.22	2.00	6.64
Na2O	4.32	4.38	3.90	4.03	5.08	6.78
K2O	1.23	1.96	0.43	1.87	1.66	0.42
P2O5	0.13	0.12	0.43	0.15	0.13	0.13
Cr2O3	0.00	0.00	0.00	0.00	0.00	0.00
TOTAL	100	100	100	100	100	100
LOI	3.64	3.98	5.33	3.05	3.19	5.42
S/TOT	0.01	0.29	< D.L.	0.01	0.09	0.14
C/TOT	0.71	0.87	0.94	0.54	0.63	1.57
Zr ppm	173	154	158	174	149	146
Y	14	12	14	14	12	13
Nb	5	4	6	5	4	4
Ag	< D.L.	< D.L.	< D.L.	< D.L.	< D.L.	< D.L.
As	0.9	7.5	2.3	0.25	10.6	10.5
Mo	< D.L.	< D.L.	< D.L.	< D.L.	< D.L.	< D.L.
Cu	20	32	14	13	11	22
Pb	7	11	6	10	8	6
Zn	63	56	102	46	70	81
Ni	6	4	8	6	8	7
V	53	57	65	59	58	59
Ba	311	424	153	439	215	116
W	< D.L.	4	1	< D.L.	< D.L.	5
Cr	18	19	21	21	17	75
Hg	< D.L.	< D.L.	< D.L.	< D.L.	< D.L.	8
Sr	202	190	227	285	199	265
Be	1	< D.L.	2	1	1	< D.L.
Co	4	4	8	3	7	4
Cs	3	4	0.5	4	3	0.5
Hf	3	3	4	3	3	2
Rb	37	61	10	56	41	13
Sb	0.5	0.7	0.7	0.6	0.6	0.8
Sn	10	8	6	13	2.5	14
Ta	< D.L.	< D.L.	< D.L.	< D.L.	< D.L.	1.4
Th	3	3.5	4.2	4.3	2.8	2
U	< D.L.	1	1.2	< D.L.	1.7	< D.L.
Ga	16	17	11	17	16	12
Se	0.3	0.3	0.4	0.3	0.3	0.3
Te	< D.L.	0.1	< D.L.	< D.L.	< D.L.	< D.L.
La	18.7	17.7	29.4	28	18	15.2
Ce	32	31	49	47	34	22
Nd	9	8	18	16	10	2.5
Sm	2.3	2.1	3	3	2.5	1.7
Eu	0.6	0.6	0.7	0.9	0.7	0.4
Yb	0.7	0.7	1.3	0.9	0.6	0.6
Lu	0.11	0.12	0.15	0.12	0.09	0.09
Dy	-	-	-	-	-	-
Er	-	-	-	-	-	-
Gd	-	-	-	-	-	-
Ho	-	-	-	-	-	-
Pr	-	-	-	-	-	-
Tm	-	-	-	-	-	-

	ONA97-1-1011	ONA97-1-1014	ONA98x-7106	ONA98x-7107	ONA97-9-1635	ONA97-9-1636
	Ryne Lapilli tuff	Ryne Lapilli tuff	Ryne Lapilli tuff	Ryne Lapilli tuff	Ryne Lapilli tuff	Ryne Lapilli tuff
Au g/t	0.893	0.004	0.63	0.0025	0.87	0.25
SiO2 wt%	64.30	72.34	70.54	68.99	64.55	62.81
TiO2	0.39	0.42	0.47	0.53	1.14	0.77
Al2O3	14.88	15.39	13.95	15.08	16.72	15.29
Fe2O3	8.48	1.52	3.79	4.86	4.76	5.56
MnO	0.22	0.03	0.04	0.06	0.09	0.12
MgO	1.52	0.37	1.97	3.05	1.34	2.36
CaO	5.71	3.43	3.01	2.12	4.03	6.18
Na2O	2.31	3.76	4.01	2.49	4.19	3.95
K2O	2.08	2.63	2.13	2.69	3.06	2.83
P2O5	0.11	0.12	0.08	0.13	0.13	0.12
Cr2O3	0.00	0.00	0.01	0.01	0.01	0.01
TOTAL	100	100	100	100	100	100
LOI	6.05	3.37	4.29	4.51	5.7	8.11
S/TOT	1.84	0.07	-	-	-	-
C/TOT	1.23	0.82	-	-	-	-
Zr ppm	150	168	121	120.5	-	-
Y	15	13	9.5	8.5	-	-
Nb	5	5	4	4	-	-
Ag	1	< D.L.	< D.L.	< D.L.	-	-
As	7	4.2	-	-	46	36
Mo	< D.L.	< D.L.	< D.L.	< D.L.	1	3
Cu	167	26	25	< D.L.	-	-
Pb	5	7	20	20	-	-
Zn	95	50	20	25	-	-
Ni	8	3	30	25	-	-
V	78	49	75	60	-	-
Ba	494	483	298	424	-	-
W	< D.L.	4	43	2	-	-
Cr	74	58	-	-	-	-
Hg	11	6	-	-	-	-
Sr	175	165	215	145	-	-
Be	1	2	-	-	-	-
Co	10	4	11.5	10.5	-	-
Cs	5	4	3	2.9	-	-
Hf	3	3	4	3	-	-
Rb	69	74	61.6	72.6	-	-
Sb	0.7	0.5	-	-	-	-
Sn	10	11	1	1	-	-
Ta	< D.L.	< D.L.	0.5	0.5	-	-
Th	3.3	2.7	1	1	-	-
U	< D.L.	0.7	0.5	0.5	-	-
Ga	11	15	16	20	-	-
Se	0.6	0.3	-	-	-	-
Te	4.6	< D.L.	-	-	-	-
La	16	16.1	21.5	18	-	-
Ce	27	29	42	36	-	-
Nd	12	12	17	15.5	-	-
Sm	2.1	2.1	2.6	2.3	-	-
Eu	0.5	0.5	1	0.8	-	-
Yb	1	0.6	1.1	0.9	-	-
Lu	0.15	0.1	0.1	0.1	-	-
Dy	-	-	1.7	1.6	-	-
Er	-	-	0.9	0.9	-	-
Gd	-	-	2.9	2.2	-	-
Ho	-	-	0.4	0.3	-	-
Pr	-	-	4.6	4.3	-	-
Tm	-	-	0.1	0.1	-	-

	ONA97-8-1637	ONA98C-8030	ONA97-1-1029	ONA97-1-1031	ONA97-1-1033	ONA97-1-1036
	Ryne Lapilli tuff	Hourglass Lapilli tuff	Ryne Metavolc.	Ryne Metavolc.	Ryne Metavolc.	Ryne Metavolc.
Au g/t	3.3	0.01	7.5	0.292	1.23	1.2
SiO2 wt%	64.22	69.81	58.10	57.61	61.92	69.26
TiO2	0.52	0.43	0.57	0.52	0.43	0.28
Al2O3	15.36	15.90	13.57	12.68	10.90	10.56
Fe2O3	5.24	3.49	8.17	8.04	9.92	9.36
MnO	0.07	0.06	0.18	0.21	0.26	0.21
MgO	2.15	1.11	3.59	4.25	3.73	2.09
CaO	3.96	3.02	8.44	9.87	8.73	4.68
Na2O	7.61	3.43	6.58	5.89	1.37	1.06
K2O	0.82	2.63	0.76	0.89	2.69	2.51
P2O5	0.04	0.12	0.03	0.04	0.06	0.01
Cr2O3	0.01	0.01	0.00	0.00	0.00	0.00
TOTAL	100	100	100	100	100	100
LOI	5.06	4.05	10.89	12.8	12.29	9.63
S/TOT	-	-	1.75	0.59	2.15	4.87
C/TOT	-	-	3.19	3.78	3.27	1.79
Zr ppm	-	129	84	54	57	93
Y	-	8	14	11	14	11
Nb	-	3	3	1	2	3
Ag	-	< D.L.	2.9	< D.L.	0.6	0.7
As	88	-	691	163	6720	1570
Mo	20	1	2	2	2	5
Cu	-	25	118	84	124	127
Pb	-	20	10	5	8	10
Zn	-	75	76	83	71	68
Ni	-	15	57	58	60	23
V	-	45	128	143	133	80
Ba	-	459	170	149	356	336
W	-	< D.L.	35	36	16	13
Cr	-	-	93	172	183	14
Hg	-	-	8	< D.L.	5	6
Sr	-	226	462	544	296	187
Be	-	-	1	1	1	1
Co	-	8	24	23	40	15
Cs	-	6.7	1	1	3	2
Hf	-	4	2	2	1	2
Rb	-	67.2	22	25	66	62
Sb	-	-	1.9	1.5	2.3	< D.L.
Sn	-	1	11	9	14	11
Ta	-	< D.L.	< D.L.	< D.L.	< D.L.	< D.L.
Th	-	1	2.7	1.5	1.2	1.5
U	-	0.5	< D.L.	< D.L.	< D.L.	< D.L.
Ga	-	19	10	9	10	11
Se	-	-	0.6	0.3	1.3	2.1
Te	-	-	2.2	0.2	0.4	0.7
La	-	20	14	9.4	8.9	10
Ce	-	38	20	14	15	17
Nd	-	14.5	14	9	2.5	2.5
Sm	-	2.9	2.3	1.6	1.7	1.3
Eu	-	0.6	0.6	0.6	0.8	0.5
Yb	-	0.5	1	0.8	0.7	0.6
Lu	-	0.1	0.17	0.12	0.11	0.09
Dy	-	1.5	-	-	-	-
Er	-	0.7	-	-	-	-
Gd	-	2.4	-	-	-	-
Ho	-	0.3	-	-	-	-
Pr	-	4	-	-	-	-
Tm	-	0.1	-	-	-	-

	ONA97-1-1037	ONA97-1-1038	ONA97-1-1039	ONA97-1-1044	ONA98-28-2606	ONA97-8-1641
	Ryne Metavolc.	Ryne Metavolc.	Ryne Metavolc.	Ryne Metavolc.	Ryne Metavolc.	Ryne Metavolc.
Au g/t	0.142	1.06	0.084	0.893	1.73	0.275
SiO2 wt%	54.30	60.60	45.76	58.82	45.36	64.54
TiO2	0.57	0.53	0.57	0.54	0.47	0.50
Al2O3	14.71	13.96	15.75	14.00	14.25	15.78
Fe2O3	9.92	7.22	11.40	8.04	10.14	4.29
MnO	0.29	0.18	0.28	0.24	0.20	0.06
MgO	4.57	3.64	7.68	3.42	7.08	2.45
CaO	10.08	7.85	13.14	8.42	15.14	5.01
Na2O	2.24	3.36	1.49	3.86	5.69	4.60
K2O	3.22	2.58	3.88	2.57	1.60	2.64
P2O5	0.09	0.08	0.05	0.09	0.08	0.13
Cr2O3	0.00	0.00	0.00	0.00	0.00	0.01
TOTAL	100	100	100	100	100	100
LOI	13.68	10.98	17.64	10.94	17.11	6.86
S/TOT	0.5	0.43	0.16	0.84	1.4	-
C/TOT	3.82	2.91	4.86	3.16	5.23	-
Zr ppm	62	80	39	63	35	110
Y	12	13	14	10	11	8
Nb	3	1	1	3	1	4
Ag	< D.L.	< D.L.	< D.L.	< D.L.	0.7	< D.L.
As	721	1930	809	3580	712	-
Mo	< D.L.	7	2	26	13	3
Cu	56	48	17	71	46	15
Pb	< D.L.	6	< D.L.	7	55	25
Zn	86	86	108	84	97	30
Ni	81	46	75	62	73	35
V	160	142	218	149	177	55
Ba	421	335	440	333	288	412
W	22	20	17	17	29	30
Cr	298	138	355	188	156	-
Hg	< D.L.	< D.L.	< D.L.	5	< D.L.	-
Sr	362	380	461	348	653	277
Be	1	2	1	1	1	-
Co	28	25	35	23	30	14.5
Cs	3	3	5	0.5	3	3
Hf	1	2	1	1	0.5	3
Rb	80	63	90	63	40	73.4
Sb	< D.L.	< D.L.	< D.L.	< D.L.	< D.L.	-
Sn	6	7	7	2.5	12	1
Ta	< D.L.	< D.L.	< D.L.	< D.L.	< D.L.	0.5
Th	1.2	2	0.1	2.3	0.1	8
U	< D.L.	1.4	< D.L.	< D.L.	< D.L.	0.5
Ga	10	10	12	12	11	18
Se	0.5	0.4	0.4	0.2	0.4	-
Te	< D.L.	0.2	< D.L.	0.2	1.4	-
La	8.4	10.4	3.2	9.4	3.5	17
Ce	17	18	9	13	8	33.5
Nd	2.5	2.5	2.5	2.5	5	16
Sm	1.6	1.7	1	1.6	0.8	2.8
Eu	0.6	0.6	0.5	0.6	0.1	0.9
Yb	1.2	1.3	1.3	1	1.1	0.9
Lu	0.19	0.2	0.2	0.16	0.14	0.1
Dy	-	-	-	-	-	2.1
Er	-	-	-	-	-	0.8
Gd	-	-	-	-	-	2.5
Ho	-	-	-	-	-	0.4
Pr	-	-	-	-	-	4.2
Tm	-	-	-	-	-	0.1

	ONA97-9-1643	ONA97-9-1639	ONA97-9-1640	ONA98x-7119	ONA97-9-1652	ONA98C-8451
	Ryne Metavolc.	Ryne Metavolc.	Ryne Metavolc.	Ryne Metavolc.	Ryne Metavolc.	Ryne Metavolc.
Au g/t	0.12	1.2	1.2	1.3	0.34	1.62
SiO2 wt%	65.89	64.27	65.80	61.03	65.03	66.10
TiO2	0.45	0.60	0.49	0.72	0.46	0.72
Al2O3	15.00	15.91	14.80	18.81	16.97	16.60
Fe2O3	4.42	5.99	5.64	6.92	4.10	6.83
MnO	0.08	0.09	0.09	0.10	0.04	0.06
MgO	2.28	2.38	2.26	2.71	2.04	1.24
CaO	4.49	3.52	3.57	2.53	3.29	1.35
Na2O	4.73	4.44	5.46	2.61	5.44	3.14
K2O	2.54	2.70	1.80	4.40	2.58	3.89
P2O5	0.13	0.09	0.10	0.16	0.04	0.06
Cr2O3	0.01	0.01	0.01	0.02	0.01	0.01
TOTAL	100	100	100	100	100	100
LOI	6.44	6.14	5.85	5.23	4.94	4.67
S/TOT	-	-	-	-	-	-
C/TOT	-	-	-	-	-	-
Zr ppm	123	160.5	143	103.5	-	140
Y	8	13	12	17	-	14
Nb	4	6	6	5	-	5
Ag	< D.L.	1	1	< D.L.	-	1
As	-	-	-	-	18	-
Mo	8	21	5	4	-	3
Cu	10	30	70	80	-	40
Pb	25	25	40	15	-	5
Zn	35	60	60	90	-	25
Ni	30	100	70	85	-	60
V	50	110	85	115	-	135
Ba	336	419	243	699	-	502
W	31	42	51	29	-	39
Cr	-	-	-	-	-	-
Hg	-	-	-	-	-	-
Sr	270	320	297	203	-	162
Be	-	-	-	-	-	-
Co	13	19.5	19	25	-	21
Cs	3.2	5.4	3.1	5.9	-	4
Hf	3	5	4	4	-	4
Rb	68.2	87.8	53.6	121	-	107
Sb	-	-	-	-	-	-
Sn	1	1	1	< D.L.	-	< D.L.
Ta	0.5	0.5	0.5	0.5	-	0.5
Th	6	18	16	6	-	5
U	0.5	3.5	3.5	3	-	2.5
Ga	16	22	18	25	-	21
Se	-	-	-	-	-	-
Te	-	-	-	-	-	-
La	16	33	26.5	32	-	28.5
Ce	31	61.5	50.5	61.5	-	56
Nd	14.5	27	22.5	26	-	23
Sm	2.6	4.9	3.9	4.9	-	3.7
Eu	0.9	1.3	0.9	1.1	-	1.1
Yb	0.7	1.3	1.3	1.8	-	1.3
Lu	0.1	0.2	0.2	0.2	-	0.1
Dy	1.7	2.7	2.5	3.1	-	2.3
Er	1	1.7	1.5	1.9	-	1.2
Gd	2.3	4.2	3.3	4.5	-	3.6
Ho	0.4	0.6	0.4	0.6	-	0.4
Pr	4	7.7	6.3	7	-	6.1
Tm	0.1	0.2	0.2	0.3	-	0.1

	ONA98x-7109	ONA98x-7110	ONA98C-8672	ONA98x-7047	ONA98x-7048	ONA98C-8012
	Ryne Metavolc.	Ryne Metavolc.	Ryne Metavolc.	Hourglass Metavolc.	Hourglass Metavolc.	Hourglass Metavolc.
Au g/t	0.225	1.53	0.01	0.0025	0.4	0.15
SiO2 wt%	66.16	69.88	70.88	62.73	68.24	70.44
TiO2	0.62	0.52	0.45	0.46	0.53	0.41
Al2O3	16.79	13.64	12.93	14.18	15.88	15.41
Fe2O3	6.20	3.38	3.36	11.46	5.33	3.46
MnO	0.06	0.16	0.13	0.19	0.12	0.05
MgO	2.25	1.41	1.74	2.30	1.14	1.18
CaO	0.95	4.63	3.80	4.30	2.40	2.92
Na2O	3.44	3.75	1.84	3.09	4.00	3.57
K2O	3.41	2.43	4.75	1.17	2.22	2.44
P2O5	0.09	0.18	0.12	0.11	0.13	0.10
Cr2O3	0.02	0.01	0.01	0.01	0.01	0.01
TOTAL	100	100	100	100	100	100
LOI	3.32	5.92	4.45	5.68	3.78	3.87
S/TOT	-	-	-	-	-	-
C/TOT	-	-	-	-	-	-
Zr ppm	128	121.5	116.5	112	134	134
Y	14	9.5	10	9	9.5	9.5
Nb	6	4	4	3	4	5
Ag	< D.L.	< D.L.	< D.L.	< D.L.	< D.L.	< D.L.
As	-	-	-	-	-	-
Mo	2	< D.L.	1	1	1	1
Cu	45	10	< D.L.	20	15	15
Pb	45	15	< D.L.	20	20	20
Zn	75	95	25	105	50	60
Ni	60	20	15	20	10	15
V	145	55	50	30	35	35
Ba	327	542	701	134.5	219	284
W	33	18	2	< D.L.	< D.L.	< D.L.
Cr	-	-	-	-	-	-
Hg	-	-	-	-	-	-
Sr	182	151	75.2	154.5	160	202
Be	-	-	-	-	-	-
Co	18	8.5	8	13.5	8	7.5
Cs	5.7	2.3	10.4	2.8	5.3	6.6
Hf	4	4	3	3	4	4
Rb	114.5	57.8	90.8	47.4	67.6	63.8
Sb	-	-	-	-	-	-
Sn	1	1	< D.L.	1	1	1
Ta	0.5	0.5	< D.L.	0.5	0.5	0.5
Th	6	1	3	2	2	1
U	2.5	0.5	0.5	0.5	0.5	1
Ga	24	16	15	19	19	17
Se	-	-	-	-	-	-
Te	-	-	-	-	-	-
La	33	19.5	20	19	22.5	20
Ce	63.5	38.5	39	36	44.5	37
Nd	25.5	16.5	16	14	18	15
Sm	4.1	2.8	3.5	2.9	3.2	3.3
Eu	1	0.8	0.7	0.9	0.9	0.7
Yb	1	1	0.8	0.9	0.8	0.8
Lu	0.2	0.1	0.1	0.1	0.1	0.1
Dy	2.7	1.7	2	2.1	1.8	1.7
Er	1.5	0.9	1	0.8	1	1
Gd	3.5	2.6	2.2	2.1	2.5	2.5
Ho	0.5	0.4	0.4	0.3	0.4	0.3
Pr	7.1	4.5	4.5	3.9	4.8	4.2
Tm	0.1	0.1	0.1	0.1	0.1	0.1

	ONA98x-7112	ONA98x-7500	OG99C-8867	OG99C-1150	OG99C-8194	ONA98C-8196B
	Hourglass Metavolc.	Hourglass Metavolc.	Hourglass Felsite dyke	Hourglass Felsite dyke	Hourglass Felsite dyke	Hourglass Felsite dyke
Au g/t	0.0025	0.0025	52.5	48.2	49.2	78.03
SiO2 wt%	67.74	68.79	70.55	73.86	76.73	74.27
TiO2	0.36	0.57	0.43	0.31	0.39	0.41
Al2O3	14.15	16.99	14.42	12.90	12.30	12.19
Fe2O3	3.84	3.91	2.83	2.43	3.07	2.97
MnO	0.08	0.06	0.04	0.04	0.04	0.06
MgO	2.79	1.61	0.82	0.60	0.31	0.81
CaO	5.48	2.21	2.41	2.14	0.92	2.49
Na2O	3.69	2.98	8.23	7.45	4.91	6.38
K2O	1.80	2.73	0.17	0.19	1.22	0.31
P2O5	0.08	0.15	0.10	0.09	0.11	0.10
Cr2O3	0.01	0.01	0.00	0.00	0.00	0.01
TOTAL	100	100	100	100	100	100
LOI	7.45	3.59	3.57	3.03	1.89	3.61
S/TOT	-	-	0.91	0.44	0.21	-
C/TOT	-	-	0.92	0.75	0.25	-
Zr ppm	92.5	-	116	84	96	114
Y	7	-	10	8	12	7
Nb	2	-	4	2	3	3
Ag	< D.L.	-	2.9	1.9	0.8	8
As	-	-	40.2	37.1	31.7	-
Mo	2	< D.L.	< D.L.	< D.L.	< D.L.	2
Cu	< D.L.	-	16	5	41	10
Pb	25	-	8	8	9	20
Zn	80	-	40	33	43	45
Ni	20	-	9	7	8	15
V	60	-	20	14	54	20
Ba	288	-	54	31	162	46.5
W	1	-	< D.L.	4	< D.L.	3
Cr	-	-	39	39	19	-
Hg	-	-	63	20	47	-
Sr	190.5	-	247	201	125	225
Be	-	-	1	< D.L.	< D.L.	-
Co	9	-	8	9	16	6.5
Cs	3.6	-	0.5	0.5	4	0.5
Hf	3	-	3	2	3	3
Rb	40.8	-	7	6	33	6.4
Sb	-	-	0.8	0.5	0.7	-
Sn	< D.L.	-	9	2.5	5	< D.L.
Ta	< D.L.	-	< D.L.	< D.L.	< D.L.	< D.L.
Th	1	-	2.5	2.9	2.5	1
U	0.5	-	< D.L.	< D.L.	< D.L.	0.5
Ga	18	-	13	11	10	13
Se	-	-	0.4	0.3	0.3	-
Te	-	-	0.1	< D.L.	< D.L.	-
La	11.5	-	17.7	14.2	21.9	17.5
Ce	21	-	35	23	37	32.5
Nd	9	-	12	6	24	14
Sm	1.6	-	2.8	1.8	3.2	2.4
Eu	0.6	-	0.7	0.4	0.8	0.6
Yb	0.8	-	0.5	0.8	0.9	0.7
Lu	0.1	-	0.07	0.12	0.13	< D.L.
Dy	1.5	-	-	-	-	1.3
Er	0.8	-	-	-	-	0.7
Gd	1.8	-	-	-	-	1.9
Ho	0.3	-	-	-	-	0.3
Pr	2.5	-	-	-	-	3.7
Tm	0.1	-	-	-	-	0.1

	ONA98-27-2559	ONA98C-8472B	ONA98C-8484A	ONA98x-7017	ONA98x-7018	ONA98x-7118
	Ryne QFP	Ryne QFP	Ryne QFP	Ryne QFP	Ryne QFP	Ryne FQP
Au g/t	0.118	0.33	0.1	0.0025	0.0025	0.01
SiO2 wt%	75.93	74.92	74.10	71.90	71.95	57.58
TiO2	0.14	0.21	0.21	0.28	0.37	1.04
Al2O3	13.00	14.12	14.72	15.65	14.71	15.76
Fe2O3	1.61	1.96	1.57	2.39	3.46	9.08
MnO	0.03	0.01	0.03	0.05	0.06	0.13
MgO	0.46	0.01	0.09	0.91	1.39	4.59
CaO	1.45	0.26	0.48	2.33	2.30	5.44
Na2O	6.74	8.32	8.55	4.51	4.63	4.45
K2O	0.50	0.08	0.10	1.92	1.07	1.72
P2O5	0.14	0.10	0.11	0.05	0.05	0.20
Cr2O3	0.00	0.01	0.02	0.01	0.01	0.01
TOTAL	100	100	100	100	100	100
LOI	1.75	0.97	1	2.55	1.72	8.76
S/TOT	0.66	-	-	-	-	-
C/TOT	0.48	-	-	-	-	-
Zr ppm	82	88	72.5	120	97	92
Y	7	3	3	4.5	6.5	12.5
Nb	1	0.5	0.5	3	3	4
Ag	< D.L.	< D.L.	< D.L.	< D.L.	< D.L.	< D.L.
As	10.1	-	-	-	10	-
Mo	7	1	< D.L.	1	-	< D.L.
Cu	5	< D.L.	< D.L.	20	40	40
Pb	5	5	5	20	20	5
Zn	19	15	< D.L.	60	75	65
Ni	8	5	5	15	30	70
V	20	20	15	25	50	120
Ba	148	45	39	329	237	405
W	10	22	17	< D.L.	< D.L.	1
Cr	93	-	-	-	-	-
Hg	< D.L.	-	-	-	-	-
Sr	124	74.1	100	277	254	333
Be	< D.L.	-	-	-	-	-
Co	4	3.5	4.5	5.5	12	27
Cs	0.5	0.1	0.1	1.7	1.1	2.6
Hf	1	3	3	3	3	3
Rb	14	1.2	1.6	62.8	30	55.8
Sb	0.4	-	-	-	-	-
Sn	6	< D.L.	< D.L.	1	1	< D.L.
Ta	< D.L.	< D.L.	< D.L.	1	0.5	< D.L.
Th	1.5	0.5	0.5	5	5	2
U	< D.L.	0.5	0.5	0.5	1	1
Ga	17	18	18	21	17	19
Se	< D.L.	-	-	-	-	-
Te	0.9	-	-	-	-	-
La	6.1	9	9.5	12.5	12.5	19.5
Ce	11	18	17.5	21.5	23.5	41.5
Nd	2.5	7	6.5	9	9.5	20.5
Sm	0.8	1.3	1.4	1.4	1.4	3.9
Eu	0.2	0.3	0.3	0.6	0.7	0.9
Yb	0.2	0.3	0.2	0.5	0.8	1.1
Lu	0.025	< D.L.	< D.L.	< D.L.	0.1	0.1
Dy	-	0.5	0.8	0.8	1.3	2.2
Er	-	0.3	0.2	0.5	0.7	1.3
Gd	-	1	1.1	1.4	1.7	3.3
Ho	-	< D.L.	< D.L.	0.1	0.3	0.4
Pr	-	1.8	1.8	2.6	2.7	4.8
Tm	-	< D.L.	< D.L.	0.1	0.1	0.1

	ONA98C-8012	ONA97-9-139	ONA97-9-287	ONA98-24-115	ONA97-1-1051	ONA97-1-1050
	Hourglass QFP	Ryne Gabbro	Ryne Gabbro	Ryne Gabbro	Ryne Gabbro	Ryne Gabbro
Au g/t	0.15	0.012	0.013	0.004	2.43	0.83
SiO2 wt%	70.44	52.41	50.72	56.43	54.90	54.07
TiO2	0.41	0.70	0.32	0.91	1.13	1.30
Al2O3	15.41	11.11	8.67	14.62	12.48	12.26
Fe2O3	3.46	10.49	11.06	9.05	13.72	14.93
MnO	0.05	0.19	0.25	0.12	0.20	0.17
MgO	1.18	11.14	16.33	5.85	4.16	5.04
CaO	2.92	10.71	11.82	7.83	8.05	7.63
Na2O	3.57	2.85	0.46	4.02	3.99	2.34
K2O	2.44	0.15	0.35	1.00	1.26	2.14
P2O5	0.10	0.25	0.04	0.17	0.11	0.11
Cr2O3	0.01	0.00	0.00	0.00	0.00	0.01
TOTAL	100	100	100	100	100	100
LOI	3.87	15.05	16.55	9.07	11.59	8.63
S/TOT	-	0.17	0.13	0.16	0.94	-
C/TOT	-	3.84	3.99	1.96	3.29	-
Zr ppm	134	70	27	87	77	93
Y	9.5	13	9	13	22	20
Nb	5	3	1	4	3	4
Ag	< D.L.	< D.L.	< D.L.	< D.L.	1	< D.L.
As	-	0.9	8.9	2.6	3280	-
Mo	1	< D.L.	68	< D.L.	< D.L.	2
Cu	15	115	8	33	134	130
Pb	20	10	< D.L.	< D.L.	6	20
Zn	60	133	88	106	100	105
Ni	15	104	321	97	23	75
V	35	176	154	142	330	340
Ba	284	69	47	296	179	261
W	< D.L.	< D.L.	< D.L.	< D.L.	23	17
Cr	-	680	1230	181	37	-
Hg	-	< D.L.	< D.L.	< D.L.	7	-
Sr	202	503	195	339	272	255
Be	-	< D.L.	< D.L.	1	2	-
Co	7.5	43	65	31	39	42
Cs	6.6	0.5	3	3	6	5.9
Hf	4	1	0.5	2	0.5	3
Rb	63.8	6	12	27	35	62
Sb	-	2.4	0.8	1.7	< D.L.	-
Sn	1	7	8	9	8	1
Ta	0.5	< D.L.	< D.L.	< D.L.	0.9	0.5
Th	1	3.3	0.1	3	1.8	5
U	1	< D.L.	< D.L.	1	< D.L.	< D.L.
Ga	17	8	3	12	12	18
Se	-	0.5	0.2	0.4	0.6	-
Te	-	< D.L.	1.6	< D.L.	0.4	-
La	20	19.1	1.4	15.9	5.9	6.5
Ce	37	39	1.5	29	10	15.5
Nd	15	16	2.5	18	2.5	9.5
Sm	3.3	3.7	0.6	2.9	2.3	2.9
Eu	0.7	0.9	0.2	0.9	0.4	0.9
Yb	0.8	1	0.8	1	2.5	2.5
Lu	0.1	0.14	0.12	0.13	0.34	0.5
Dy	1.7	-	-	-	-	4
Er	1	-	-	-	-	2.7
Gd	2.5	-	-	-	-	3.7
Ho	0.3	-	-	-	-	0.9
Pr	4.2	-	-	-	-	2.1
Tm	0.1	-	-	-	-	0.5

	ONA97-1-1051	ONA97-9-1654	ONA98x-7108	ONA98x-7104	ONA98x-7105	ONA98x-7111
	Ryne Gabbro	Ryne Gabbro	Ryne Gabbro	Ryne Mafic intrusion	Ryne Mafic intrusion	Ryne Mafic intrusion
Au g/t	2.34	0.0025	0.01	0.0025	0.015	0.025
SiO2 wt%	54.38	51.59	53.18	51.95	53.62	52.92
TiO2	1.17	0.22	0.64	1.02	0.60	1.33
Al2O3	12.02	5.94	15.60	15.90	15.63	17.54
Fe2O3	14.01	12.04	11.24	13.42	10.50	11.16
MnO	0.20	0.25	0.19	0.28	0.18	0.22
MgO	4.36	20.30	6.25	5.10	7.48	3.03
CaO	8.32	9.30	8.17	8.19	8.91	8.06
Na2O	4.00	0.04	1.48	3.47	0.98	2.81
K2O	1.40	0.05	3.16	0.56	2.02	2.84
P2O5	0.11	0.01	0.08	0.11	0.07	0.07
Cr2O3	0.01	0.28	0.01	0.01	0.01	0.02
TOTAL	100	100	100	100	100	100
LOI	10.12	14.42	12.51	8.55	10.19	8.06
S/TOT	-	-	-	-	-	-
C/TOT	-	-	-	-	-	-
Zr ppm	84	-	41	68	35.5	55.5
Y	21	-	13	17	13	19.5
Nb	3	-	1	3	1	1
Ag	< D.L.	-	< D.L.	< D.L.	< D.L.	< D.L.
As	-	24	-	-	-	-
Mo	1	-	< D.L.	8	2	< D.L.
Cu	140	-	60	10	155	125
Pb	25	-	20	15	25	10
Zn	90	-	75	90	60	100
Ni	60	-	75	60	80	130
V	295	-	220	345	225	185
Ba	196	-	368	226	527	373
W	24	-	10	3	3	9
Cr	-	-	-	-	-	-
Hg	-	-	-	-	-	-
Sr	281	-	173.5	101	99.8	203
Be	-	-	-	-	-	-
Co	39	-	35.5	34	35.5	54.5
Cs	5.8	-	3.1	0.8	2	3
Hf	2	-	1	2	1	2
Rb	38.6	-	83.4	12	54	78
Sb	-	-	-	-	-	-
Sn	1	-	< D.L.	< D.L.	< D.L.	< D.L.
Ta	< D.L.	-	< D.L.	< D.L.	< D.L.	< D.L.
Th	3	-	0.5	0.5	0.5	0.5
U	< D.L.	-	< D.L.	< D.L.	< D.L.	< D.L.
Ga	15	-	15	17	14	20
Se	-	-	-	-	-	-
Te	-	-	-	-	-	-
La	6	-	3.5	6.5	3.5	4
Ce	14	-	7.5	12.5	7.5	11
Nd	9	-	5	8	5	8
Sm	2.6	-	1	1.9	1.1	2
Eu	0.9	-	0.6	0.8	0.3	0.8
Yb	2.3	-	1.3	1.5	1.4	2.4
Lu	0.4	-	0.2	0.2	0.2	0.3
Dy	3.9	-	2.2	3.4	2.2	3.4
Er	2.7	-	1.2	1.8	1.5	2
Gd	3.2	-	1.7	2.8	1.8	3.7
Ho	0.9	-	0.5	0.6	0.5	0.8
Pr	2	-	1	1.8	1	1.7
Tm	0.4	-	0.2	0.3	0.2	0.3

	ONA98x-7113	ONA98x-7114	ONA98x-7116	ONA98x-7117	ONA97-1-1028	ONA98x-7045A
	Ryne Ultramafic intr.	Ryne Ultramafic intr.	Ryne Mafic intrusion	Ryne Lamprophyre	Ryne Lamprophyre	Ryne Mafic intrusion
Au g/t	0.015	< D.L.5	0.02	0.02	0.005	< D.L.
SiO2 wt%	42.40	51.33	47.68	54.03	53.84	55.68
TiO2	0.22	0.24	0.73	0.63	1.94	1.27
Al2O3	7.84	11.30	14.21	12.84	14.86	14.24
Fe2O3	9.85	8.08	12.34	9.70	12.69	14.39
MnO	0.28	0.17	0.28	0.16	0.19	0.21
MgO	12.81	12.17	6.80	8.78	3.32	4.89
CaO	23.73	13.50	12.48	8.91	6.21	5.00
Na2O	0.03	0.42	1.96	2.46	3.37	2.17
K2O	2.59	2.65	3.44	2.25	2.62	2.01
P2O5	0.01	0.01	0.06	0.19	0.95	0.13
Cr2O3	0.26	0.12	0.01	0.04	0.01	0.01
TOTAL	100	100	100	100	100	100
LOI	27.16	19.28	13.91	5.87	3.39	5.17
S/TOT	-	-	-	-	-	-
C/TOT	-	-	-	-	-	-
Zr ppm	14	13.5	34	62	268	75.5
Y	6	4	14	11.5	33	24
Nb	0.5	0.5	1	3	58	3
Ag	< D.L.	< D.L.	< D.L.	< D.L.	1	< D.L.
As	-	-	-	-	-	-
Mo	31	251	4	1	3	1
Cu	< D.L.	5	75	65	25	20
Pb	20	20	< D.L.	< D.L.	25	< D.L.
Zn	180	90	70	95	150	55
Ni	350	225	60	55	60	35
V	-	60	180	130	95	245
Ba	239	303	452	504	1475	234
W	11	9	4	< D.L.	2	6
Cr	-	-	-	-	-	-
Hg	-	-	-	-	-	-
Sr	908	598	191	259	503	97.2
Be	-	-	-	-	-	-
Co	54.5	43	41.5	40	40.5	37.5
Cs	2.7	3.5	5	8.2	3.3	3.7
Hf	0.5	0.5	1	2	6	3
Rb	61.2	64	71.2	53	58.8	39.4
Sb	-	-	-	-	-	-
Sn	< D.L.	< D.L.	< D.L.	< D.L.	2	< D.L.
Ta	< D.L.	< D.L.	< D.L.	< D.L.	< D.L.	< D.L.
Th	0.5	0.5	0.5	1	25	0.5
U	< D.L.	< D.L.	< D.L.	< D.L.	2	< D.L.
Ga	10	8	14	14	22	18
Se	-	-	-	-	-	-
Te	-	-	-	-	-	-
La	2	1	2.5	12.5	114.5	7
Ce	4	2	7	28.5	211	16
Nd	2.5	1	4.5	16.5	88	10
Sm	0.8	0.4	1.7	3.7	13.8	2.9
Eu	0.5	0.1	0.4	1.1	3.8	0.9
Yb	0.6	0.5	1.6	1.2	2.8	2.4
Lu	< D.L.	< D.L.	0.2	0.2	0.6	0.4
Dy	1.1	0.7	2.1	2.3	7	4.1
Er	0.7	0.5	1.6	1.2	3.9	2.6
Gd	0.9	0.7	2.1	3.4	11.6	4.1
Ho	0.2	0.1	0.5	0.6	1.4	0.9
Pr	0.5	0.3	0.9	3.8	25.5	2.2
Tm	< D.L.	< D.L.	0.3	0.1	0.6	0.4

	ONA98x-7049	ONA98x-7001	ONA98x-7037	ONA98x-7504A	ONA98x-7015	ONA98x-7032
	Hourglass Mafic intrusion	Green Jimmy Lapilli tuff	Cabin Mafic lapilli tuff	Knu. Lake Mafic metavolc.	Jaz area Metavolcaniclastic	Cabin Felsic metavolc.
Au g/t	0.0025	0.0025	0.015	0.0025	0.0025	0.0025
SiO2 wt%	45.37	70.35	52.60	48.56	70.91	79.63
TiO2	1.95	0.56	1.50	1.36	0.50	0.32
Al2O3	13.82	15.22	15.97	15.17	16.02	13.68
Fe2O3	21.00	5.55	13.99	14.13	3.36	1.21
MnO	0.25	0.11	0.18	0.52	0.04	0.03
MgO	8.39	3.30	5.00	2.92	1.90	0.18
CaO	7.73	1.45	7.10	13.90	0.69	1.51
Na2O	1.34	2.55	1.91	3.06	4.27	1.59
K2O	0.04	0.83	1.62	0.28	2.20	1.77
P2O5	0.10	0.07	0.11	0.10	0.11	0.08
Cr2O3	0.01	0.01	0.01	0.01	0.01	0.01
TOTAL	100	100	100	100	100	100
LOI	8.69	3.67	7.65	6.01	2.27	1.66
S/TOT	-	-	-	-	-	-
C/TOT	-	-	-	-	-	-
Zr ppm	53.5	124.5	73	57.5	145.5	113
Y	14.5	10	12	23.5	10	4.5
Nb	3	4	4	2	6	3
Ag	< D.L.	< D.L.	< D.L.	< D.L.	< D.L.	< D.L.
As	-	-	-	-	-	-
Mo	1	-	1	1	1	< D.L.
Cu	105	40	155	65	15	15
Pb	5	< D.L.	170	5	15	15
Zn	120	150	250	135	70	35
Ni	130	20	50	170	30	5
V	355	95	355	150	45	25
Ba	22	159.5	300	73.5	290	314
W	< D.L.	1	4	1	< D.L.	1
Cr	-	-	-	-	-	-
Hg	-	-	-	-	-	-
Sr	101	127.5	171.5	263	115.5	271
Be	-	-	-	-	-	-
Co	73	8.5	45.5	53.5	10	6
Cs	0.6	2.5	3.2	0.6	2.7	5.6
Hf	1	3	1	1	4	3
Rb	2.6	19.6	40	6.2	47.2	43.2
Sb	-	-	-	-	-	-
Sn	1	1	6	2	1	3
Ta	< D.L.	1	0.5	0.25	0.25	0.5
Th	0.5	9	< D.L.	< D.L.	5	1
U	< D.L.	1	0.5	< D.L.	1	1
Ga	17	21	22	18	21	19
Se	-	-	-	-	-	-
Te	-	-	-	-	-	-
La	5	14.5	9	6	19.5	13.5
Ce	14	26	17.5	14	37.5	26
Nd	8	11	9.5	10.5	17	10
Sm	2.3	2.1	2.4	3.2	3.1	1.8
Eu	1	0.6	0.9	1.2	0.9	0.6
Yb	1.7	0.9	1.4	2.3	1	0.5
Lu	0.2	0.1	0.2	0.4	0.2	< D.L.
Dy	3.1	1.5	2	4	2.1	0.9
Er	1.9	1	1.6	3	1.2	0.5
Gd	2.5	1.6	2.9	4.5	2.9	1.7
Ho	0.6	0.3	0.5	0.9	0.4	0.1
Pr	2	2.7	2.5	2.3	4.6	3.2
Tm	0.2	< D.L.	0.1	0.4	0.2	< D.L.

	ONA98x-7038	ONA98x-7034	ONA98x-7012	ONA98x-7125	ONA98x-7031	ONA98x-7124
	Cabin Mafic flow bx	Cabin Mafic volcanic	Green Jimmy Felsic dyke	MVP QP	Cabin QFP	MVP Gabbro
Au g/t	0.085	0.0025	0.0025	0.03	0.0025	0.03
SiO2 wt%	56.64	51.99	70.56	65.89	66.68	46.18
TiO2	1.82	1.21	0.46	0.83	0.43	1.06
Al2O3	16.94	16.73	15.90	15.58	17.14	17.70
Fe2O3	11.43	13.48	3.88	6.96	3.04	20.15
MnO	0.13	0.23	0.05	0.06	0.05	0.16
MgO	2.87	5.62	1.57	2.52	1.43	8.21
CaO	5.18	8.15	3.06	2.30	2.32	3.34
Na2O	3.79	2.08	2.16	4.39	7.01	2.85
K2O	1.07	0.38	2.25	1.35	1.69	0.13
P2O5	0.12	0.10	0.10	0.12	0.20	0.19
Cr2O3	0.01	0.01	0.01	0.01	0.01	0.03
TOTAL	100	100	100	100	100	100
LOI	5.09	8.85	4.31	3.65	1.34	6.81
S/TOT	-	-	-	-	-	-
C/TOT	-	-	-	-	-	-
Zr ppm	82	55.5	152.5	123	178	112
Y	19	20	6.5	11	12	25.5
Nb	5	3	3	4	14	5
Ag	< D.L.	< D.L.	< D.L.	< D.L.	< D.L.	< D.L.
As	-	-	-	-	-	-
Mo	1	< D.L.	-	1	< D.L.	2
Cu	115	115	2.5	40	10	10
Pb	5	5	5	< D.L.	15	< D.L.
Zn	170	120	50	20	20	140
Ni	160	110	10	25	15	50
V	155	285	60	110	45	375
Ba	234	72	425	214	539	36
W	< D.L.	1	< D.L.	3	< D.L.	5
Cr	-	-	-	-	-	-
Hg	-	-	-	-	-	-
Sr	243	85.6	125.5	111	554	91.6
Be	-	-	-	-	-	-
Co	50.5	51.5	8.5	19.5	10.5	56
Cs	1.8	1.3	3	2.8	0.4	0.7
Hf	2	1	3	4	4	3
Rb	28	8.6	60	33.4	35.6	6.2
Sb	-	-	-	-	-	-
Sn	3	2	< D.L.	< D.L.	3	1
Ta	0.5	0.25	0.25	0.5	1.5	0.5
Th	< D.L.	< D.L.	3	3	4	1
U	< D.L.	< D.L.	0.5	0.5	3.5	< D.L.
Ga	22	18	23	19	21	27
Se	-	-	-	-	-	-
Te	-	-	-	-	-	-
La	7.5	3.5	16	8	44	7.5
Ce	18.5	8	29.5	18.5	87	18
Nd	12.5	6	13	9.5	37	13
Sm	3.9	2.2	2.2	2.2	6.4	3.3
Eu	1.3	0.7	0.6	0.7	1.8	1
Yb	2.1	2.4	0.6	0.7	1	2.3
Lu	0.2	0.4	< D.L.	0.1	0.1	0.4
Dy	3.5	3.2	1.1	2.1	2.3	4.5
Er	2.3	2.3	0.5	1.1	1.1	2.5
Gd	4.9	3.2	1.9	1.8	5.3	4.4
Ho	0.8	0.8	0.3	0.3	0.5	0.9
Pr	3	1.5	3.3	2.3	10.9	2.6
Tm	0.3	0.3	0.1	0.1	0.1	0.4

	ONA98x-7002	ONA98x-7007	ONA98x-7010	ONA98x-7013	ONA98x-7103	ONA98x-7120
	Green Jimmy Gabbro	MVP Mafic flow	MVP Mafic flow	MVP Mafic flow	Ryne Mafic schist	Ryne Mafic schist
Au g/t	0.01	0.0025	0.0025	0.0025	0.02	0.12
SiO2 wt%	50.33	50.88	52.21	49.94	52.97	47.57
TiO2	1.71	0.92	0.89	0.88	0.35	0.36
Al2O3	13.54	16.29	16.38	15.93	11.85	12.12
Fe2O3	19.67	12.13	12.07	12.83	12.51	11.17
MnO	0.24	0.21	0.17	0.19	0.28	0.22
MgO	5.72	7.14	6.13	7.51	12.35	13.40
CaO	5.35	8.68	10.03	10.58	8.11	12.44
Na2O	3.23	3.51	1.91	1.97	0.21	0.75
K2O	0.08	0.18	0.14	0.11	1.16	1.89
P2O5	0.13	0.05	0.07	0.05	0.05	0.01
Cr2O3	0.01	0.01	0.01	0.01	0.15	0.06
TOTAL	100	100	100	100	100	100
LOI	6.49	2.67	4.1	2.74	14.06	18.17
S/TOT	-	-	-	-	-	-
C/TOT	-	-	-	-	-	-
Zr ppm	75	45	56	44.5	21.5	24
Y	28	16.5	17.5	17	5	7
Nb	3	1	1	1	0.5	0.5
Ag	< D.L.	< D.L.	< D.L.	< D.L.	< D.L.	< D.L.
As	-	-	-	-	-	-
Mo	-	-	-	-	229	3
Cu	90	95	70	110	5	20
Pb	< D.L.	< D.L.	< D.L.	< D.L.	15	< D.L.
Zn	100	70	80	85	80	80
Ni	25	125	110	110	335	230
V	460	305	285	275	80	80
Ba	28.5	46.5	53	46	362	334
W	< D.L.	< D.L.	< D.L.	< D.L.	7	13
Cr	-	-	-	-	-	-
Hg	-	-	-	-	-	-
Sr	57.9	108	147.5	109.5	119.5	726
Be	-	-	-	-	-	-
Co	51.5	54.5	47.5	52	69.5	47.5
Cs	1	0.4	0.8	0.3	1.5	2.9
Hf	1	1	1	1	< D.L.	< D.L.
Rb	5.2	3.6	6.2	3.6	36.2	57.6
Sb	-	-	-	-	-	-
Sn	< D.L.	< D.L.	< D.L.	< D.L.	< D.L.	< D.L.
Ta	< D.L.	< D.L.	< D.L.	< D.L.	< D.L.	< D.L.
Th	4	< D.L.	< D.L.	< D.L.	< D.L.	< D.L.
U	< D.L.	< D.L.	< D.L.	< D.L.	< D.L.	< D.L.
Ga	22	18	17	18	10	9
Se	-	-	-	-	-	-
Te	-	-	-	-	-	-
La	3	2.5	3	2.5	2	2
Ce	8	5.5	6.5	6.5	4.5	4
Nd	7.5	4.5	5	5.5	2.5	2.5
Sm	1.9	1.7	1.7	2	0.3	0.6
Eu	0.7	0.5	0.8	0.5	0.2	0.1
Yb	2.8	1.8	1.7	1.8	0.7	1
Lu	0.3	0.3	0.2	0.3	< D.L.	< D.L.
Dy	4.5	2.4	2.9	2.3	1.1	1.2
Er	3	1.7	1.7	1.5	0.8	0.7
Gd	3.3	2.1	2.6	2.5	0.9	0.8
Ho	0.9	0.6	0.5	0.6	0.2	0.2
Pr	1.2	0.9	1.1	1.2	0.5	0.5
Tm	0.4	0.3	0.2	0.3	< D.L.	0.1

	ONA98x-7021	ONA98C-8195B	ONA98x-7025	ONA98x-7033	ONA98x-7008	ONA98x-7009
	Ryne Inter. schist	Hourglass Felsic schist	Claimline Felsic schist	Cabin Felsic schist	Green Jimmy Felsic schist	Green Jimmy Felsic schist
Au g/t	< D.L.5	0.14	0.0025	0.01	0.0025	0.0025
SiO2 wt%	64.73	74.48	71.01	69.12	72.77	72.31
TiO2	0.49	0.48	0.40	0.60	0.47	0.45
Al2O3	16.77	13.39	15.22	14.73	16.56	16.09
Fe2O3	6.16	2.69	3.77	5.97	3.51	3.63
MnO	0.18	0.05	0.05	0.11	0.05	0.05
MgO	1.52	0.50	1.82	2.56	1.56	1.49
CaO	3.84	1.52	3.10	3.03	1.38	2.03
Na2O	3.84	5.97	2.53	1.68	1.08	1.46
K2O	2.34	0.79	1.98	2.11	2.53	2.37
P2O5	0.13	0.12	0.10	0.10	0.08	0.10
Cr2O3	0.01	0.01	0.01	0.01	0.01	0.01
TOTAL	100	100	100	100	100	100
LOI	4.63	2.31	4.1	4.33	3.61	4.13
S/TOT	-	-	-	-	-	-
C/TOT	-	-	-	-	-	-
Zr ppm	145	131	-	104	116	142
Y	9.5	8.5	-	11.5	6	6.5
Nb	5	4	-	4	2	3
Ag	< D.L.	< D.L.	-	< D.L.	< D.L.	< D.L.
As	-	-	-	-	-	-
Mo	1	2	1	1	-	-
Cu	15	320	-	25	10	2.5
Pb	25	10	-	15	< D.L.	5
Zn	75	55	-	75	85	80
Ni	15	10	-	25	5	5
V	45	35	-	85	55	55
Ba	365	114.5	-	222	308	450
W	< D.L.	3	-	6	< D.L.	< D.L.
Cr	-	-	-	-	-	-
Hg	-	-	-	-	-	-
Sr	170	221	-	251	85.6	130.5
Be	-	-	-	-	-	-
Co	9	6	-	11.5	7	8.5
Cs	4.1	1.5	-	2.4	3.7	4
Hf	4	3	-	3	3	3
Rb	47.6	22.2	-	56.4	57.6	59.8
Sb	-	-	-	-	-	-
Sn	< D.L.	< D.L.	-	3	< D.L.	< D.L.
Ta	0.5	< D.L.	-	0.5	< D.L.	< D.L.
Th	5	1	-	< D.L.	2	3
U	0.5	1	-	< D.L.	0.5	0.5
Ga	21	14	-	19	21	21
Se	-	-	-	-	-	-
Te	-	-	-	-	-	-
La	20	18.5	-	12.5	13.5	14.5
Ce	39.5	35	-	24.5	23.5	25.5
Nd	19.5	16	-	11.5	9	9
Sm	2.9	2.5	-	2.6	1.5	1.7
Eu	0.9	0.7	-	0.7	0.5	0.3
Yb	0.9	0.7	-	1.3	0.7	0.7
Lu	0.1	0.1	-	0.2	0.1	< D.L.
Dy	2	1.5	-	2	0.9	0.7
Er	1.3	0.8	-	1.4	0.6	0.5
Gd	2.9	2.5	-	2.5	1.4	1.6
Ho	0.5	0.3		0.4	0.3	0.1
Pr	4.9	4.1		3.4	2.6	2.9
Tm	0.1	0.1		0.1	0.1	< D.L.

	ONA98x-7011	ONA98x-7005	ONA98x-7006	ONA98x-7035	ONA98x-7036	ONA98x-7102
	Green Jimmy Felsic schist	Green Jimmy Inter. schist	Green Jimmy Mafic schist	Green Jimmy Mafic schist	Green Jimmy Mafic schist	Ryne Inter. dyke
Au g/t	0.0025	0.0025	0.0025	0.02	0.0025	0.065
SiO2 wt%	74.14	58.64	49.30	50.64	50.17	56.64
TiO2	0.47	1.23	0.96	1.11	1.08	0.40
Al2O3	16.64	21.60	17.42	16.05	15.63	12.20
Fe2O3	2.64	8.30	12.37	14.04	16.83	7.67
MnO	0.04	0.10	0.21	0.20	0.29	0.24
MgO	1.27	3.09	5.28	4.07	6.23	4.78
CaO	0.80	2.14	10.59	11.43	8.09	11.35
Na2O	1.33	2.08	3.26	1.92	1.04	6.05
K2O	2.58	2.74	0.53	0.44	0.54	0.65
P2O5	0.09	0.07	0.07	0.09	0.09	0.01
Cr2O3	0.01	0.01	0.01	0.01	0.01	0.01
TOTAL	100	100	100	100	100	100
LOI	2.81	5.45	10.54	9.62	9.62	13.91
S/TOT	-	-	-	-	-	-
C/TOT	-	-	-	-	-	-
Zr ppm	142	58	41.5	67.5	50	46.5
Y	7	17	17	18.5	20.5	8.5
Nb	3	2	1	3	3	1
Ag	< D.L.	< D.L.	< D.L.	< D.L.	< D.L.	< D.L.
As	-	-	-	-	-	-
Mo	-	-	-	2	1	4
Cu	2.5	90	150	115	130	10
Pb	10	< D.L.	< D.L.	5	5	25
Zn	50	60	75	125	155	75
Ni	5	210	130	110	110	60
V	65	390	290	250	240	65
Ba	342	448	98	66.5	109	112.5
W	< D.L.	< D.L.	< D.L.	< D.L.	< D.L.	16
Cr	-	-	-	-	-	-
Hg	-	-	-	-	-	-
Sr	67.2	127.5	111.5	114.5	70.1	591
Be	-	-	-	-	-	-
Co	6.5	64.5	56.5	47.5	53	18.5
Cs	3.5	3.7	1	1.1	1.4	0.8
Hf	3	1	1	1	1	1
Rb	62.6	70.8	16	8.6	11.4	15
Sb	-	-	-	-	-	-
Sn	< D.L.	< D.L.	< D.L.	2	2	< D.L.
Ta	< D.L.	< D.L.	< D.L.	< D.L.	0.5	< D.L.
Th	3	< D.L.	< D.L.	< D.L.	< D.L.	< D.L.
U	0.5	< D.L.	< D.L.	< D.L.	< D.L.	< D.L.
Ga	23	23	18	17	17	13
Se	-	-	-	-	-	-
Te	-	-	-	-	-	-
La	15	3.5	2.5	3.5	3	7.5
Ce	28	9	5.5	8.5	8	14.5
Nd	10.5	6	4.5	6.5	6.5	6.5
Sm	2	2	1.8	2.3	2.1	1.3
Eu	0.7	0.6	0.6	0.8	0.8	0.5
Yb	0.6	1.3	1.9	2.3	2.5	0.7
Lu	< D.L.	0.2	0.2	0.4	0.4	0.1
Dy	1.4	3.2	2	3.2	3.6	1.6
Er	0.5	1.8	1.6	2.3	2.6	0.8
Gd	1.6	2.3	1.9	3.5	3.3	1.3
Ho	0.3	0.6	0.6	0.8	0.8	0.3
Pr	2.7	1.3	1	1.4	1.4	1.5
Tm	0.1	0.3	0.2	0.3	0.4	0.1

	ONA98x-7121	ONA98x-7115	ONA98x-7026	ONA97-1-1052	ONA97-1-1053	ONA97-1-1054
	Ryne Diorite sill	Ryne Monzonite	MVP Monzonite	Ryne Conglomerate	Ryne Conglomerate	Ryne Conglomerate
Au g/t	0.015	0.01	0.0025	0.715	0.02	0.02
SiO2 wt%	51.98	63.87	71.69	56.51	57.98	55.49
TiO2	0.61	0.55	0.21	0.82	0.68	0.63
Al2O3	9.70	17.31	15.61	13.47	14.88	14.90
Fe2O3	9.93	4.98	1.86	9.86	7.87	7.94
MnO	0.18	0.10	0.04	0.18	0.16	0.20
MgO	12.26	1.43	0.83	4.82	4.55	4.83
CaO	10.87	2.75	1.29	9.04	8.33	10.14
Na2O	1.89	5.53	5.01	2.44	1.42	2.07
K2O	2.29	3.21	3.36	2.74	4.04	3.69
P2O5	0.19	0.27	0.08	0.11	0.08	0.09
Cr2O3	0.11	0.01	0.01	0.01	0.01	0.01
TOTAL	100	100	100	100	100	100
LOI	15.18	3.34	1	10.48	11.75	13.49
S/TOT	-	-	-	-	-	-
C/TOT	-	-	-	-	-	-
Zr ppm	51	158.5	91	78	76.5	-
Y	9.5	14	4	16	10	-
Nb	4	8	5	3	3	-
Ag	< D.L.	< D.L.	< D.L.	< D.L.	< D.L.	-
As	-	-	-	-	-	134
Mo	2	< D.L.	< D.L.	1	1	-
Cu	55	15	5	75	45	-
Pb	5	20	20	20	15	-
Zn	45	95	40	75	60	-
Ni	115	5	5	90	105	-
V	110	60	15	150	120	-
Ba	233	1085	912	334	535	-
W	4	1	< D.L.	9	5	-
Cr	-	-	-	-	-	-
Hg	-	-	-	-	-	-
Sr	520	707	666	220	133	-
Be	-	-	-	-	-	-
Co	43	9	4.5	37.5	29.5	-
Cs	45.4	2.7	2.1	2.7	3.4	-
Hf	1	5	3	2	2	-
Rb	100.5	69	112.5	63.8	82.2	-
Sb	-	-	-	-	-	-
Sn	< D.L.	< D.L.	3	1	< D.L.	-
Ta	1.5	0.5	0.5	< D.L.	0.5	-
Th	3	5	1	3	3	-
U	0.5	2.5	1.5	< D.L.	< D.L.	-
Ga	11	22	21	16	15	-
Se	-	-	-	-	-	-
Te	-	-	-	-	-	-
La	19	54	10.5	7.5	8	-
Ce	38.5	107	23	16	16.5	-
Nd	18.5	45	9.5	9.5	9	-
Sm	3.8	7.3	1.9	2.5	2.1	-
Eu	0.9	1.7	0.6	0.7	0.6	-
Yb	0.7	1.2	0.4	1.8	1.1	-
Lu	0.1	0.1	< D.L.	0.3	0.1	-
Dy	2.2	2.9	0.7	3.3	2.2	-
Er	0.9	1.1	0.4	2.2	1.2	-
Gd	3.5	6.3	1.6	2.7	2	-
Ho	0.4	0.5	0.1	0.7	0.5	-
Pr	4.8	12.1	2.7	2.3	2.1	-
Tm	0.1	0.1	< D.L.	0.3	0.1	-

	ONA97-1-1055	ONA97-1-1056	OG99C-4134
	Ryne Conglomerate	Ryne Conglomerate	Big Bear Gabbro
Au g/t	0.08	0.17	0.018
SiO2 wt%	58.33	53.57	48.07
TiO2	0.60	0.54	1.75
Al2O3	14.17	13.69	16.02
Fe2O3	6.98	11.02	18.14
MnO	0.23	0.24	0.17
MgO	3.18	3.79	5.47
CaO	10.73	11.68	5.63
Na2O	3.70	3.34	4.54
K2O	1.98	2.05	0.07
P2O5	0.09	0.07	0.16
Cr2O3	0.01	0.01	0.00
TOTAL	100	100	100
LOI	10.52	9.49	7.44
S/TOT	-	-	-
C/TOT	-	-	-
Zr ppm	-	68.5	105
Y	-	10.5	26
Nb	-	2	3
Ag	-	< D.L.	0.2
As	58	-	2.5
Mo	-	3	< D.L.
Cu	-	290	41
Pb	-	20	< D.L.
Zn	-	75	135
Ni	-	100	59
V	-	100	384
Ba	-	309	32
W	-	9	< D.L.
Cr	-	-	55
Hg	-	-	2.5
Sr	-	210	183
Be	-	-	1
Co	-	30	49
Cs	-	2.4	1
Hf	-	1	2
Rb	-	45.4	3
Sb	-	-	0.2
Sn	-	< D.L.	2.5
Ta	-	< D.L.	< D.L.
Th	-	2	< D.L.
U	-	< D.L.	< D.L.
Ga	-	12	18
Se	-	-	0.3
Te	-	-	< D.L.
La	-	7.5	4.6
Ce	-	15.5	9
Nd	-	8	2.5
Sm	-	1.9	2.6
Eu	-	0.6	0.9
Yb	-	1.1	2.4
Lu	-	0.1	0.34
Dy	-	2.1	-
Er	-	1.2	-
Gd	-	2.4	-
Ho	-	0.4	-
Pr	-	2.1	-
Tm	-	0.1	-

APPENDIX B

Microprobe analyses

Microprobe analyse results of gold and electrum

Detection limit in wt%: Au, 0.1; Ag, 0.15; Hg, 0.3; Cu, 0.08

Sample #	Au (ppb)	Location	Au wt%	Ag wt%	Hg wt%	Cu wt%	Total wt%
172a-2a1	25000	Hourglass	79.25	18.03	0.19	-	97.47
172a-2a2	25000	Hourglass	78.30	17.78	0.09	-	96.17
172a-2a3	25000	Hourglass	80.11	17.46	0.15	-	97.72
172a-2a4	25000	Hourglass	78.95	17.86	0.26	-	97.08
172a-2a5	25000	Hourglass	82.52	11.14	0.12	-	93.78
22-1a1	8090	Ryne	89.78	7.42	0.17	-	97.37
22-1a2	8090	Ryne	86.59	10.53	0.11	-	97.23
22-2a1	8090	Ryne	79.56	16.28	0.11	-	95.95
22-2a2	8090	Ryne	72.30	19.36	0.16	-	91.84
172a-2a2	25000	Hourglass	80.65	17.91	0.10	0.04	98.70
172a-2a3	25000	Hourglass	80.30	17.89	0.01	0.02	98.22
172a-2a4	25000	Hourglass	80.04	17.82	0.12	0.04	98.02
22-1a1	8090	Ryne	91.63	7.44	0.00	0.03	99.10
148C1#1	13000	Big Bear	88.66	6.48	0.00	0.04	95.18
173C2#1	60000	Claimline	88.04	11.37	0.01	0.03	99.45
173C2#2	60000	Claimline	87.61	11.31	0.05	0.04	99.02
173C2#3	60000	Claimline	87.99	11.48	0.00	0.04	99.52
176C10#1	48000	Hourglass	83.81	13.39	0.00	0.02	97.22
176C12#1	48000	Hourglass	83.00	13.04	0.03	0.03	96.10
176C12#2	48000	Hourglass	79.91	11.77	0.12	0.05	91.84
176C12#3	48000	Hourglass	82.39	12.96	0.19	0.00	95.54
066C6#1	1200	Ryne	78.69	18.64	0.00	0.03	97.36
R2C10#1	200000	Ryne	94.24	6.66	0.00	0.02	100.92
R3C3#1	200000	Ryne	90.58	8.64	0.00	0.06	99.28
R3C3#2	200000	Ryne	91.98	8.54	0.05	0.02	100.59
R3C9#1	200000	Ryne	93.53	6.80	0.00	0.03	100.36
R3C9#2	200000	Ryne	92.85	6.69	0.08	0.05	99.67
R3C10#1	200000	Ryne	92.46	6.71	0.00	0.05	99.23
R3C10#2	200000	Ryne	92.09	6.97	0.00	0.05	99.12
R3C10#3	200000	Ryne	93.23	6.62	0.14	0.06	100.05
R3C10#4	200000	Ryne	91.54	6.73	0.00	0.08	98.35
R1aC1#1	200000	Ryne	94.65	5.92	0.00	0.04	100.60
R1aC2#1	200000	Ryne	94.06	6.05	0.00	0.13	100.23
R1aC2#2	200000	Ryne	94.77	6.17	0.00	0.07	101.02
R1aC2#3	200000	Ryne	94.27	6.01	0.00	0.06	100.33
R1aC2#4	200000	Ryne	92.46	6.06	0.00	0.02	98.53
R1aC3#1	200000	Ryne	92.60	5.87	0.00	0.01	98.47
R1aC3#2	200000	Ryne	92.30	6.02	0.00	0.04	98.36
R1aC9#1	200000	Ryne	92.41	6.25	0.00	0.09	98.76
R1aC9#2	200000	Ryne	92.14	6.44	0.00	0.06	98.64
R1aC9#3	200000	Ryne	92.36	6.45	0.00	0.06	98.86
R1bC1#1	200000	Ryne	92.36	6.27	0.00	0.05	98.68
R1bC1#2	200000	Ryne	91.78	6.55	0.00	0.02	98.35
R1bC1#3	200000	Ryne	92.35	6.42	0.00	0.07	98.84
R1bC1#4	200000	Ryne	92.20	6.31	0.00	0.07	98.58
R1bC11#1	200000	Ryne	92.55	6.05	0.00	0.03	98.64
R1bC11#2	200000	Ryne	92.61	5.92	0.00	0.04	98.58
H2C7#1	65000	Hourglass	78.50	18.55	0.00	0.03	97.07
H2C7#2	65000	Hourglass	79.39	18.71	0.03	0.04	98.18
H2C7#3	65000	Hourglass	78.34	18.47	0.00	0.00	96.81
H2C7#4	65000	Hourglass	70.02	26.34	0.19	0.00	96.55
022C1#1	8090	Ryne	90.24	7.21	0.00	0.05	97.50
022C1#2	8090	Ryne	86.85	10.40	0.00	0.02	97.27

Sample #	Au (ppb)	Location	Au wt%	Ag wt%	Hg wt%	Cu wt%	Total wt%
022C2#1	8090	Ryne	80.01	15.93	0.00	0.08	96.01
148C1#1	13750	Big Bear	89.93	6.79	0.00	0.02	96.74
128C1#1	7400	Ryne	93.25	6.98	0.00	0.08	100.31
088C1#1	3690	Ryne	68.71	29.17	0.00	0.03	98.00
088C1#2	3690	Ryne	69.29	28.92	0.00	0.04	98.27
088C1#3	3690	Ryne	69.02	29.18	0.00	0.00	98.22
088C1#4	3690	Ryne	69.37	28.58	0.00	0.05	98.02
088C1#5	3690	Ryne	66.75	28.70	0.17	0.03	97.78
081C1#1	2530	Hourglass	75.58	22.64	0.05	0.02	99.92
081C1#2	2530	Hourglass	75.61	22.85	0.08	0.01	100.12
090C1#1	480	Ryne	78.93	20.12	0.00	0.00	99.05
090C1#2	480	Ryne	78.54	20.12	0.00	0.01	98.68
090C1#3	480	Ryne	77.97	19.97	0.00	0.05	98.01
090C1#4	480	Ryne	79.52	19.82	0.00	0.00	99.34
090C1#5	480	Ryne	79.39	20.01	0.00	0.02	99.42
090C1#6	480	Ryne	81.98	16.87	0.00	0.01	98.87
090C1#7	480	Ryne	82.80	17.19	0.00	0.02	100.01
090C1#8	480	Ryne	81.00	17.96	0.04	0.00	99.00
090C1#9	480	Ryne	82.35	16.96	0.00	0.04	99.35
090C2#1	480	Ryne	73.98	21.21	0.00	0.03	97.91
090C2#2	480	Ryne	74.79	20.12	0.00	0.02	97.19
021C1#1	8090	Ryne	79.42	20.50	0.00	0.02	100.03
021C1#2	8090	Ryne	78.90	18.99	0.00	0.01	97.98
021C1#3	8090	Ryne	78.96	18.84	0.00	0.00	97.89
142C1#1	14710	Ryne	85.57	7.66	0.00	0.03	98.06
142C1#2	14710	Ryne	93.19	8.74	0.00	0.06	103.62
150C1#1	730	Big Bear	88.85	11.40	0.07	0.19	101.69
150C1#2	730	Big Bear	87.82	11.09	0.00	0.30	100.53
065C1#1	3300	Ryne	89.25	10.00	0.00	0.08	101.66
065C1#2	3300	Ryne	89.15	9.89	0.00	0.04	100.81
065C1#3	3300	Ryne	88.31	9.44	0.00	0.06	100.56
065C2#1	3300	Ryne	92.57	7.59	0.00	0.09	101.48
065C2#2	3300	Ryne	92.20	7.80	0.00	0.06	101.27
065C2#3	3300	Ryne	91.66	7.81	0.00	0.07	100.69
140C1#1	3200	Ryne	79.95	19.37	0.00	0.07	101.12
140C1#2	3200	Ryne	79.75	18.83	0.02	0.06	100.35
140C1#3	3200	Ryne	79.66	18.98	0.00	0.04	100.44
140C2#1	3200	Ryne	96.70	4.18	0.00	0.09	103.24
140C2#2	3200	Ryne	98.23	4.10	0.00	0.07	102.58
140C2#3	3200	Ryne	95.89	4.17	0.00	0.08	102.08
140C2#4	3200	Ryne	96.53	4.35	0.00	0.06	102.79
140C3#1	3200	Ryne	80.77	12.77	0.00	0.02	94.52
140C3#2	3200	Ryne	81.17	13.00	0.00	0.02	95.07
138BC2#1	12980	Ryne	71.50	25.49	0.00	0.05	97.88
138BC2#2	12980	Ryne	73.00	25.30	0.00	0.02	99.08
138BC3#1	12980	Ryne	81.97	9.81	0.13	0.05	97.27
138BC3#2	12980	Ryne	85.54	10.03	0.07	0.04	99.72
138BC3#3	12980	Ryne	88.71	10.44	0.00	0.06	102.01
H1C1#1	65000	Hourglass	88.05	11.54	0.00	0.05	99.65
H1C1#2	65000	Hourglass	87.60	10.98	0.00	0.03	98.61
H1C1#3	65000	Hourglass	89.05	11.33	0.00	0.00	100.38
H1C1#4	65000	Hourglass	88.07	11.20	0.00	0.00	99.27
H1C1#5	65000	Hourglass	88.23	11.05	0.00	0.05	99.33
H1C1#6	65000	Hourglass	88.04	11.49	0.00	0.00	99.61
H1C1#7	65000	Hourglass	88.04	11.23	0.00	0.04	99.69
H1C1#8	65000	Hourglass	87.89	11.49	0.00	0.02	99.80

Sample #	Au (ppb)	Location	Au wt%	Ag wt%	Hg wt%	Cu wt%	Total wt%
H1C1#9	65000	Hourglass	88.15	11.37	0.03	0.02	99.57
H1C1#10	65000	Hourglass	87.71	11.01	0.00	0.00	98.74
H1C2#1	65000	Hourglass	88.09	11.94	0.00	0.00	100.03
H1C2#2	65000	Hourglass	88.00	11.87	0.00	0.00	99.87
H1C2#3	65000	Hourglass	86.90	11.73	0.02	0.00	98.67
H1C2#4	65000	Hourglass	87.05	11.93	0.00	0.01	99.01
H1C2#5	65000	Hourglass	87.40	11.88	0.00	0.00	99.28
H1C2#6	65000	Hourglass	86.96	12.03	0.00	0.02	99.01
H1C3#1	65000	Hourglass	86.43	12.00	0.00	0.04	98.55
H1C4#1	65000	Hourglass	88.03	11.25	0.00	0.03	99.31
H1C4#2	65000	Hourglass	87.24	11.70	0.00	0.01	98.96
H1C4#3	65000	Hourglass	87.38	11.64	0.00	0.04	99.10
H1C4#4	65000	Hourglass	87.41	11.75	0.00	0.00	99.16
H1C4#5	65000	Hourglass	87.37	11.87	0.00	0.00	99.24
H1C5#1	65000	Hourglass	86.96	12.30	0.00	0.02	99.31
H1C6#1	65000	Hourglass	86.24	11.49	0.00	0.03	97.94
H1C7#1	65000	Hourglass	86.68	12.02	0.00	0.01	98.75
H1C7#2	65000	Hourglass	87.31	11.77	0.00	0.03	99.11
H1C7#3	65000	Hourglass	88.11	11.98	0.00	0.05	100.19
H1C8#1	65000	Hourglass	87.74	11.83	0.00	0.04	99.61
H1C8#2	65000	Hourglass	87.92	11.91	0.00	0.02	99.85

Microprobe analyse results of pyrite

Detection limit in wt%: Fe, 0.05; As, 0.03; Co, Ni, S, 0.01; Cu, 0.04; Zn, 0.03

Sample #	Au (ppb)	Location	Fe wt%	As wt%	Co wt%	Cu wt%	Ni wt%	Zn wt%	S wt%	Total wt%
172a-1a	25000	Hourglass	46.56	0.02	0.07	-	0.00	-	53.49	100.13
172a-1b	25000	Hourglass	46.58	0.02	0.05	-	0.00	-	53.66	100.31
172a-2a1	25000	Hourglass	46.16	0.33	0.10	-	0.02	-	53.03	99.63
172a-2a2	25000	Hourglass	46.14	0.39	0.05	-	0.00	-	52.85	99.42
172a-3	25000	Hourglass	46.42	0.06	0.05	-	0.00	-	53.34	99.87
172a-4core	25000	Hourglass	46.52	0.46	0.06	-	0.02	-	53.08	100.14
172a-4rim	25000	Hourglass	42.96	0.07	0.11	-	0.05	-	51.78	94.96
22-1a	8090	Ryne	46.48	0.07	0.05	-	0.00	-	53.22	99.82
22-2a	8090	Ryne	46.61	0.10	0.07	-	0.00	-	53.40	100.18
22-3a	8090	Ryne	46.28	0.09	0.05	-	0.02	-	53.10	99.52
23C1#1	1270	Ryne	46.12	0.44	0.20	0.02	0.01	0.01	53.15	99.96
23C1#2	1270	Ryne	45.40	0.22	0.20	0.05	0.01	0.01	53.45	99.34
23C3#1	1270	Ryne	46.50	0.22	0.01	0.04	0.01	0.02	53.51	100.31
23C4#1	1270	Ryne	46.70	0.45	0.00	0.00	0.01	0.02	53.18	100.36
23C5#1	1270	Ryne	46.49	0.08	0.00	0.04	0.00	0.02	52.82	99.44
23C5#2	1270	Ryne	46.18	0.53	0.00	0.00	0.00	0.00	52.76	99.48
23C8#1	1270	Ryne	46.41	0.12	0.00	0.03	0.01	0.00	53.30	99.88
23C8#2	1270	Ryne	46.64	0.51	0.00	0.02	0.01	0.00	53.03	100.21
23C8#3	1270	Ryne	46.35	0.07	0.00	0.03	0.01	0.03	53.16	99.65
30C2#1	2340	Ryne	46.17	0.08	0.01	0.04	0.00	0.00	53.31	99.59
21C1#1	8090	Ryne	45.70	0.11	0.21	0.01	0.01	0.01	52.32	98.39
21C2#1	8090	Ryne	45.85	0.16	0.44	0.03	0.08	0.02	53.20	99.79
21C3#1	8090	Ryne	46.20	0.18	0.00	0.00	0.07	0.00	53.37	99.81
21C4#1	8090	Ryne	46.45	0.09	0.06	0.04	0.04	0.00	53.10	99.78
148C1#1	13750	Big Bear	46.31	1.12	0.00	0.00	0.01	0.03	52.41	99.88
148C1#2	13750	Big Bear	46.74	0.04	0.00	0.02	0.01	0.00	53.50	100.31
148C2#1	13750	Big Bear	46.71	0.03	0.01	0.04	0.02	0.00	53.40	100.21
148C2#2	13750	Big Bear	46.34	0.09	0.01	0.01	0.08	0.01	53.28	99.80
173C1#1	60000	Claimline	46.37	0.02	0.17	0.03	0.03	0.00	53.50	100.12
175C3#1	78oz	Ryne	46.53	0.07	0.00	0.02	0.02	0.00	53.27	99.92
175C4#1	78oz	Ryne	46.33	0.03	0.00	0.04	0.01	0.03	53.56	100.00
175C4#2	78oz	Ryne	46.03	0.66	0.01	0.01	0.04	0.00	52.85	99.60
175C4#3	78oz	Ryne	46.27	0.05	0.04	0.01	0.01	0.04	53.55	99.97
175C5#1	78oz	Ryne	44.34	1.63	1.83	0.00	0.01	0.03	52.22	100.08
175C7#1	78oz	Ryne	45.16	1.03	0.33	0.00	0.03	0.03	52.67	99.25
175C7#2	78oz	Ryne	46.45	0.08	0.00	0.00	0.00	0.00	53.49	100.00
175C8#1	78oz	Ryne	46.80	0.08	0.00	0.00	0.02	0.04	53.09	100.03
175C9#1	78oz	Ryne	46.64	0.08	0.00	0.00	0.00	0.00	53.01	99.74
175C9#2	78oz	Ryne	46.46	0.20	0.03	0.01	0.03	0.00	53.08	99.80
175C9#3	78oz	Ryne	46.56	0.02	0.00	0.03	0.01	0.00	53.35	99.97
176C2#1	45000	Hourglass	46.61	0.07	0.00	0.04	0.02	0.00	52.94	99.69
176C3#1	45000	Hourglass	46.64	0.02	0.04	0.03	0.13	0.01	53.05	99.93
176C3#2	45000	Hourglass	46.56	0.17	0.15	0.05	0.10	0.00	52.97	100.00
176C4#1	45000	Hourglass	46.54	0.20	0.13	0.03	0.07	0.00	52.88	99.85
176C5#1	45000	Hourglass	46.43	0.12	0.22	0.04	0.04	0.02	52.88	99.76
176C5#2	45000	Hourglass	46.42	0.74	0.12	0.03	0.28	0.00	52.49	100.07
176C5#3	45000	Hourglass	45.95	0.62	0.11	0.06	0.26	0.01	52.70	99.70
176C8#1	45000	Hourglass	46.59	0.06	0.02	0.06	0.05	0.01	52.92	99.71
176C9#1	45000	Hourglass	45.63	0.69	0.00	0.02	0.02	0.02	52.60	98.98
176C9#2	45000	Hourglass	44.77	2.77	0.90	0.03	0.10	0.00	51.23	99.80
176C9#3	45000	Hourglass	45.58	0.20	0.33	0.04	0.53	0.01	52.69	99.37
176C11#1	45000	Hourglass	46.45	0.20	0.02	0.03	0.18	0.00	53.00	99.89
176C11#2	45000	Hourglass	46.71	0.08	0.00	0.04	0.01	0.02	53.12	99.99
176C11#3	45000	Hourglass	46.74	1.89	0.00	0.03	0.01	0.00	51.79	100.45
176C11#4	45000	Hourglass	46.63	1.65	0.00	0.03	0.00	0.01	51.90	100.22
176C11#5	45000	Hourglass	46.85	0.20	0.00	0.03	0.01	0.00	52.95	100.05
176C11#6	45000	Hourglass	46.44	0.18	0.06	0.05	0.12	0.02	52.88	99.75
003C2#1	85	Ryne	46.43	0.24	0.00	0.03	0.01	0.00	53.21	99.92
003C2#2	85	Ryne	46.50	0.16	0.00	0.03	0.01	0.03	53.48	100.22
003C2#3	85	Ryne	45.07	0.24	0.10	0.04	0.04	0.00	52.62	98.14
003C2#4	85	Ryne	46.60	0.08	0.00	0.01	0.01	0.02	53.48	100.17
003C2#5	85	Ryne	46.87	0.23	0.00	0.04	0.03	0.04	53.17	100.37

Sample #	Au (ppb)	Location	Fe wt%	As wt%	Co wt%	Cu wt%	Ni wt%	Zn wt%	S wt%	Total wt%
003C2#6	85	Ryne	46.95	0.15	0.00	0.04	0.03	0.00	53.38	100.55
003C7#1	85	Ryne	46.57	0.07	0.08	0.08	0.02	0.00	53.78	100.57
003C8#1	85	Ryne	46.87	0.08	0.12	0.02	0.02	0.00	53.72	100.81
003C9#1	85	Ryne	46.52	0.03	0.00	0.04	0.04	0.00	53.52	100.15
003C11#1	85	Ryne	46.79	0.13	0.00	0.02	0.03	0.02	53.58	100.56
066C1#1	1200	Ryne	46.86	0.07	0.00	0.03	0.05	0.00	53.41	100.21
066C1#2	1200	Ryne	46.39	0.10	0.01	0.02	0.05	0.01	53.32	99.91
066C1#3	1200	Ryne	46.79	0.08	0.07	0.02	0.02	0.01	53.45	100.45
066C1#4	1200	Ryne	46.33	0.40	0.08	0.01	0.08	0.00	53.13	100.00
066C1#5	1200	Ryne	46.49	0.09	0.00	0.01	0.04	0.03	53.58	100.24
066C1#6	1200	Ryne	45.89	0.14	0.03	0.04	0.08	0.00	53.25	99.43
066C3#1	1200	Ryne	46.54	0.02	0.00	0.08	0.02	0.02	53.42	100.08
066C4#1	1200	Ryne	46.73	0.05	0.03	0.03	0.21	0.00	53.07	100.11
066C4#2	1200	Ryne	46.32	0.08	0.10	0.03	0.07	0.03	53.54	100.16
066C4#3	1200	Ryne	46.33	0.05	0.01	0.02	0.01	0.02	53.58	100.02
066C5#1	1200	Ryne	46.24	0.04	0.00	0.05	0.03	0.00	53.72	100.08
066C6#1	1200	Ryne	46.74	0.10	0.02	0.04	0.02	0.00	53.58	100.49
066C6#2	1200	Ryne	46.72	0.08	0.00	0.05	0.08	0.00	53.40	100.33
066C6#3	1200	Ryne	46.45	0.08	0.00	0.02	0.02	0.00	53.05	99.60
066C9#1	1200	Ryne	45.51	0.03	0.01	0.01	0.11	0.00	52.42	98.09
066C9#2	1200	Ryne	46.84	0.05	0.00	0.00	0.12	0.03	37.96	85.02
066C9#3	1200	Ryne	46.22	0.08	0.02	0.00	0.11	0.00	50.27	96.69
R2C2#1	78oz	Ryne	46.54	0.51	0.00	0.03	0.01	0.00	53.11	100.19
R2C5#1	78oz	Ryne	46.62	0.70	0.00	0.02	0.01	0.00	52.76	100.12
R2C5#2	78oz	Ryne	28.60	0.12	0.01	0.03	0.03	0.00	45.24	74.03
R2C6#1	78oz	Ryne	46.76	0.11	0.00	0.01	0.01	0.02	53.43	100.33
R2C7#1	78oz	Ryne	46.69	0.09	0.04	0.01	0.02	0.01	53.62	100.49
R2C7#2	78oz	Ryne	46.72	0.13	0.00	0.01	0.01	0.00	53.74	100.61
R3C2#1	78oz	Ryne	46.77	0.17	0.02	0.01	0.04	0.00	53.62	100.64
R3C2#2	78oz	Ryne	46.77	0.96	0.00	0.04	0.02	0.00	52.86	100.65
R3C2#3	78oz	Ryne	46.07	0.37	0.02	0.00	0.02	0.01	52.75	99.24
R3C6#1	78oz	Ryne	46.99	0.13	0.00	0.02	0.03	0.04	53.46	100.66
R3C9#1	78oz	Ryne	46.74	0.20	0.00	0.02	0.04	0.00	53.58	100.57
R3C9#2	78oz	Ryne	46.97	0.11	0.00	0.00	0.02	0.00	53.55	100.66
R3C10#1	78oz	Ryne	46.85	0.19	0.04	0.00	0.03	0.00	53.25	100.37
R3C10#2	78oz	Ryne	46.28	0.35	0.01	0.03	0.08	0.00	53.68	100.44
022C1#1	8090	Ryne	46.45	0.13	0.00	0.04	0.02	0.00	54.15	100.79
022C1#2	8090	Ryne	46.37	0.06	0.01	0.00	0.01	0.00	53.98	100.43
022C2#1	8090	Ryne	46.46	0.39	0.00	0.04	0.01	0.00	54.08	100.96
022C2#2	8090	Ryne	46.78	0.07	0.00	0.01	0.02	0.00	54.07	100.94
022C2#3	8090	Ryne	46.66	0.07	0.01	0.02	0.03	0.00	54.08	100.86
022C3#1	8090	Ryne	46.08	0.04	0.00	0.05	0.02	0.00	54.79	100.99
022C3#2	8090	Ryne	46.76	0.06	0.00	0.04	0.03	0.01	53.93	100.84
022C3#3	8090	Ryne	45.64	1.17	0.00	0.03	0.07	0.00	53.48	100.39
023C4#1	8090	Ryne	46.39	0.09	0.02	0.04	0.02	0.02	54.34	100.91
023C4#2	8090	Ryne	46.22	0.47	0.00	0.03	0.02	0.01	53.92	100.66
023C4#3	8090	Ryne	46.39	0.44	0.00	0.01	0.01	0.02	53.93	100.81
023C4#4	8090	Ryne	46.55	0.14	0.02	0.01	0.02	0.00	54.09	100.84
023C4#5	8090	Ryne	46.40	0.02	0.00	0.04	0.00	0.01	54.41	100.88
148C1#1	13750	Big Bear	46.98	0.04	0.04	0.02	0.03	0.00	53.86	100.97
148C1#2	13750	Big Bear	46.97	0.01	0.00	0.00	0.01	0.00	53.84	100.83
148C1#3	13750	Big Bear	46.67	1.08	0.00	0.00	0.02	0.00	52.93	100.70
148C1#4	13750	Big Bear	46.96	0.44	0.00	0.02	0.01	0.02	53.51	100.97
148C1#5	13750	Big Bear	47.45	0.04	0.00	0.02	0.01	0.02	53.51	101.05
148C1#6	13750	Big Bear	46.55	0.02	0.00	0.01	0.01	0.00	53.59	100.19
148C2#1	13750	Big Bear	46.45	0.08	0.10	0.00	0.02	0.00	53.64	100.26
148C2#2	13750	Big Bear	46.90	0.05	0.00	0.00	0.03	0.01	53.68	100.68
148C2#3	13750	Big Bear	46.71	0.32	0.00	0.01	0.01	0.00	53.61	100.67
175C8#1	78oz	Ryne	46.79	0.10	0.00	0.01	0.03	0.00	53.88	100.81
128C1#1	7400	Ryne	46.13	0.04	0.00	0.02	0.02	0.03	53.15	99.39
128C1#2	7400	Ryne	45.77	0.07	0.00	0.01	0.01	0.00	53.20	99.05
128C2#1	7400	Ryne	45.71	0.14	0.00	0.02	0.01	0.00	53.26	99.13
128C2#2	7400	Ryne	45.83	0.01	0.00	0.01	0.00	0.00	53.54	99.39
128C2#3	7400	Ryne	45.96	0.14	0.00	0.00	0.02	0.00	52.95	99.07
128C3#1	7400	Ryne	45.90	0.07	0.00	0.03	0.02	0.00	53.10	99.12

Sample #	Au (ppb)	Location	Fe wt%	As wt%	Co wt%	Cu wt%	Ni wt%	Zn wt%	S wt%	Total wt%
128C3#2	7400	Ryne	45.87	0.10	0.00	0.00	0.02	0.00	53.03	99.03
128C4#1	7400	Ryne	45.65	0.80	0.00	0.03	0.01	0.00	52.68	99.18
128C4#2	7400	Ryne	45.96	0.17	0.00	0.02	0.02	0.07	53.08	99.34
128C4#3	7400	Ryne	46.30	0.07	0.03	0.03	0.02	0.03	53.27	99.76
128C8#1	7400	Ryne	46.13	0.16	0.00	0.00	0.01	0.00	53.06	99.36
128C8#2	7400	Ryne	45.80	0.10	0.00	0.02	0.03	0.00	52.86	98.91
R1aC3#1	78oz	Ryne	45.36	0.48	0.67	0.00	0.02	0.00	52.80	99.16
R1aC5#1	78oz	Ryne	45.89	0.06	0.00	0.02	0.02	0.00	53.18	99.17
R1aC5#2	78oz	Ryne	45.82	0.05	0.06	0.01	0.01	0.00	52.89	98.86
R1aC8#1	78oz	Ryne	46.20	0.05	0.00	0.03	0.01	0.01	53.12	99.42
R1aC9#1	78oz	Ryne	46.37	0.12	0.00	0.02	0.04	0.01	53.06	99.64
R1aC9#2	78oz	Ryne	45.99	0.15	0.00	0.00	0.03	0.02	53.29	99.49
R1aC11#1	78oz	Ryne	46.41	0.02	0.00	0.02	0.03	0.00	53.31	99.80
R1aC14#1	78oz	Ryne	45.89	0.03	0.00	0.00	0.01	0.01	53.05	98.99
R1bC1#1	78oz	Ryne	45.46	0.13	0.00	0.00	0.07	0.01	53.40	99.06
R1bC2#1	78oz	Ryne	45.50	0.09	0.01	0.01	0.01	0.00	53.39	99.00
R1bC2#2	78oz	Ryne	45.70	0.26	0.00	0.01	0.01	0.00	53.16	99.14
R1bC3#1	78oz	Ryne	45.90	0.03	0.00	0.02	0.00	0.00	53.19	99.15
R1bC8#1	78oz	Ryne	45.75	0.03	0.02	0.03	0.01	0.00	53.42	99.27
R1bC8#1	78oz	Ryne	45.40	0.85	0.00	0.03	0.01	0.03	52.60	98.92
R1bC8#2	78oz	Ryne	45.37	1.61	0.00	0.02	0.02	0.04	52.08	99.14
R1bC9#1	78oz	Ryne	45.75	0.18	0.06	0.02	0.02	0.00	53.30	99.35
R1bC12#1	78oz	Ryne	45.72	0.06	0.00	0.03	0.15	0.00	53.28	99.24
R1bC12#2	78oz	Ryne	46.06	0.01	0.00	0.02	0.03	0.01	53.41	99.56
R1bC12#3	78oz	Ryne	45.57	0.01	0.10	0.02	0.02	0.00	53.37	99.08
R1bC12#4	78oz	Ryne	45.36	0.06	0.00	0.02	0.20	0.01	53.36	99.01
H2C4#1	~60g/t	Hourglass	46.38	0.02	0.00	0.01	0.02	0.01	53.12	99.56
H2C8#1	~60g/t	Hourglass	45.56	0.06	0.09	0.03	0.02	0.00	53.41	99.15
H2C8#2	~60g/t	Hourglass	45.37	0.31	0.11	0.01	0.11	0.01	52.58	98.51
H2C8#3	~60g/t	Hourglass	45.96	0.05	0.00	0.03	0.06	0.00	53.30	99.41
H2C10#1	~60g/t	Hourglass	45.83	0.02	0.00	0.01	0.01	0.00	52.93	98.80
H2C10#2	~60g/t	Hourglass	45.58	1.06	0.00	0.03	0.03	0.00	52.44	99.15

Microprobe analyse results of pyrrhotite

Detection limit in wt%: Fe, 0.06; As, Cu, 0.04; Co, Ni, S, Zn, 0.02

Sample #	Au (ppb)	Location	Fe wt%	As wt%	Co wt%	Cu wt%	Ni wt%	Zn wt%	S wt%	Total wt%
23C1#1	1270	Ryne	58.35	0.07	0.00	0.04	0.10	0.00	39.12	97.67
23C2#1	1270	Ryne	58.07	0.05	0.00	0.05	0.08	0.03	39.16	97.44
23C3#1	1270	Ryne	58.87	0.05	0.00	0.04	0.09	0.00	39.10	98.15
23C4#1	1270	Ryne	59.42	0.04	0.00	0.01	0.08	0.00	38.31	97.84
30C2#1	2340	Ryne	58.41	0.00	0.00	0.12	0.01	0.01	38.23	97.78
21C2#1	8080	Ryne	58.92	0.08	0.00	0.01	0.09	0.03	39.12	98.23
21C3#1	8080	Ryne	58.74	0.00	0.00	0.02	0.09	0.03	38.94	97.82
21C4#1	8080	Ryne	58.90	0.05	0.00	0.01	0.08	0.00	38.85	97.91
148C2#1	13000	Big Bear	59.32	0.04	0.00	0.03	0.32	0.03	38.53	98.28
175C2#1	200000	Ryne	58.93	0.06	0.02	0.03	0.15	0.00	38.39	97.59
175C2#2	200000	Ryne	59.12	0.05	0.03	0.03	0.15	0.03	38.47	97.87
175C3#1	200000	Ryne	58.87	0.02	0.00	0.04	0.11	0.00	38.52	97.57
175C3#2	200000	Ryne	34.80	0.03	0.00	0.02	0.01	0.00	0.40	35.27
175C5#1	200000	Ryne	59.21	0.04	0.01	0.09	0.30	0.03	38.57	98.24
175C8#1	200000	Ryne	58.77	0.05	0.00	0.03	0.26	0.02	39.02	98.16
175C8#1	200000	Ryne	59.89	0.04	0.00	0.04	0.29	0.00	38.20	98.46
088CC5#1	1200	Ryne	60.08	0.06	0.01	0.06	0.17	0.00	37.96	98.36
R2C1#1	200000	Ryne	59.88	0.05	0.00	0.10	0.22	0.01	39.40	99.66
R2C3#1	200000	Ryne	46.75	0.05	0.02	0.13	0.38	0.01	43.72	91.06
R2C8#1	200000	Ryne	60.87	0.02	0.00	0.02	0.15	0.01	38.95	100.02
128C4#1	7400	Ryne	61.47	0.06	0.09	0.00	0.04	0.00	39.34	101.00
128C8#1	7400	Ryne	61.02	0.09	0.06	0.00	0.13	0.02	39.04	100.35
R1aC1#1	200000	Ryne	58.57	0.05	0.00	0.02	0.91	0.01	39.81	99.35
R1aC10#1	200000	Ryne	60.91	0.04	0.11	0.00	0.31	0.01	39.12	100.50
R1bC8#1	200000	Ryne	60.72	0.06	0.10	0.00	0.06	0.00	39.01	99.96
R1bC12#1	200000	Ryne	60.52	0.05	0.05	0.00	0.07	0.01	39.15	99.83
H2C8#1	65000	Hourglass	60.07	0.03	0.03	0.00	0.61	0.01	39.22	99.98
H2C8#2	65000	Hourglass	60.70	0.04	0.04	0.00	0.24	0.00	39.14	100.16
H2C8#3	65000	Hourglass	60.92	0.05	0.05	0.00	0.24	0.00	39.23	100.48
023C1#1	1270	Ryne	59.47	0.03	0.03	0.00	0.09	0.04	38.74	98.40
023C1#2	1270	Ryne	58.45	0.05	0.01	0.00	0.11	0.00	39.26	97.89
023C2#1	1270	Ryne	59.13	0.06	0.07	0.00	0.06	0.02	39.78	99.16
023C2#2	1270	Ryne	58.16	0.06	0.05	0.00	0.06	0.01	39.33	97.71
023C2#3	1270	Ryne	59.27	0.04	0.17	0.00	0.06	0.00	39.74	99.31
023C2#4	1270	Ryne	59.53	0.06	0.05	0.00	0.09	0.00	39.64	99.38
023C2#5	1270	Ryne	59.69	0.04	0.03	0.00	0.06	0.01	39.80	99.67
023C2#6	1270	Ryne	59.23	0.05	0.02	0.00	0.06	0.01	39.75	99.15
023C3#1	1270	Ryne	59.66	0.04	0.03	0.00	0.09	0.06	39.86	99.74
023C3#2	1270	Ryne	59.58	0.06	0.00	0.00	0.11	0.00	39.81	99.57
023C4#1	1270	Ryne	60.50	0.02	0.06	0.00	0.07	0.01	39.19	99.85
148C2#1	13750	Big Bear	60.37	0.05	0.03	0.00	0.34	0.00	38.97	99.77
175C2#1	200000	Ryne	60.03	0.07	0.05	0.03	0.16	0.02	38.80	99.17
175C2#2	200000	Ryne	59.82	0.04	0.04	0.04	0.17	0.01	38.99	99.11
175C2#3	200000	Ryne	59.69	0.03	0.07	0.03	0.17	0.00	38.86	98.84
175C2#4	200000	Ryne	59.87	0.04	0.05	0.00	0.16	0.00	38.83	98.96
175C4#1	200000	Ryne	59.66	0.05	0.02	0.00	0.49	0.00	38.62	98.84
175C5#1	200000	Ryne	60.29	0.03	0.07	0.02	0.33	0.00	38.89	99.63
175C5#2	200000	Ryne	60.33	0.01	0.05	0.00	0.31	0.00	39.24	99.95
175C5#3	200000	Ryne	60.22	0.05	0.05	0.00	0.33	0.00	38.95	99.61
175C5#4	200000	Ryne	60.41	0.05	0.05	0.01	0.25	0.02	39.19	99.98
175C8#1	200000	Ryne	61.07	0.03	0.07	0.00	0.30	0.01	39.32	100.81
175C8#2	200000	Ryne	59.46	0.05	0.03	0.00	0.30	0.00	39.69	99.53
175C8#3	200000	Ryne	59.69	0.06	0.02	0.00	0.25	0.00	39.81	99.83

Sample #	Au (ppb)	Location	Fe wt%	As wt%	Co wt%	Cu wt%	Ni wt%	Zn wt%	S wt%	Total wt%
175C8#4	200000	Ryne	59.86	0.04	0.02	0.01	0.25	0.00	39.67	99.86
175C8#1	200000	Ryne	59.79	0.04	0.04	0.00	0.17	0.02	39.62	99.69
175C8#2	200000	Ryne	60.71	0.07	0.01	0.00	0.30	0.02	39.09	100.21
175C8#3	200000	Ryne	59.60	0.04	0.01	0.00	0.24	0.00	39.58	99.46

Microprobe analyse results of other sulfides

Sphalerite

Detection limit in wt%: Zn, 0.11; Fe, 0.06; Ni, 0.01; Mn, S, 0.02

Sample #	Au (ppb)	Location	Zn wt%	Fe wt%	Ni wt%	Mn wt%	S wt%	Total wt%
023C3#1	1270	Ryne	59.85	7.26	0.01	0.00	31.76	98.89
148C2#1	13750	Big Bear	59.60	7.82	0.01	0.01	32.53	99.97
148C2#2	13750	Big Bear	59.34	7.57	0.01	0.00	32.73	99.66
148C2#3	13750	Big Bear	59.35	7.68	0.01	0.01	32.44	99.49

Chalcopyrite

Detection limit in wt%: Cu, 0.04; Fe, 0.05; As, 0.03; Ni, 0.01; S, 0.02

Sample #	Au (ppb)	Location	Cu wt%	Fe wt%	As wt%	Ni wt%	S wt%	Total wt%
172AC1#1	25000	Hourglass	33.78	30.93	0.05	0.02	34.93	99.71
22C3#1	8090	Ryne	33.67	30.90	0.07	0.04	34.30	98.99
23C1#1	1270	Ryne	0.03	59.05	0.06	0.13	39.32	98.61
23C2#1	1270	Ryne	33.92	30.17	0.03	0.02	34.39	98.52
23C6#1	1270	Ryne	34.05	30.66	0.03	0.01	34.72	99.46
30C2#1	2340	Ryne	34.49	30.52	0.03	0.01	34.92	99.98
148C1#1	13750	Big Bear	33.72	30.99	0.01	0.03	34.64	99.36
175C2#1	200000	Ryne	34.10	30.53	0.04	0.01	34.48	99.15
175C5#1	200000	Ryne	34.37	30.85	0.04	0.00	34.43	99.68
176C3#1	45000	Hourglass	33.74	31.49	0.07	0.01	34.53	99.84

Arsenopyrite

Detection limit in wt%: Fe, Cu, 0.05; As, 0.07; Ni, Co, S, Mn, 0.02; Zn, 0.03

Sample #	Au (ppb)	Location	Fe wt%	As wt%	Cu wt%	Ni wt%	Zn wt%	Mn wt%	Co wt%	S wt%	Total wt%
23C1#1	1270	Ryne	35.62	43.13	0.02	0.01	0.00	0.01	0.00	21.32	100.11
23C1#2	1270	Ryne	34.21	44.57	0.00	0.04	0.00	0.00	0.69	20.43	99.94
23C2#1	1270	Ryne	35.08	43.49	0.02	0.01	0.02	0.00	0.01	21.13	99.76
23C2#2	1270	Ryne	35.02	43.03	0.02	0.02	0.03	0.00	0.00	21.31	99.42
23C3#1	1270	Ryne	35.19	43.29	0.02	0.02	0.00	0.00	0.00	21.14	99.67
30C1#1	2340	Ryne	27.41	48.10	0.00	0.22	0.00	0.01	6.78	18.52	101.04
H2C6#1	65000	Hourglass	35.52	43.03	0.00	0.13	0.03	0.00	0.01	21.53	100.26
H2C10#1	65000	Hourglass	35.16	42.79	0.01	0.23	0.00	0.00	0.00	21.18	99.38
023C2#1	1270	Ryne	34.85	42.42	0.06	0.03	0.02	0.01	0.06	21.59	99.04
023C2#2	1270	Ryne	34.68	41.61	0.03	0.02	0.00	0.00	0.00	21.84	98.18
023C2#3	1270	Ryne	35.09	42.72	0.02	0.02	0.00	0.01	0.00	21.31	99.17
023C2#4	1270	Ryne	35.07	42.64	0.01	0.02	0.00	0.00	0.00	21.28	99.03

Microprobe analyse results of carbonate minerals

Detection limit in wt%: CaO, MnO, 0.03; MgO, 0.02; FeO, 0.04; SrO, 0.05

Sample #	Au (ppb)	Location	CaO wt%	MgO wt%	FeO wt%	MnO wt%	SrO wt%	CO2 wt%	Total wt%
066C2AK#1	1200	Ryne	28.13	12.92	13.38	0.46	0.010	45.12	100.0
066C2AK#2	1200	Ryne	28.35	13.62	12.61	0.49	0.004	44.92	100.0
066C2AK#3	1200	Ryne	28.54	13.54	12.87	0.52	0.000	44.54	100.0
066C7CB#1	1200	Ryne	28.52	13.72	13.22	0.49	0.000	44.05	100.0
066C7CB#2	1200	Ryne	28.93	13.32	12.82	0.39	0.025	44.52	100.0
066C8CB#1	1200	Ryne	28.27	13.55	13.43	0.32	0.047	44.38	100.0
066C8CB#2	1200	Ryne	28.37	13.21	13.81	0.35	0.057	44.20	100.0
066C8CB#3	1200	Ryne	28.09	12.66	14.33	0.36	0.107	44.45	100.0
066C12CB#1	1200	Ryne	28.03	12.14	14.81	0.35	0.183	44.48	100.0
066C12CB#2	1200	Ryne	28.11	12.23	14.60	0.36	0.189	44.51	100.0
003C1CB#1	85	Ryne	53.93	0.34	0.94	0.22	0.000	44.57	100.0
003C2CB#1	85	Ryne	52.83	0.32	1.02	0.20	0.000	45.62	100.0
003C2CB#2	85	Ryne	53.42	0.58	0.33	0.24	0.000	45.43	100.0
003C4CB#1	85	Ryne	56.53	0.26	0.12	0.23	0.000	42.87	100.0
003C4CB#2	85	Ryne	53.69	0.36	0.24	0.26	0.000	45.45	100.0
003C5CB#1	85	Ryne	53.02	0.03	0.88	0.66	0.000	45.41	100.0
003C5CB#2	85	Ryne	53.45	0.04	0.59	0.66	0.000	45.26	100.0
003C5CB#3	85	Ryne	53.08	0.48	1.53	0.17	0.000	44.74	100.0
003C5CB#4	85	Ryne	54.26	0.20	0.61	0.16	0.000	44.78	100.0
003C6CB#1	85	Ryne	53.42	0.12	0.58	0.30	0.000	45.57	100.0
003C7CB#1	85	Ryne	54.32	0.39	0.45	0.30	0.000	44.54	100.0
003C7CB#2	85	Ryne	54.02	0.39	0.41	0.25	0.000	44.94	100.0
003C10CB#1	85	Ryne	54.42	0.12	0.77	0.65	0.000	44.06	100.0
R1aC4CB#1	200000	Ryne	29.31	12.93	12.67	0.74	0.000	44.35	100.0
R1aC4CB#2	200000	Ryne	29.19	12.73	12.89	0.68	0.000	44.51	100.0
R1aC6CB#1	200000	Ryne	28.47	11.60	14.60	0.73	0.000	44.60	100.0
R1aC7CB#1	200000	Ryne	27.87	11.00	16.55	0.57	0.000	44.02	100.0
R1aC10CB#1	200000	Ryne	52.83	0.13	0.59	0.33	0.000	46.13	100.0
R1aC11CB#1	200000	Ryne	27.76	11.81	15.71	0.64	0.000	44.08	100.0
R1aC12CB#1	200000	Ryne	28.39	11.87	14.59	0.84	0.000	44.30	100.0
R1aC12CB#2	200000	Ryne	28.49	11.98	14.56	0.68	0.000	44.30	100.0
R1aC12CB#3	200000	Ryne	28.57	12.37	12.98	1.08	0.000	45.01	100.0
R1aC13CB#1	200000	Ryne	30.91	17.84	2.79	0.84	0.000	47.62	100.0
R1aC13CB#2	200000	Ryne	30.35	12.85	9.85	1.91	0.000	45.04	100.0
R1aC13CB#3	200000	Ryne	30.27	18.16	2.98	0.95	0.000	47.63	100.0
R1aC13CB#4	200000	Ryne	53.27	0.13	0.44	0.21	0.000	45.95	100.0
R1aC13CB#5	200000	Ryne	53.20	0.11	0.43	0.24	0.000	46.02	100.0
R1bC2CB#1	200000	Ryne	29.24	18.26	3.27	1.08	0.000	48.14	100.0
R1bC3CB#1	200000	Ryne	29.62	18.55	3.57	1.01	0.000	47.25	100.0
R1bC3CB#2	200000	Ryne	48.45	2.78	2.93	0.91	0.000	44.93	100.0
R1bC7CB#1	200000	Ryne	27.79	11.82	15.64	0.59	0.010	44.15	100.0
R1bC7CB#2	200000	Ryne	27.80	11.83	15.33	0.60	0.000	44.45	100.0
126C1CB#1	7400	Ryne	29.12	13.14	11.34	1.63	0.000	44.76	100.0
126C1CB#2	7400	Ryne	28.73	13.07	11.22	1.76	0.000	45.23	100.0
126C1CB#3	7400	Ryne	29.03	13.38	10.35	1.96	0.000	45.28	100.0
126C2CB#1	7400	Ryne	28.12	13.64	11.24	1.37	0.000	45.62	100.0
R2C2CB#1	200000	Ryne	29.06	19.18	4.27	0.59	0.029	46.87	100.0
R2C7CB#1	200000	Ryne	28.54	11.48	15.60	0.56	0.025	43.80	100.0

Sample #	Au (ppb)	Location	CaO wt%	MgO wt%	FeO wt%	MnO wt%	SrO wt%	CO2 wt%	Total wt%
R2C7CB#2	200000	Ryne	28.74	11.29	15.49	0.59	0.107	43.78	100.0
R2C7CB#3	200000	Ryne	28.56	10.88	16.02	0.54	0.018	43.99	100.0
R3C1CB#1	200000	Ryne	28.63	10.86	15.75	0.51	0.019	44.23	100.0
R3C1CB#2	200000	Ryne	28.46	10.57	16.56	0.59	0.017	43.80	100.0
R3C1CB#3	200000	Ryne	28.43	10.78	16.33	0.56	0.034	43.87	100.0
R3C1CB#4	200000	Ryne	27.77	10.25	16.87	0.60	0.019	44.49	100.0
R3C1CB#5	200000	Ryne	27.89	10.26	16.78	0.55	0.000	44.52	100.0
R3C2CB#1	200000	Ryne	28.17	11.56	15.42	0.57	0.013	44.27	100.0
R3C2CB#2	200000	Ryne	28.37	11.43	15.44	0.72	0.011	44.04	100.0
R3C3CB#1	200000	Ryne	54.31	1.50	0.30	0.02	0.000	43.87	100.0
R3C3CB#2	200000	Ryne	52.18	1.52	0.40	0.01	0.000	45.89	100.0
R3C8CB#1	200000	Ryne	28.29	11.18	15.68	0.58	0.021	44.25	100.0
R3C8CB#2	200000	Ryne	28.37	11.34	15.70	0.54	0.000	44.05	100.0
R3C8CB#3	200000	Ryne	28.43	11.41	15.38	0.62	0.000	44.15	100.0
H2C4CB#1	69000	Hourglass	50.64	1.13	1.86	0.48	0.000	45.90	100.0
009C1CB#1	815	Ryne	53.09	0.51	1.59	1.00	0.000	43.81	100.0
009C1CB#2	815	Ryne	52.70	0.32	1.35	0.96	0.000	44.66	100.0
009C2CB#1	815	Ryne	53.54	0.16	0.64	0.84	0.000	44.83	100.0
009C3CB#1	815	Ryne	52.42	0.32	1.42	0.99	0.000	44.86	100.0
009C4CB#1	815	Ryne	52.70	0.36	1.25	0.95	0.000	44.73	100.0
009C5CB#1	815	Ryne	52.63	0.39	1.49	1.03	0.000	44.47	100.0
009C6CB#1	815	Ryne	54.01	0.35	0.97	1.17	0.000	43.51	100.0
009C7CB#1	815	Ryne	52.46	0.34	1.43	1.06	0.000	44.71	100.0
009C8CB#1	815	Ryne	51.92	0.50	1.72	1.02	0.000	44.83	100.0
009C9CB#1	815	Ryne	52.30	0.52	1.80	1.06	0.000	44.32	100.0
009C10CB#1	815	Ryne	52.27	0.54	1.79	1.09	0.000	44.32	100.0
009C11CB#1	815	Ryne	53.24	0.44	1.17	1.19	0.000	43.97	100.0
009C12CB#1	815	Ryne	51.47	0.53	2.20	1.17	0.000	44.63	100.0
009C12CB#2	815	Ryne	51.52	0.70	2.21	1.02	0.000	44.55	100.0
009C12CB#3	815	Ryne	53.23	0.62	1.77	1.12	0.000	43.26	100.0
009C12CB#4	815	Ryne	52.65	0.64	1.99	1.16	0.000	43.57	100.0
009C13CB#1	815	Ryne	49.49	0.89	4.02	0.65	0.072	44.88	100.0
013C1CB#1	4	Ryne	54.75	0.35	0.28	0.48	0.000	44.14	100.0
013C1CB#2	4	Ryne	53.57	0.44	1.06	0.34	0.000	44.60	100.0
013C2CB#1	4	Ryne	54.54	0.07	0.29	0.42	0.000	44.68	100.0
013C3CB#1	4	Ryne	54.66	0.08	0.31	0.33	0.000	44.62	100.0
013C4CB#1	4	Ryne	55.28	0.22	0.35	0.44	0.000	43.70	100.0
013C5CB#1	4	Ryne	54.79	0.27	0.30	0.41	0.000	44.24	100.0
013C5CB#2	4	Ryne	53.05	0.45	1.20	0.25	0.000	45.06	100.0
013C6CB#1	4	Ryne	54.02	0.40	1.14	0.37	0.000	44.08	100.0
013C7CB#1	4	Ryne	55.34	0.19	0.24	0.50	0.000	43.73	100.0
013C8CB#1	4	Ryne	53.02	0.57	1.76	0.29	0.000	44.36	100.0
013C9CB#1	4	Ryne	53.51	0.30	1.10	0.25	0.000	44.85	100.0
013C10CB#1	4	Ryne	54.47	0.15	0.51	0.45	0.000	44.42	100.0
013C11CB#1	4	Ryne	54.92	0.45	0.43	0.62	0.000	43.59	100.0
013C12CB#1	4	Ryne	53.66	0.45	0.55	0.53	0.000	44.82	100.0
013C12CB#2	4	Ryne	52.13	0.58	1.75	0.26	0.000	45.29	100.0
011C1CB#1	140	Ryne	50.85	0.51	2.42	1.43	0.000	44.80	100.0
011C1CB#2	140	Ryne	50.47	0.58	2.72	1.51	0.000	44.71	100.0
011C2CB#1	140	Ryne	50.00	0.58	2.90	1.55	0.000	44.96	100.0
011C3CB#1	140	Ryne	49.20	0.97	3.14	2.13	0.000	44.56	100.0
011C4CB#1	140	Ryne	50.61	0.54	2.60	1.58	0.000	44.68	100.0

Sample #	Au (ppb)	Location	CaO wt%	MgO wt%	FeO wt%	MnO wt%	SrO wt%	CO2 wt%	Total wt%
011C5CB#1	140	Ryne	50.97	0.48	2.46	1.55	0.000	44.54	100.0
011C6CB#1	140	Ryne	53.48	0.21	0.93	1.35	0.000	44.04	100.0
011C7CB#1	140	Ryne	52.25	0.19	0.92	1.32	0.000	45.32	100.0
011C8CB#1	140	Ryne	50.43	0.52	2.66	1.61	0.000	44.77	100.0
005C1CB#1	6	Ryne	54.98	0.03	0.06	0.26	0.000	44.69	100.0
005C2CB#1	6	Ryne	53.20	0.49	1.34	0.53	0.000	44.45	100.0
005C3CB#1	6	Ryne	53.18	0.40	1.02	0.44	0.000	44.95	100.0
005C3CB#2	6	Ryne	55.05	0.05	0.18	0.20	0.000	44.53	100.0
005C4CB#1	6	Ryne	52.80	0.53	1.21	0.50	0.000	44.96	100.0
005C5CB#1	6	Ryne	52.95	0.55	1.29	0.44	0.000	44.76	100.0
005C6CB#1	6	Ryne	54.82	0.47	1.17	0.48	0.000	43.06	100.0
005C7CB#1	6	Ryne	55.60	0.05	0.08	0.31	0.000	43.97	100.0
005C7CB#2	6	Ryne	55.32	0.03	0.06	0.32	0.000	44.28	100.0
005C7CB#3	6	Ryne	53.52	0.45	1.01	0.51	0.000	44.52	100.0
005C7CB#4	6	Ryne	54.00	0.34	0.74	0.42	0.000	44.51	100.0
021C1CB#1	8090	Ryne	28.20	9.66	17.98	0.47	0.146	43.54	100.0
021C2CB#1	8090	Ryne	51.04	0.51	1.67	2.02	0.000	44.75	100.0
021C2CB#2	8090	Ryne	28.18	13.36	13.00	0.43	0.000	45.04	100.0
021C3CB#1	8090	Ryne	28.35	9.47	18.52	0.51	0.140	43.01	100.0
021C4CB#1	8090	Ryne	54.57	0.11	0.52	0.67	0.000	44.12	100.0
021C5CB#1	8090	Ryne	53.43	0.15	0.74	0.19	0.000	45.50	100.0
021C6CB#1	8090	Ryne	29.15	8.95	18.23	0.67	0.000	43.01	100.0
021C6CB#2	8090	Ryne	28.47	9.43	18.28	0.70	0.000	43.12	100.0
021C6CB#3	8090	Ryne	28.55	9.09	18.41	0.76	0.000	43.19	100.0
021C6CB#4	8090	Ryne	28.11	8.09	20.25	1.03	0.000	42.52	100.0
021C7CB#1	8090	Ryne	53.90	0.09	0.35	1.45	0.000	44.21	100.0
090C1CB#1	480	Ryne	28.72	13.19	13.02	0.29	0.237	44.55	100.0
090C1CB#2	480	Ryne	28.57	15.79	8.61	1.15	0.000	45.88	100.0
090C2CB#1	480	Ryne	28.69	13.36	13.57	0.31	0.108	43.96	100.0
090C3CB#1	480	Ryne	28.26	13.61	13.15	0.46	0.000	44.54	100.0
090C4CB#1	480	Ryne	28.56	13.70	13.08	0.29	0.071	44.30	100.0
090C5CB#1	480	Ryne	28.34	12.61	14.49	0.27	0.097	44.21	100.0
090C6CB#1	480	Ryne	29.07	13.61	11.99	0.59	0.000	44.74	100.0
024C1CB#1	1320	Ryne	28.38	12.34	14.85	0.55	0.017	43.87	100.0
024C2CB#1	1320	Ryne	28.57	12.96	13.28	0.62	0.000	44.57	100.0
024C3CB#1	1320	Ryne	28.25	12.02	14.84	0.58	0.057	44.26	100.0
024C4CB#1	1320	Ryne	28.45	12.05	14.38	0.60	0.019	44.49	100.0
024C5CB#1	1320	Ryne	55.04	0.05	0.26	0.18	0.000	44.48	100.0
024C6CB#1	1320	Ryne	28.45	10.86	15.79	0.54	0.162	44.21	100.0
018C1CB#1	60	Ryne	53.30	0.87	2.18	0.26	0.000	43.39	100.0
018C2CB#1	60	Ryne	54.16	0.44	0.77	0.73	0.000	43.91	100.0
018C3CB#1	60	Ryne	54.74	0.40	0.41	0.31	0.000	44.15	100.0
018C4CB#1	60	Ryne	53.63	0.28	0.75	0.55	0.000	44.79	100.0
018C5CB#1	60	Ryne	54.22	0.07	0.77	0.37	0.000	44.57	100.0
018C6CB#1	60	Ryne	54.33	0.09	0.70	0.40	0.000	44.49	100.0
018C7CB#1	60	Ryne	55.10	0.07	0.71	0.39	0.000	43.73	100.0
018C8CB#1	60	Ryne	50.40	0.28	0.73	0.43	0.000	48.16	100.0
018C9CB#1	60	Ryne	54.77	0.28	0.71	0.19	0.000	44.05	100.0
018C10CB#1	60	Ryne	52.66	1.05	1.23	0.61	0.000	44.46	100.0
026C1CB#1	800	Ryne	27.84	10.54	16.73	1.00	0.000	43.90	100.0
026C2CB#1	800	Ryne	28.34	10.70	16.59	0.83	0.066	43.49	100.0
026C3CB#1	800	Ryne	28.31	8.97	17.92	1.68	0.019	43.10	100.0

Sample #	Au (ppb)	Location	CaO wt%	MgO wt%	FeO wt%	MnO wt%	SrO wt%	CO2 wt%	Total wt%
026C4CB#1	800	Ryne	28.72	10.86	15.47	1.09	0.000	43.86	100.0
026C5CB#1	800	Ryne	28.02	10.56	16.64	1.02	0.056	43.70	100.0
026C6CB#1	800	Ryne	28.95	9.41	16.72	1.19	0.037	43.70	100.0
026C7CB#1	800	Ryne	28.86	10.98	15.31	0.93	0.000	43.93	100.0
026C8CB#1	800	Ryne	27.74	10.36	17.01	1.37	0.000	43.52	100.0
026C9CB#1	800	Ryne	28.04	10.39	16.44	1.14	0.000	43.99	100.0
026C10CB#1	800	Ryne	27.52	7.77	19.70	1.63	0.027	43.36	100.0
081C1CB#1	2530	Hourglass	27.94	8.92	18.78	0.76	0.000	43.61	100.0
081C2CB#1	2530	Hourglass	28.43	9.65	18.16	0.64	0.097	43.03	100.0
081C2CB#2	2530	Hourglass	28.25	10.11	17.73	0.55	0.002	43.36	100.0
081C3CB#1	2530	Hourglass	27.89	10.02	18.40	0.59	0.010	43.10	100.0
081C4CB#1	2530	Hourglass	28.89	9.46	17.89	0.72	0.000	43.05	100.0
081C5CB#1	2530	Hourglass	28.56	9.69	18.30	0.59	0.077	42.79	100.0
081C5CB#2	2530	Hourglass	28.10	8.30	20.34	0.58	0.009	42.67	100.0
081C5CB#3	2530	Hourglass	28.24	10.88	16.93	0.45	0.079	43.42	100.0
081C5CB#4	2530	Hourglass	28.39	12.47	14.30	0.57	0.178	44.10	100.0
081C5CB#5	2530	Hourglass	28.70	9.92	17.73	0.51	0.054	43.09	100.0
081C6CB#1	2530	Hourglass	28.04	9.83	18.32	0.55	0.013	43.25	100.0
081C7CB#1	2530	Hourglass	54.85	0.09	0.06	0.18	0.000	44.83	100.0
081C8CB#1	2530	Hourglass	28.54	8.54	19.32	0.75	0.000	42.85	100.0
081C9CB#1	2530	Hourglass	28.52	7.29	21.26	0.59	0.019	42.31	100.0
081C10CB#1	2530	Hourglass	28.51	9.56	17.96	0.84	0.000	43.13	100.0
081C11CB#1	2530	Hourglass	28.01	9.84	18.24	0.71	0.000	43.20	100.0
022C1CB#1	8090	Ryne	28.46	12.00	14.88	0.49	0.048	44.12	100.0
022C2CB#1	8090	Ryne	28.31	12.65	14.06	0.56	0.096	44.33	100.0
022C3CB#1	8090	Ryne	28.61	11.37	15.29	0.57	0.060	44.10	100.0
022C4CB#1	8090	Ryne	28.33	11.54	15.50	0.50	0.057	44.06	100.0
022C5CB#1	8090	Ryne	28.41	11.14	15.97	0.49	0.000	43.98	100.0
022C6CB#1	8090	Ryne	28.36	11.89	15.17	0.63	0.025	43.93	100.0
022C7CB#1	8090	Ryne	28.26	12.03	14.61	0.55	0.041	44.51	100.0
023C1CB#1	1270	Ryne	27.92	10.55	17.09	1.16	0.047	43.24	100.0
023C2CB#1	1270	Ryne	28.38	11.57	15.23	0.82	0.076	43.91	100.0
023C3CB#1	1270	Ryne	28.13	10.47	16.81	1.43	0.038	43.11	100.0
023C4CB#1	1270	Ryne	28.16	11.33	15.39	0.79	0.080	44.25	100.0
023C5CB#1	1270	Ryne	27.80	8.98	18.96	1.16	0.044	43.07	100.0
023C6CB#1	1270	Ryne	28.49	9.32	17.96	0.92	0.000	43.32	100.0
127C1CB#1	4	Ryne	52.97	0.23	0.85	1.24	0.000	44.71	100.0
127C2CB#1	4	Ryne	52.21	0.32	1.88	1.77	0.000	43.83	100.0
127C3CB#1	4	Ryne	52.89	0.15	1.03	1.13	0.000	44.80	100.0
127C4CB#1	4	Ryne	54.87	0.55	0.29	0.95	0.000	43.34	100.0
127C5CB#1	4	Ryne	51.65	0.27	1.49	1.57	0.000	45.03	100.0
127C6CB#1	4	Ryne	50.26	0.36	2.24	1.86	0.000	45.28	100.0
127C7CB#1	4	Ryne	54.25	0.14	0.48	1.52	0.000	43.61	100.0
127C8CB#1	4	Ryne	53.76	0.34	0.47	1.43	0.000	43.99	100.0
127C9CB#1	4	Ryne	50.29	0.23	2.10	2.85	0.016	44.52	100.0
127C10CB#1	4	Ryne	53.22	0.17	1.01	1.21	0.000	44.39	100.0
127C10CB#2	4	Ryne	52.76	0.19	1.18	1.35	0.000	44.52	100.0
127C10CB#3	4	Ryne	54.26	0.05	0.30	0.81	0.000	44.60	100.0
127C10CB#4	4	Ryne	52.15	0.21	1.41	1.43	0.000	44.80	100.0
128C1CB#1	5	Ryne	53.72	0.29	1.05	0.58	0.000	44.36	100.0
128C2CB#1	5	Ryne	52.86	0.13	0.96	1.18	0.000	44.89	100.0
128C3CB#1	5	Ryne	54.08	0.23	0.83	0.54	0.000	44.31	100.0

Sample #	Au (ppb)	Location	CaO wt%	MgO wt%	FeO wt%	MnO wt%	SrO wt%	CO2 wt%	Total wt%
128C4CB#1	5	Ryne	53.04	0.34	1.26	0.67	0.000	44.69	100.0
128C5CB#1	5	Ryne	54.71	0.18	0.77	0.92	0.000	43.42	100.0
128C6CB#1	5	Ryne	53.00	0.29	1.32	0.64	0.000	44.75	100.0
128C7CB#1	5	Ryne	52.33	0.49	1.10	1.29	0.000	44.80	100.0
128C7CB#2	5	Ryne	53.85	0.20	0.85	0.54	0.000	44.55	100.0
128C7CB#3	5	Ryne	53.42	0.21	0.97	0.54	0.000	44.85	100.0
128C8CB#1	5	Ryne	52.75	0.34	1.30	0.87	0.000	44.75	100.0
128C8CB#2	5	Ryne	54.26	0.12	0.40	0.54	0.000	44.68	100.0
128C8CB#3	5	Ryne	56.68	0.06	0.23	0.43	0.000	42.60	100.0
128C8CB#4	5	Ryne	54.44	0.21	0.93	0.51	0.000	43.92	100.0
138BC1CB#1	12960	Ryne	29.23	15.97	7.60	1.05	0.000	46.14	100.0
138BC2CB#1	12960	Ryne	28.14	12.75	13.81	0.53	0.092	44.68	100.0
138BC3CB#1	12960	Ryne	28.78	12.73	14.03	0.28	0.000	44.18	100.0
138BC3CB#2	12960	Ryne	28.68	12.69	13.95	0.25	0.000	44.43	100.0
138BC3CB#3	12960	Ryne	28.56	13.06	13.66	0.31	0.010	44.40	100.0
138BC3CB#4	12960	Ryne	28.39	12.52	14.27	0.24	0.044	44.54	100.0
138BC3CB#5	12960	Ryne	28.62	13.78	12.16	0.44	0.022	44.98	100.0
138BC4CB#1	12960	Ryne	28.61	12.90	13.32	0.45	0.129	44.59	100.0
138BC5CB#1	12960	Ryne	28.64	13.43	12.81	0.45	0.111	44.57	100.0
138BC6CB#1	12960	Ryne	28.60	13.74	12.22	0.40	0.078	44.96	100.0
138BC7CB#1	12960	Ryne	28.72	14.04	12.02	0.38	0.012	44.83	100.0
138BC7CB#2	12960	Ryne	28.86	13.33	13.05	0.43	0.031	44.30	100.0
138BC7CB#3	12960	Ryne	28.89	11.79	14.75	0.50	0.031	44.05	100.0
138BC7CB#4	12960	Ryne	28.84	13.98	11.90	0.37	0.005	44.91	100.0
154C1CB#1	51450	Houglass	28.39	10.20	17.41	0.36	0.080	43.55	100.0
154C2CB#1	51450	Houglass	29.37	14.41	10.32	0.62	0.000	45.29	100.0
154C2CB#2	51450	Houglass	29.17	14.01	10.85	0.58	0.000	45.39	100.0
154C2CB#3	51450	Houglass	27.78	9.44	18.67	0.41	0.010	43.68	100.0
154C2CB#4	51450	Houglass	28.38	10.34	16.64	0.39	0.000	44.26	100.0
154C3CB#1	51450	Houglass	28.29	11.17	16.01	0.38	0.043	44.12	100.0
154C4CB#1	51450	Houglass	28.66	11.00	15.75	0.44	0.000	44.15	100.0
154C5CB#1	51450	Houglass	28.24	11.47	15.99	0.33	0.030	43.93	100.0
154C6CB#1	51450	Houglass	28.04	10.19	17.15	0.37	0.060	44.18	100.0
154C6CB#2	51450	Houglass	28.40	10.04	17.67	0.42	0.030	43.44	100.0
154C6CB#3	51450	Houglass	28.15	10.62	16.94	0.37	0.020	43.90	100.0
154C6CB#4	51450	Houglass	28.23	12.57	13.99	0.37	0.089	44.75	100.0
154C6CB#5	51450	Houglass	28.49	9.79	18.04	0.41	0.064	43.20	100.0
154C6CB#6	51450	Houglass	28.40	9.66	17.33	0.42	0.000	44.19	100.0
154C6CB#7	51450	Houglass	28.26	9.50	17.94	0.39	0.010	43.90	100.0
154C6CB#8	51450	Houglass	28.45	10.04	17.55	0.44	0.086	43.43	100.0
154C7CB#1	51450	Houglass	28.29	9.74	18.04	0.41	0.118	43.40	100.0
154C8CB#1	51450	Houglass	29.12	11.86	14.14	0.47	0.211	44.21	100.0
154C9CB#1	51450	Houglass	28.39	10.38	17.21	0.46	0.055	43.51	100.0
154C10CB#1	51450	Houglass	28.47	11.59	15.32	0.37	0.000	44.25	100.0
165C1CB#1	32	Houglass	27.76	9.58	18.96	0.50	0.031	43.17	100.0
165C1CB#2	32	Houglass	53.85	0.29	0.83	0.31	0.000	44.72	100.0
165C2CB#1	32	Houglass	28.14	9.04	19.42	0.33	0.108	42.96	100.0
165C2CB#2	32	Houglass	27.86	9.98	18.33	0.42	0.000	43.42	100.0
165C3CB#1	32	Houglass	28.86	10.85	15.86	0.65	0.000	43.79	100.0
165C3CB#2	32	Houglass	28.14	8.65	20.37	0.45	0.000	42.40	100.0
165C3CB#3	32	Houglass	28.39	12.52	13.29	1.38	0.000	44.42	100.0
165C3CB#4	32	Houglass	28.37	11.07	15.32	0.91	0.000	44.33	100.0

Sample #	Au (ppb)	Location	CaO wt%	MgO wt%	FeO wt%	MnO wt%	SrO wt%	CO2 wt%	Total wt%
165C3CB#5	32	Hougiass	27.86	8.93	19.72	0.47	0.001	43.01	100.0
165C4CB#1	32	Hougiass	27.96	9.26	19.15	0.45	0.000	43.18	100.0
165C5CB#1	32	Hougiass	27.91	8.98	19.49	0.57	0.004	43.05	100.0
165C6CB#1	32	Hougiass	28.24	9.21	18.86	0.54	0.012	43.15	100.0
165C6CB#2	32	Hougiass	28.21	9.92	17.64	0.44	0.000	43.79	100.0
165C6CB#3	32	Hougiass	28.14	10.68	15.94	0.54	0.000	44.70	100.0
165C7CB#1	32	Hougiass	28.95	9.09	18.07	0.40	0.000	43.50	100.0
165C7CB#2	32	Hougiass	29.08	9.33	18.05	0.50	0.000	43.04	100.0
165C7CB#3	32	Hougiass	28.96	9.87	16.70	0.81	0.000	43.65	100.0
172AC1CB#1	52500	Hougiass	27.94	9.80	17.88	0.38	0.018	43.99	100.0
172AC2CB#1	52500	Hougiass	28.20	10.97	17.24	0.34	0.098	43.15	100.0
172AC2CB#2	52500	Hougiass	28.38	11.70	15.84	0.28	0.002	43.79	100.0
172AC3CB#1	52500	Hougiass	28.94	10.06	17.35	0.41	0.084	43.17	100.0
172AC4CB#1	52500	Hougiass	28.73	10.58	16.97	0.48	0.000	43.24	100.0
172AC4CB#2	52500	Hougiass	28.20	11.05	16.40	0.33	0.158	43.87	100.0
172AC4CB#3	52500	Hougiass	28.40	12.56	14.14	0.40	0.208	44.29	100.0
172AC4CB#4	52500	Hougiass	28.22	10.53	16.87	0.39	0.105	43.89	100.0
172AC4CB#5	52500	Hougiass	28.36	10.96	16.68	0.37	0.103	43.54	100.0
172AC4CB#6	52500	Hougiass	28.39	11.98	15.38	0.40	0.143	43.71	100.0
172AC4CB#7	52500	Hougiass	28.60	10.60	16.60	0.45	0.000	43.75	100.0
172AC4CB#8	52500	Hougiass	28.57	11.93	15.36	0.35	0.114	43.68	100.0
172AC4CB#9	52500	Hougiass	28.36	11.14	16.23	0.39	0.122	43.76	100.0
172AC4CB#10	52500	Hougiass	28.48	12.88	13.57	0.41	0.212	44.44	100.0
172AC4CB#11	52500	Hougiass	28.33	11.30	16.25	0.36	0.123	43.65	100.0
172AC4CB#12	52500	Hougiass	28.09	9.27	19.10	0.34	0.064	43.15	100.0
172AC4CB#13	52500	Hougiass	28.34	9.71	18.55	0.31	0.060	43.02	100.0
172AC4CB#14	52500	Hougiass	28.67	11.71	15.27	0.40	0.159	43.79	100.0
172AC4CB#15	52500	Hougiass	28.26	11.37	15.50	0.39	0.066	44.42	100.0
172AC4CB#16	52500	Hougiass	28.59	12.92	13.65	0.42	0.175	44.24	100.0
172AC4CB#17	52500	Hougiass	28.51	12.60	14.20	0.41	0.120	44.17	100.0
172AC4CB#18	52500	Hougiass	28.49	11.26	16.56	0.32	0.169	43.20	100.0
172AC4CB#19	52500	Hougiass	28.56	11.40	16.25	0.36	0.097	43.34	100.0
172AC4CB#20	52500	Hougiass	28.78	12.02	15.10	0.48	0.036	43.58	100.0
172AC4CB#21	52500	Hougiass	28.53	12.66	13.70	0.43	0.000	44.68	100.0
172AC5CB#1	52500	Hougiass	54.55	0.09	0.73	0.26	0.000	44.37	100.0
172AC6CB#1	52500	Hougiass	28.27	10.53	16.83	0.45	0.000	43.93	100.0
172AC6CB#2	52500	Hougiass	28.01	10.61	16.78	0.45	0.000	44.15	100.0
172AC6CB#3	52500	Hougiass	54.82	0.04	0.44	0.19	0.000	44.51	100.0
172AC6CB#4	52500	Hougiass	54.15	0.13	0.41	0.35	0.000	44.96	100.0
175C1CB#1	200000	Ryne	29.55	14.01	10.27	1.10	0.000	45.07	100.0
175C2CB#1	200000	Ryne	29.56	13.08	13.02	0.31	0.128	43.90	100.0
175C3CB#1	200000	Ryne	28.66	10.87	16.45	0.38	0.126	43.51	100.0
175C4CB#1	200000	Ryne	28.31	13.05	14.10	0.42	0.020	44.10	100.0
175C4CB#2	200000	Ryne	28.97	9.26	18.62	0.28	0.033	42.83	100.0
175C4CB#3	200000	Ryne	28.18	11.59	16.12	0.49	0.000	43.63	100.0
175C4CB#4	200000	Ryne	29.04	9.18	18.60	0.28	0.042	42.86	100.0
175C5CB#1	200000	Ryne	29.03	15.44	9.75	0.30	0.006	45.47	100.0
175C5CB#2	200000	Ryne	28.89	12.86	13.27	0.55	0.000	44.42	100.0
175C5CB#3	200000	Ryne	28.30	10.69	17.14	0.44	0.000	43.43	100.0
175C5CB#4	200000	Ryne	28.65	13.78	12.44	0.32	0.000	44.82	100.0
175C6CB#1	200000	Ryne	28.84	10.77	16.80	0.52	0.011	43.07	100.0
175C7CB#1	200000	Ryne	29.06	17.77	5.80	0.57	0.000	46.80	100.0

Sample #	Au (ppb)	Location	CaO wt%	MgO wt%	FeO wt%	MnO wt%	SrO wt%	CO2 wt%	Total wt%
175C8CB#1	200000	Ryne	54.23	0.11	0.35	0.60	0.000	44.72	100.0
175C9CB#1	200000	Ryne	29.42	10.87	16.12	0.44	0.106	43.05	100.0
175C9CB#2	200000	Ryne	54.54	0.12	0.35	0.57	0.000	44.43	100.0
176C1CB#1	48200	Hourglass	53.85	1.83	0.02	0.00	0.000	44.30	100.0
176C2CB#1	48200	Hourglass	27.96	9.58	18.21	0.32	0.000	43.93	100.0
176C3CB#1	48200	Hourglass	29.08	13.56	12.27	0.38	0.075	44.64	100.0
176C3CB#2	48200	Hourglass	28.08	11.11	16.70	0.36	0.005	43.75	100.0
176C3CB#3	48200	Hourglass	28.23	11.51	16.13	0.25	0.030	43.85	100.0
176C3CB#4	48200	Hourglass	28.43	9.81	18.18	0.36	0.022	43.21	100.0
176C3CB#5	48200	Hourglass	28.03	11.35	16.42	0.39	0.054	43.75	100.0
176C3CB#6	48200	Hourglass	29.00	14.02	11.42	0.45	0.043	45.07	100.0
176C3CB#7	48200	Hourglass	29.15	13.86	11.63	0.52	0.000	44.85	100.0
176C4CB#1	48200	Hourglass	28.61	10.46	16.80	0.34	0.000	43.80	100.0
176C5CB#1	48200	Hourglass	28.23	11.38	15.81	0.36	0.114	44.10	100.0
176C5CB#2	48200	Hourglass	28.32	11.43	15.83	0.40	0.158	43.85	100.0
176C5CB#3	48200	Hourglass	28.50	13.53	12.71	0.43	0.147	44.69	100.0
176C5CB#4	48200	Hourglass	28.48	11.74	15.53	0.43	0.159	43.65	100.0
176C5CB#5	48200	Hourglass	28.15	11.18	16.60	0.38	0.181	43.51	100.0
176C5CB#6	48200	Hourglass	28.30	11.99	15.08	0.38	0.140	44.11	100.0
176C5CB#7	48200	Hourglass	28.06	11.38	16.31	0.29	0.055	43.91	100.0
176C6CB#1	48200	Hourglass	28.87	9.79	17.58	0.39	0.000	43.36	100.0
176C6CB#2	48200	Hourglass	29.13	13.47	12.58	0.49	0.000	44.34	100.0
176C7CB#1	48200	Hourglass	28.76	10.35	17.47	0.36	0.000	43.06	100.0
176C7CB#2	48200	Hourglass	28.65	14.05	11.31	0.46	0.000	45.53	100.0
176C8CB#1	48200	Hourglass	28.34	10.31	17.40	0.37	0.000	43.57	100.0

Microprobe analyse results of plagioclase

Detection limit in wt%: NaO, MgO, Al2O3, K2O, 0.02; CaO, SiO2, 0.03; FeO 0.04

Sample #	Au (ppb)	Location	Na2O wt%	CaO wt%	K2O wt%	MgO wt%	FeO wt%	Al2O3 wt%	SiO2 wt%	Total wt%
086C2PG#1	1200	Ryne	11.67	0.08	0.06	0.00	0.05	19.29	68.65	99.80
086C2PG#2	1200	Ryne	11.23	0.14	0.31	0.03	0.07	19.74	67.41	98.93
086C2PG#3	1200	Ryne	11.44	0.11	0.15	0.02	0.03	19.40	67.88	99.03
086C2PG#4	1200	Ryne	11.46	0.14	0.26	0.03	0.03	19.67	68.74	100.31
086C2PG#5	1200	Ryne	11.45	0.09	0.09	0.01	0.02	19.61	67.93	99.20
086C2PG#6	1200	Ryne	11.46	0.10	0.04	0.00	0.00	19.38	68.83	99.82
086C12PG#1	1200	Ryne	11.16	0.44	0.06	0.00	0.04	19.82	67.59	99.12
003C1PG#1	85	Ryne	11.67	0.07	0.01	0.00	0.01	19.31	69.40	100.47
003C1PG#2	85	Ryne	11.62	0.06	0.04	0.01	0.01	19.44	69.21	100.41
003C5PG#1	85	Ryne	11.65	0.06	0.02	0.00	0.00	19.47	68.44	99.66
003C7PG#1	85	Ryne	11.57	0.06	0.02	0.00	0.02	19.43	68.87	99.96
003C8PG#1	85	Ryne	11.58	0.10	0.01	0.00	0.02	19.59	68.79	100.09
003C8PG#2	85	Ryne	11.56	0.11	0.02	0.01	0.00	19.44	69.81	100.93
003C10PG#1	85	Ryne	11.50	0.20	0.06	0.00	0.01	19.69	69.27	100.74
R1aC7PG#1	200000	Ryne	11.54	0.09	0.06	0.00	0.06	19.32	68.10	99.21
R1aC7PG#2	200000	Ryne	11.50	0.21	0.06	0.01	0.03	19.47	68.57	99.84
R1aC9PG#1	200000	Ryne	11.43	0.07	0.14	0.01	0.06	19.40	68.60	99.73
R1aC11PG#1	200000	Ryne	11.66	0.16	0.07	0.00	0.13	19.49	68.92	100.43
R1aC14PG#1	200000	Ryne	11.48	0.07	0.06	0.01	0.06	19.32	68.12	99.13
R1bC4PG#1	200000	Ryne	11.60	0.02	0.05	0.00	0.02	19.19	67.98	98.85
R1bC4PG#2	200000	Ryne	11.65	0.10	0.06	0.01	0.03	19.34	67.60	98.78
R1bC7PG#1	200000	Ryne	11.53	0.10	0.07	0.00	0.06	19.45	68.14	99.37
R1bC10PG#1	200000	Ryne	11.58	0.02	0.05	0.00	0.06	19.27	68.58	99.56
128C1PG#1	7400	Ryne	11.27	0.18	0.37	0.05	0.11	19.75	67.94	99.65
128C1PG#2	7400	Ryne	11.40	0.13	0.05	0.01	0.06	19.34	68.56	99.54
128C1PG#3	7400	Ryne	11.03	0.21	0.58	0.05	0.15	19.90	67.48	99.39
128C1PG#4	7400	Ryne	9.05	0.08	2.67	0.36	0.72	21.71	64.26	98.86
128C1PG#5	7400	Ryne	11.54	0.08	0.06	0.00	0.05	19.30	69.00	100.03
128C1PG#6	7400	Ryne	11.55	0.03	0.06	0.00	0.04	19.23	68.64	99.54
128C2PG#1	7400	Ryne	11.66	0.02	0.07	0.02	0.02	18.88	67.53	98.19
128C2PG#2	7400	Ryne	11.48	0.03	0.07	0.00	0.03	18.98	68.47	99.07
128C3PG#1	7400	Ryne	11.51	0.07	0.05	0.01	0.05	18.99	67.54	98.22
128C3PG#2	7400	Ryne	11.38	0.06	0.32	0.00	0.02	18.86	67.72	98.36
R2C1PG#1	200000	Ryne	11.47	0.04	0.05	0.01	0.02	19.26	68.53	99.38
R2C1PG#2	200000	Ryne	11.40	0.10	0.06	0.01	0.05	19.40	68.33	99.36
R2C7PG#1	200000	Ryne	10.40	0.22	1.25	0.12	0.33	20.88	66.67	99.87
R2C8PG#1	200000	Ryne	11.44	0.04	0.05	0.00	0.06	19.34	68.90	99.82
R2C8PG#2	200000	Ryne	11.06	0.12	0.37	0.01	0.12	19.70	67.86	99.24
R2C8PG#3	200000	Ryne	11.40	0.10	0.05	0.00	0.05	19.46	68.82	99.88
R2C9PG#1	200000	Ryne	11.34	0.22	0.12	0.02	0.11	19.84	68.35	100.00
R2C9PG#2	200000	Ryne	11.61	0.18	0.04	0.02	0.13	19.52	68.83	100.34
R3C3PG#1	200000	Ryne	11.21	0.26	0.06	0.00	0.03	18.92	69.69	100.16
R3C3PG#3	200000	Ryne	11.45	0.05	0.06	0.01	0.05	19.40	68.31	99.33
R3C3PG#4	200000	Ryne	11.36	0.14	0.06	0.00	0.06	19.59	67.97	99.19
R3C7PG#1	200000	Ryne	11.22	0.30	0.33	0.02	0.06	19.94	68.34	100.24
R3C10PG#1	200000	Ryne	11.63	0.14	0.05	0.00	0.05	19.45	68.69	100.00
H2C1PG#1	69000	Hourglass	11.52	0.14	0.05	0.00	0.01	19.31	68.53	99.57
H2C1PG#2	69000	Hourglass	11.45	0.22	0.04	0.00	0.00	19.43	68.64	99.79
H2C1PG#3	69000	Hourglass	11.56	0.07	0.05	0.00	0.01	19.34	68.78	99.81
H2C2PG#1	69000	Hourglass	9.84	0.10	0.03	0.00	0.01	16.53	73.35	99.86
H2C2PG#2	69000	Hourglass	11.28	0.20	0.07	0.00	0.00	19.32	67.85	98.71
H2C2PG#3	69000	Hourglass	11.30	0.14	0.04	0.01	0.00	19.14	69.15	99.77
H2C3PG#1	69000	Hourglass	11.52	0.23	0.07	0.00	0.00	19.59	68.44	99.85
H2C3PG#2	69000	Hourglass	11.53	0.17	0.06	0.00	0.03	19.60	68.61	100.00
H2C4PG#1	69000	Hourglass	11.32	0.24	0.05	0.01	0.00	19.43	67.99	99.03
H2C4PG#2	69000	Hourglass	11.53	0.21	0.05	0.00	0.01	19.48	68.06	99.33
H2C7PG#1	69000	Hourglass	11.53	0.13	0.04	0.00	0.00	19.54	68.76	100.01
H2C7PG#2	69000	Hourglass	11.57	0.18	0.05	0.00	0.00	19.54	68.34	99.67
H2C8PG#1	69000	Hourglass	11.58	0.18	0.06	0.00	0.01	19.58	68.53	99.94
H2C8PG#2	69000	Hourglass	11.52	0.13	0.06	0.00	0.01	19.56	68.68	99.96
H2C11PG#1	69000	Hourglass	11.59	0.10	0.06	0.00	0.01	19.50	68.66	99.92
H2C11PG#2	69000	Hourglass	11.44	0.14	0.04	0.01	0.00	19.46	68.96	100.06

Sample #	Au (ppb)	Location	Na2O wt%	CaO wt%	K2O wt%	MgO wt%	FeO wt%	Al2O3 wt%	SiO2 wt%	Total wt%
H2C12PGI#1	69000	Hourglass	11.58	0.16	0.06	0.01	0.02	19.44	68.52	99.79
H2C12PGI#2	69000	Hourglass	11.62	0.04	0.07	0.00	0.03	19.24	68.73	99.72
H2C12PGI#3	69000	Hourglass	11.56	0.09	0.06	0.01	0.02	19.48	68.68	99.86
H2C12PGI#4	69000	Hourglass	11.52	0.20	0.06	0.00	0.06	19.55	68.48	99.87

Microprobe analyse results of chlorite

Detection limit in wt%: FeO, 0.015; MgO, K2O, SiO2, 0.03; Na2O, Al2O3, 0.02; CaO, MnO, 0.04

Sample #	Au (ppb)	Location	FeO wt%	MgO wt%	Na2O wt%	K2O wt%	CaO wt%	MnO wt%	Al2O3 wt%	SiO2 wt%	Total wt%
066C6CL#1	1200	Ryne	26.36	14.43	0.02	0.01	0.05	0.03	21.97	24.75	87.61
066C6CL#2	1200	Ryne	27.01	13.80	0.01	0.07	0.03	0.03	20.97	24.46	86.35
066C6CL#3	1200	Ryne	26.04	15.29	0.01	0.03	0.03	0.06	21.16	25.32	87.94
066C7CL#1	1200	Ryne	26.52	15.46	0.01	0.01	0.00	0.04	20.33	25.10	87.48
066C7CL#2	1200	Ryne	26.92	14.50	0.00	0.02	0.01	0.06	21.65	25.42	88.57
066C10CL#1	1200	Ryne	25.67	15.05	0.00	0.04	0.02	0.06	21.44	25.15	87.42
066C10CL#2	1200	Ryne	26.46	14.54	0.02	0.06	0.01	0.02	21.53	24.92	87.56
066C11CL#1	1200	Ryne	25.92	15.02	0.01	0.02	0.05	0.03	21.07	25.44	87.55
003C3CL#1	85	Ryne	31.59	10.03	0.03	0.02	0.04	0.03	21.31	23.58	86.64
003C3CL#2	85	Ryne	31.67	10.37	0.04	0.03	0.03	0.01	21.87	24.04	88.06
003C6CL#1	85	Ryne	31.88	10.55	0.02	0.03	0.03	0.02	21.29	24.29	88.11
003C8CL#1	85	Ryne	32.14	9.60	0.02	0.02	0.00	0.04	22.26	24.04	88.11
R1eC3CL#1	200000	Ryne	28.69	13.18	0.01	0.02	0.01	0.06	21.92	24.74	88.62
R1eC3CL#2	200000	Ryne	29.17	12.94	0.01	0.03	0.00	0.05	21.77	24.93	88.89
R1bC10CL#1	200000	Ryne	28.61	13.20	0.00	0.01	0.02	0.03	21.73	24.92	88.53
R1bC10CL#2	200000	Ryne	29.25	12.83	0.03	0.03	0.01	0.06	21.81	25.11	89.12
R1bC10CL#3	200000	Ryne	29.79	12.44	0.03	0.02	0.02	0.06	21.44	25.11	88.90
126C1CL#1	7400	Ryne	31.37	11.25	0.00	0.04	0.03	0.06	21.46	24.48	88.68
126C1CL#2	7400	Ryne	31.65	11.03	0.02	0.03	0.03	0.08	21.61	24.57	89.00
126C5PG#1	7400	Ryne	33.49	9.60	0.00	0.03	0.02	0.09	20.99	24.00	88.23
126C6CL#1	7400	Ryne	32.47	10.30	0.01	0.02	0.01	0.08	21.26	24.20	88.35
126C6CL#2	7400	Ryne	32.80	10.42	0.01	0.00	0.00	0.09	21.21	24.34	88.88
H2C2CL#1	69000	Hourglass	25.99	15.58	0.01	0.02	0.01	0.05	21.07	25.52	88.24
H2C2CL#2	69000	Hourglass	24.24	16.67	0.01	0.02	0.04	0.06	20.57	25.90	87.51
H2C9CL#1	69000	Hourglass	25.58	14.76	0.00	0.01	0.03	0.04	19.89	24.74	85.04
H2C9CL#2	69000	Hourglass	27.29	14.57	0.00	0.02	0.02	0.05	21.11	25.44	88.50
H2C9CL#3	69000	Hourglass	25.96	15.00	0.01	0.02	0.04	0.05	20.95	25.81	87.83
H2C9CL#4	69000	Hourglass	24.44	16.70	0.00	0.03	0.00	0.06	21.29	25.91	88.43

Microprobe analyse results of biotite and sericite

Detection limit in wt%: K2O, Al2O3, MgO, CaO, SiO2, 0.03; Fe2O3, MnO, 0.04; TiO2, BaO, 0.05; Cr2O3, V2O3, 0.06; F, 0.12; Cl, 0.015

Sample #	Au (ppb)	Location	K2O wt%	Na2O wt%	FeO wt%	MgO wt%	Cr2O3 wt%	V2O3 wt%	CaO wt%
BIOTITE									
066C1BO#1	1200	Ryne	10.16	0.03	19.11	11.05	0.00	0.04	0.04
066C1BO#2	1200	Ryne	10.30	0.03	19.02	10.99	0.00	0.08	0.02
066C1BO#3	1200	Ryne	10.06	0.05	19.00	11.52	0.22	0.06	0.02
066C1BO#4	1200	Ryne	9.89	0.02	19.37	11.30	0.01	0.09	0.00
SERICITE									
066C7SR#1	1200	Ryne	11.40	0.27	2.66	1.89	0.00	0.05	0.00
066C7SR#2	1200	Ryne	11.46	0.28	2.49	1.83	0.03	0.03	0.02
066C10SR#1	1200	Ryne	11.60	0.20	3.64	2.18	0.02	0.08	0.02
066C10SR#2	1200	Ryne	11.49	0.27	3.53	2.08	0.21	0.08	0.05
003C10SR#1	85	Ryne	10.40	0.80	2.55	1.06	0.18	1.48	0.00
R1aC5SR#1	200000	Ryne	11.04	0.58	3.54	1.16	0.00	0.17	0.00
R1aC6SR#1	200000	Ryne	11.35	0.28	2.47	1.33	0.01	0.17	0.03
R1aC7SR#1	200000	Ryne	11.52	0.23	2.79	1.21	0.01	0.17	0.01
R1aC8SR#1	200000	Ryne	11.37	0.29	3.06	1.18	0.01	0.25	0.04
R1aC10SR#1	200000	Ryne	11.19	0.52	3.17	1.20	0.00	0.32	0.04
R1aC11SR#1	200000	Ryne	11.31	0.41	1.36	0.97	0.06	0.27	0.01
R1aC14SR#1	200000	Ryne	11.37	0.43	1.16	1.03	0.03	0.16	0.00
R1bC3SR#1	200000	Ryne	11.40	0.38	1.58	1.04	0.00	0.13	0.02
R1bC3SR#2	200000	Ryne	11.64	0.31	2.35	1.07	0.01	0.17	0.01
R1bC4SR#1	200000	Ryne	11.64	0.33	1.68	1.05	0.00	0.20	0.00
R1bC10SR#1	200000	Ryne	11.24	0.43	3.49	1.04	0.02	0.30	0.01
R1bC10SR#2	200000	Ryne	11.37	0.30	3.07	1.26	0.00	0.30	0.01
126C1SR#1	7400	Ryne	11.21	0.27	3.27	1.23	0.00	0.10	0.04
126C1SR#2	7400	Ryne	11.62	0.30	3.05	1.25	0.03	0.23	0.01
126C2SR#1	7400	Ryne	11.39	0.27	3.48	1.18	0.00	0.24	0.00
126C2SR#2	7400	Ryne	11.35	0.22	4.86	1.79	0.05	0.24	0.02
126C2SR#3	7400	Ryne	11.35	0.29	3.84	1.15	0.02	0.26	0.01
126C6SR#1	7400	Ryne	11.41	0.31	4.03	1.30	0.00	0.17	0.01
126C6SR#2	7400	Ryne	11.36	0.18	4.70	1.37	0.04	0.14	0.01
R2C7SR#1	200000	Ryne	11.46	0.38	1.87	1.22	0.02	0.19	0.00
R2C7SR#2	200000	Ryne	11.49	0.37	2.06	1.28	0.01	0.27	0.00
R3C3SR#1	200000	Ryne	11.61	0.27	3.07	1.21	0.03	0.29	0.03
R3C7SR#1	200000	Ryne	11.21	0.29	3.63	1.25	0.04	0.31	0.02
H2C4SR#1	65000	Hourglass	11.44	0.22	2.49	1.56	0.00	0.06	0.00
H2C4SR#2	65000	Hourglass	11.50	0.27	1.95	1.03	0.04	0.12	0.03
H2C5SR#1	65000	Hourglass	11.68	0.21	2.40	1.64	0.00	0.04	0.01
H2C5SR#2	65000	Hourglass	11.85	0.21	2.62	1.94	0.00	0.06	0.01
H2C9SR#1	65000	Hourglass	11.12	0.45	1.43	0.96	0.00	0.12	0.00
H2C9SR#2	65000	Hourglass	11.55	0.31	2.61	1.39	0.02	0.09	0.00
H2C9SR#3	65000	Hourglass	11.20	0.17	2.48	1.80	0.00	0.14	0.04
H2C9SR#4	65000	Hourglass	11.42	0.28	2.61	1.53	0.00	0.06	0.00
H2C11SR#1	65000	Hourglass	11.56	0.29	2.22	1.40	0.00	0.09	0.00
H2C11SR#2	65000	Hourglass	11.69	0.16	2.74	1.58	0.00	0.12	0.02
H2C11SR#3	65000	Hourglass	11.42	0.16	2.60	1.69	0.00	0.11	0.00
H2C11SR#4	65000	Hourglass	11.65	0.20	2.24	1.34	0.00	0.12	0.00
H2C12SR#1	65000	Hourglass	11.15	0.55	1.30	0.95	0.01	0.05	0.00
H2C12SR#2	65000	Hourglass	11.57	0.20	2.43	1.63	0.03	0.09	0.01
H2C12SR#3	65000	Hourglass	11.47	0.22	2.49	1.57	0.01	0.04	0.02

Microprobe analyse results of biotite and sericite (II)

Sample #	MnO wt%	BaO wt%	Al2O3 wt%	TiO2 wt%	SiO2 wt%	F wt%	Cl wt%	Total wt%
BIOTITE								
066C1BO#1	0.03	0.06	16.19	1.79	36.09	1.23	0.03	95.32
066C1BO#2	0.02	0.08	16.15	1.69	35.34	1.18	0.02	94.40
066C1BO#3	0.05	0.09	16.34	1.71	36.01	1.18	0.04	95.84
066C1BO#4	0.02	0.06	16.82	1.82	35.69	1.16	0.03	95.78
SERICITE								
066C7SR#1	0.00	0.16	29.58	0.32	46.31	0.26	0.01	92.80
066C7SR#2	0.00	0.16	30.95	0.34	47.42	0.30	0.00	95.17
066C10SR#1	0.00	0.13	30.58	0.39	46.10	0.22	0.01	95.08
066C10SR#2	0.03	0.07	29.57	1.03	46.21	0.17	0.00	94.70
003C10SR#1	0.00	1.07	32.20	0.42	44.35	0.12	0.00	94.57
R1aC5SR#1	0.00	0.14	32.32	0.26	44.75	0.22	0.00	94.08
R1aC6SR#1	0.01	0.09	31.81	0.23	46.80	0.41	0.00	94.82
R1aC7SR#1	0.00	0.11	31.97	0.16	45.92	0.33	0.00	94.29
R1aC8SR#1	0.13	0.21	31.88	0.43	45.56	0.27	0.00	94.56
R1aC10SR#1	0.01	0.16	32.60	0.59	45.32	0.24	0.00	95.28
R1aC11SR#1	0.00	0.11	34.11	0.07	46.27	0.13	0.00	95.04
R1aC14SR#1	0.00	0.16	34.44	0.08	46.51	0.19	0.00	95.47
R1bC3SR#1	0.00	0.18	33.98	0.12	46.63	0.21	0.00	95.56
R1bC3SR#2	0.01	0.14	33.24	0.10	46.48	0.25	0.00	95.68
R1bC4SR#1	0.00	0.09	33.79	0.10	46.47	0.21	0.00	95.48
R1bC10SR#1	0.01	0.20	32.61	0.35	44.97	0.21	0.00	94.78
R1bC10SR#2	0.00	0.18	32.08	0.28	45.59	0.29	0.00	94.59
126C1SR#1	0.02	0.29	32.65	0.35	47.23	0.34	0.00	96.87
126C1SR#2	0.00	0.32	31.80	0.76	45.68	0.14	0.01	95.14
126C2SR#1	0.00	0.15	31.70	0.32	44.10	0.30	0.00	93.01
126C2SR#2	0.00	0.17	30.07	0.46	43.63	0.32	0.00	93.06
126C2SR#3	0.00	0.22	31.75	0.30	43.23	0.18	0.00	92.52
126C6SR#1	0.02	0.13	31.55	0.12	45.65	0.35	0.00	94.90
126C6SR#2	0.00	0.16	31.02	0.15	45.41	0.21	0.01	94.67
R2C7SR#1	0.00	0.14	33.29	0.13	46.48	0.24	0.01	95.33
R2C7SR#2	0.01	0.11	33.22	0.12	46.65	0.23	0.00	95.73
R3C3SR#1	0.00	0.16	32.27	0.55	45.63	0.19	0.00	95.22
R3C7SR#1	0.03	0.12	31.53	0.39	45.12	0.20	0.01	94.04
H2C4SR#1	0.01	0.13	31.93	0.59	46.32	0.19	0.00	94.86
H2C4SR#2	0.00	0.09	33.82	0.15	45.96	0.26	0.00	95.08
H2C5SR#1	0.00	0.22	31.49	0.37	46.25	0.29	0.01	94.48
H2C5SR#2	0.00	0.09	31.08	0.29	46.60	0.23	0.01	95.07
H2C9SR#1	0.01	0.14	33.59	0.13	46.18	0.25	0.01	94.28
H2C9SR#2	0.00	0.17	32.53	0.40	45.88	0.24	0.01	95.09
H2C9SR#3	0.00	0.15	29.45	0.49	45.80	0.19	0.04	91.86
H2C9SR#4	0.00	0.20	31.43	0.43	46.02	0.16	0.01	94.07
H2C11SR#1	0.00	0.17	32.66	0.37	46.46	0.23	0.01	95.35
H2C11SR#2	0.01	0.17	32.03	0.41	46.44	0.28	0.01	95.52
H2C11SR#3	0.00	0.18	31.93	0.36	46.98	0.29	0.01	95.60
H2C11SR#4	0.01	0.17	32.13	0.43	44.92	0.13	0.02	93.31
H2C12SR#1	0.00	0.13	34.31	0.08	46.43	0.21	0.00	95.08
H2C12SR#2	0.00	0.22	30.75	0.48	45.81	0.29	0.00	93.39
H2C12SR#3	0.00	0.15	31.72	0.46	45.82	0.35	0.00	94.18

APPENDIX C

Log K values

Log K values from SUPCRT92 and 1998 database update
(except CuHS2-, from Mountain and Seward, 1999)
400°C, 2000 bar

Reaction		Field	Log K
HSO4-SO4	HSO4- = SO4-2 + H+		-6.381
HSO4-H2S	HSO4- = H2S + 2O2		-42.095
SO4-H2S	SO4-2 + 2H+ = H2S + 2O2		-35.714
SO4-HS	SO4-2 + H+ = HS- + 2O2		-43.102
HS-H2S	HS- + H+ = H2S		7.387
Py-Po	Py + H2O = Po + H2S + 0.5O2	H2S	-14.837
Py-Po	Py + H2O = Py + HS- + H+ + 0.5O2	HS-	-22.224
Py-Mag	3Py + 6H2O = Mag + 6HS- + 6H+ + O2	HS-	-79.624
Py-Mag	3Py + 6H2O + 11O2 = Mag + 6SO4-2 + 12H+	SO4-2	178.986
Py-Hem	2Py + 4H2O + 7.5O2 = Hem + 4SO4-2 + 8H+	SO4-2	123.367
Py-Hem	2Py + 4H2O + 7.5O2 = Hem + 4HSO4- + 4H+	HSO4	148.889
Po-Hem	3Po + 3H2O + 0.5O2 = Mag + 3HS- + 3H+	HS-	-12.952
Hem-Mag	3Hem = 2Mag + 0.5O2		-12.13
Ccp-Bn+Py	5Ccp + 2H2S + O2 = Bn + 4Py + 2H2O	H2S	26.329
Ccp-Bn+Py	5Ccp + 2HSO4- + 2H+ = Bn + 4Py + 2H2O + 3O2	HSO4-	-57.861
Ccp-Bn+Py	5Ccp + 2SO4-2 + 4H+ = Bn + 4Py + 2H2O + 3O2	SO4-2	-45.1
Ccp-Bn+Hem	Bn + 2Hem + 6HSO4- + 6H+ = 5Ccp + 6H2O + 12O2	HSO4-	-239.918
Ccp-Bn+Hem	Bn + 2Hem + 6SO4-2 + 12H+ = 5Ccp + 6H2O + 12O2	SO4-2	-201.635
Ccp-Bn+Mag	Bn + 4/3Mag + 6HS- + 6H+ + 1/3O2 = 5Ccp + 6H2O	HS-	65.092
Ccp-Bn+Mag	Bn + 4/3Mag + 6SO4-2 + 12H+ = 5Ccp + 6H2O + 35/3O2	SO4-2	-193.518
Ccp-Bn+Po	Bn + 4Po + 2HS- + 2H+ + O2 = 5Ccp + 2H2O	HS-	47.793
Ccp-Bn+Po	Bn + 4Po + 2H2S + O2 = 5Ccp + 2H2O	H2S	33.018
	Au + 2H2S + 0.25O2 = Au(HS)2- + H+ + 0.5H2O	H2S	-1.794
	Au + 2HS- + H+ + 0.25O2 = Au(HS)2- + 0.5 H2O	HS-	12.981
	Au + 2SO4-2 + 3H+ = Au(HS)2- + 0.5H2O + 15/4O2	HSO4-	-85.984
	Au + 2HSO4- + H+ = Au(HS)2- + 0.5H2O + 15/4O2	SO4-2	-73.223
	Au + 2Cl- + H+ + 0.25O2 = AuCl2- + 0.5H2O		3.368
	Ccp + 0.5H2O + 2Cl- + H+ + 0.25O2 = CuCl2- + Py + 0.5H2O	Py	6.624
	Ccp + 0.5H2O + 2Cl- + H+ = Po + CuCl2- + H2S + 0.25O2	Po	-8.212
	Cu(HS)2- + Py + H+ + 0.5H2O = Ccp + 2H2S + 0.25O2	Py	-0.8178
	Cu(HS)2- + Po + H+ + 0.25O2 = Ccp + H2S + 0.5H2O	Po	14.0232
Ms-Kfs	Ms + 2K+ + 6SiO2 = 3Kfs + 2H+		-7.521
Pg-Ab	Pg + 2Na+ + 6SiO2 = 3Ab + 2H+		-8.609
CH4-CO2	CH4 + 2O2 = CO2 + 2H2O		57.293
	Dol + 4H+ = Ca2+ + Mg2+ + 2CO2 + 2H2O	CO2	11.761
	Dol + 4H+ + 2H2O = Ca2+ + Mg2+ + 2CH4 + 4O2	CH4	-102.826